UNIVERSITÉ DE SHERBROOKE

Faculté de Génie

EFFETS DES AGENTS INTERFACIAUX COPOLYMÈRES TRIBLOC SUR LE COMPORTEMENT EN RUPTURE ET EN ÉCOULEMENT DU MÉLANGE DE POLYSTYRÈNE/ CAOUTCHOUC-ETHYLÈNE-PROPYLÈNE

INFLUENCES OF TRIBLOCK-COPOLYMER INTERFACIAL-MODIFIERS ON FRACTURE AND YIELDING BEHAVIORS OF POLYSTYRENE/ETHYLENE-PROPYLENE-RUBBER BLENDS

Mémoire de maîtrise ès sciences appliquées

Spécialité : génie mécanique

Tung Ha Anh

Sherbrooke (Québec), CANADA Avril 1999

SOMMAIRE

Au cours des dernières années, plusieurs travaux ont été réalisés dans le domaine des mélanges de polymères. Ceci est un des moyens efficaces et peu coûteux pour améliorer les propriétés mécaniques des polymères. Dans une étude précédente [1], deux copolymères de triblock de styrène/éthylène - butylène/styrène (SEBS), de différents poids moléculaires, ont été utilisés pour compatibiliser un mélange contenant en volume 80 % de polystyrène (PS) et 20 % de caoutchouc-éthylène-propylène (CEP). Les résultats montrent, premièrement, une augmentation significative de la résistance aux chocs lorsque les concentrations d'agents interfaciaux sont au-dessus de la concentration critique en émulsification pour des mélanges compatibilisés par le copolymère ayant une masse moléculaire faible (K2) et, deuxièmement, qu'une transition fragile-ductile de rupture se produit.

A partir de ces résultats, l'objectif de cette étude est d'améliorer la compréhension des effets des deux copolymères de triblock ci-dessus sur la rupture et le comportement des mélanges sur un intervalle étendu des taux de chargement et des températures. À cette fin, les mélanges de différentes concentrations de ces copolymères ont été étudiés dans de diverses conditions d'essai. L'attention est mise sur la corrélation entre temps-température et la résistance de rupture ainsi que le comportement d'écoulement de ces mélanges. L'ajout du copolymère de triblock, connu sous le nom d'agent interfacial, permet au mélange fragile de PS/CEP de devenir plus ductile. La dépendance temps-température de la transition fragile-ductile à la rupture des mélanges est contrôlée par un processus d'énergie d'activation et peut être prédit par l'équation d'Arrhenius. Ajouter un agent interfacial abaisse la température à la transition fragile-ductile et réduit la barrière d'énergie contrôlant le processus de rupture. Cet effet, cependant, est beaucoup plus prononcé pour l'agent interfacial de poids moléculaire

inférieur, K2. La résistance de rupture pendant la propagation de fissure des mélanges est déterminée en utilisant la méthode de R-courbe et elle présente une contribution distincte aux mélanges K2-20 et K2-30 pour la résistance la plus élevée de rupture du mélange de PS/CEP.

La corrélation entre la température et le taux de déformation sur le comportement d'écoulement des mélanges de polymère semble être contrôlée par la relaxation moléculaire selon la théorie de Ree-Eyring. Ce modèle, fondé sur l'hypothèse de deux processus d'Eyring (les processus α et β) agissant en parallèle, permet la prévision de la contrainte d'écoulement en tension et en compression à de divers taux de déformation et de température. L'ajout des agents interfaciaux K1 et K2 résulte en une réduction de l'énergie d'activation ΔH et une augmentation en volume d'activation V^* pour les processus α et β. En outre, la similitude de la valeur de l'énergie d'activation ΔH_β au processus β et la barrière d'énergie contrôlant la transition fragile-ductile à la rupture semble prouver une corrélation implicite entre le comportement à l'écoulement et l'approche de la rupture.

SUMMARY

For the recent years, many works have been taken into account in the field of blending existing polymers together, which is one of the effective and low cost ways of improving the mechanical properties of polymers. In a previous study [1], two triblock copolymers of styrene/ ethylene – butylene/ styrene (SEBS), of different molecular weights, were used to compatibilize a blend of 80 volume % of polystyrene (PS) and 20 volume % of ethylene – propylene rubber (EPR). Results show firstly a significant increase in impact strength at interfacial agent concentrations above the critical concentration for emulsification for blends compatibilized by the low molecular weight copolymer (K2), and secondly a transition from brittle to ductile fracture mode occurred.

The aim of this work is to foster the understanding of the effects of the two triblock copolymers above on fracture and yielding behavior of the blends over a large range of loading rates and temperatures. For this purpose, the blends of different concentrations of these two triblock copolymers were studied at various test conditions. The focus is put on the time – temperature dependence of fracture performance and yielding behavior of these blends. The addition of the triblock copolymer, known as an interfacial modifier, allows the brittle PS/EPR blend to become more ductile. The time-temperature dependence of the brittle-ductile transition in fracture performance of the blends is controlled by an energy activation process and can be predicted by the Arrhenius equation. Adding an interfacial agent lowers the temperature at brittle-ductile transition and reduces the energy barrier ΔH controlling the fracture process. This effect, however, is much more pronounced for the lower molecular weight interfacial agent, K2. The fracture resistance at crack initiation as well as during the crack propagation of the blends, which is determined by using the R-curve method, presents a

distinct contribution of K2-20 and K2-30 blends to the higher fracture resistance of the PS/EPR blend.

The correlation between temperature and loading rate in yielding behavior of the blends seems to be controlled by the molecular relaxation according to the Ree-Eyring theory. This model, based on the assumption of two Eyring processes (α and β processes) acting in parallel, allows prediction of the tensile and compression yield stress at various loading rates and temperatures. The addition of K1 and K2 interfacial agents results in a reduction of the activation energy ΔH and an increase in the activation volume V^* for both α and β processes. Furthermore, the similarity of the value of the activation energy ΔH_β in β yielding process and the energy barrier ΔH controlling the brittle-ductile transition in fracture seems to pronounce an implicit correlation between the yielding behavior and fracture approach.

REMERCIEMENTS

Ce travail a été accompli sous la supervision du professeur Toan Vu-Khanh qui m'a grandement assisté avec ses précieux conseils et ses interventions toujours bien appréciées. Je tiens donc à le remercier pour tout ce qu'il a fait.

Je tiens aussi à remercier Monsieur Magella Tremblay pour son aide technique considérable et dont la compétence a favorisé le bon déroulement de cette étude.

Finallement, un gros merci à ma famille, ma fiancée et mes amis pour leur support moral qu'il a pu me stimuler pendant tout le temps que ce travail a nécessité.

TABLE OF CONTENTS

LIST OF FIGURES

LIST OF TABLES

LIST OF SYMBOLS

K1 : low molecular weight interfacial agent

K2 : high molecular weight interfacial agent

EPR : ethylene-propylene rubber

SEBS : styrene/ethylene-butylene/styrene

C_{crit} : critical concentration value of interfacial modifier

M_n : molecular weight

LEFM : linear elastic fracture mechanics

G : strain energy release rate

P : external force

C : compliance of the specimen

A : crack surface

G_c : critical value of G

P_c : load at fracture initiation

U : elastic energy stored in the sample

B : thickness of the sample

D : width of the sample

Φ : a calibration factor which depends on the length of the crack and the size of the sample

a_{eff} : effective crack length

a_o : initial crack length of the specimen

r_p : radius of the plastic zone in front of the crack tip

U_{total} : sum of all energies dissipated during the various crack propagation

U_{st} : fracture energy during the stable propagation of the crack

U_{inst} : fracture energy at instability

Δ : displacement at the load application point

i : i^{th} stable propagation zone.

G_{st} : mean value of fracture energy absorbed during the stable propagation of crack

G_{inst} : strain energy release rate at instability

a_1 : stable crack length

A_1 : stable crack propagation zone

Φ_1 : calibration factor corresponding to the crack length a_1

dJ/da : rate of the stability of crack propagation

E : Young modulus of the material

T_{mat} : tearing modulus of the material

σ_y : yield stress of the material

G_r : actual fracture energy

G_i : fracture energy at crack initiation

T_a : rate of change of G_r with crack extension

K : stress intensity factor

υ : Poisson's ratio

K_{Ic} : material fracture toughness

S : span of bending test

K_c , K_{inst} or K_i, : stress intensity factors related to three fracture modes (brittle, semi-ductile or ductile respectively)

K_R : critical stress intensity factor during crack propagation

$\dot{\varepsilon}$: strain rate

ΔH : activation energy, the enthalpy required to take a mole of segments from the potential well to the top of the barrier

R : gas constant

T : absolute temperature

$T_{b\text{-}d}$: brittle-ductile transition temperature

ω : rate of jump of molecules

$\omega_o, \dot{\varepsilon}_0$: pre-exponential factors

σ_s : shear stress

V^* : activation volume

$\dot{\varepsilon}_0$: pre-exponential factor

$\Delta H_\alpha, \Delta H_\beta$: activation energies in α and β processes

$V_{t_\alpha}{}^*, V_{t_\beta}{}^*$: activation volumes in α and β processes for tensile tests

$V_{c_\alpha}{}^*, V_{c_\beta}{}^*$: activation volumes in α and β processes for compression tests

$\dot{\varepsilon}_\beta$: critical strain rate

$\varepsilon_t, \varepsilon_c$: strains at yield point for tensile and compression tests

V : loading rate

d_c : slanting straight line separating α and β processes

INTRODUCTION

Polymer alloys and blends represent one of the fastest growing sectors of the plastics industry. Blending existing polymers together has long been known to be an effective, low cost way of developing novel materials. Polymer blends by definition are physical mixtures of structurally different homo or copolymers. However, the vast majority of polymer pairs is mutually immiscible, and, when blended, display very poor mechanical properties, due to their coarse, heterogeneous morphology and weak adhesion. In the past twenty years, research in polymer blends has increased significantly with more than 4500 patents produced annually word-wide (Utracki, 1989). The use of polymer blends in the market place is growing at approximately 10 % per year compared to 4 % for all of plastics [15]. It has been shown recently that the compatibilization of polymer blends could be carried out by incorporating a third component, or interfacial agent, into the incompatible blend.

The most common form of physical compatibilization has been the use of block copolymers. Each block of a diblock of multiblock copolymer is usually either miscible, or has strong affinities, with one of the two homopolymer phases. Thus, block copolymers can act by migrating to the interface between the homopolymers. They are known to reduce the interfacial tension, homogenize the morphology and improve adhesion between phases. This effect results in an improvement in mechanical properties and fracture performance of the material. However, the relationship between morphology, the state of the interface, and mechanical properties is still unclear. Extensive work has been carried out on various rubber-toughened polymer systems, such as HIPS/PPO blends [16, 17], ABS emulsion polymer [18], PP/EPR [19] and PA/EPR [20]. By using tensile dilatometry the effects of shear yielding and crazing phenomena in the tensile deformation of these blends have been demonstrated. In

another approach [21], the copolymer was deposited directly at the interface, and the force required to separate the homopolymers from each other was measured. A mechanical reinforcement effect due to the presence of the copolymer at the interface has been observed, and a failure mechanism map [22] has been developed which distinguishes two different regimes of failure at a compatibilized interface. If the block copolymer molecules themselves fail at the interface, the mechanism is known as chain scission. This can be expected to occur for long chains occupying the interface at a low areal density. Conversely, chain pull-out is more likely to occur with more densely packed, short interfacial agent chains.

In previous study [1], two triblock copolymers of styrene/ ethylene- butylene/ styrene (SEBS), of different molecular weights, used to compatibilize a blend of 80 volume % polystyrene (PS) and 20% ethylene- propylene rubber (EPR) were studied. The emulsification curve, which relates the average minor phase particle diameter to the concentration of interfacial agent added, was used to quantify the effect of the interfacial agents on the blend morphology. Links between morphology, interface and properties were established by combining the emulsification curve with a fracture mechanics approach. The results suggest that for the lower molecular weight interfacial agent (denoted as K2), a transition in fracture mechanisms, from brittle to ductile, occurs at around 20% interfacial agent (based on the volume of the minor phase). This transition, however, is not observed with the high molecular weight interfacial agent (denoted as K1). Following the same approach, the two same types of interfacial agents (K1 and K2 with their different molecular weights: M_n (K1) = 174 000 g/mol and M_n (K2) = 50 000 g/mol) were studied in this work for varying the adhesion between the phases in the blend of Polystyrene/ Ethylene-Propylene Rubber (PS/EPR). In order to consider the effect of the quantity of these interfacial modifiers on morphology and mechanical properties, the blends were prepared with interfacial agent concentrations of 2.5, 5,

10, 15, 20 and 30 % based on the volume of the EPR, the minor phase of the blends. The aim of this work is to foster the understanding of the influences of the two triblock copolymers above on fracture behavior of the PS/EPR blend over a large range of loading rates and temperatures. For this purpose, the blends of different concentrations of these two interfacial agents were studied at various test conditions.

In fact, it has been pointed out that the fracture behavior of polymers is a very complex process and the fracture performance depends on both the initiation and the propagation of a defect in the material [2-6]. At various levels of loading rate and temperature, the fracture mode and performance can be very different. Depending on the amount of plastic deformation at the crack tip and the stability of crack propagation, a given polymer can break in a brittle, semi-ductile, or ductile manner. For each type, an appropriate analysis must be used to determine the fracture resistance of the blend, that is represented either by the strain energy release rate (G_c, G_{inst}, or G_i) or by the stress intensity factor (K_c, K_{inst}, or K_i) of material. In this study, the method using the stress intensity factor was proposed to examine the fracture performance of the blends. This method allows us to determine the fracture resistance of the blends at crack initiation as well as during the propagation of the crack according to the $K_R(\Delta a_{eff})$ curve.

The development of copolymers and polymer blends has resulted in materials exhibiting more and more ductile behavior in fracture. Ductile fracture generally occurs under a stable crack propagation, with more plastic deformation. For this mode of fracture, after initiation, the cracks can only propagate with additional supply of energy by external loads so that the character of the failure is less catastrophic. For this reason, much effort is being put on making plastics tougher. However, toughened plastics exhibit a ductile behavior only under a

certain range of temperature and loading rates. Many polymers, regarded as tough under normal conditions, become brittle when the temperature is lowered or the loading rate is increased. Therefore, another purpose of this work is to put the focus on the effects of time and temperature on the ductile fracture behavior of PS/EPR blend, modified by various concentrations of the two different interfacial agents. The Ree-Eyring's model was used to predict the tensile and the compression yield stress of the blends at various temperatures and loading rates. This model has also shown that the correlation between temperature and loading rate seems to be controlled by the molecular relaxation according to the Ree- Eyring theory. A relationship between the activation energy ΔH_β in the β process from the Ree-Eyring equation and the energy barrier ΔH of the Arrhenius form controlling the brittle-ductile transition in fracture performance of the blends, is found to give a link between the yield behavior with the fracture process.

In this thesis, we will address the following issues: First, the theoretical background will be presented in Chapter 1. Then the experimental study will be given in Chapter 2. Chapter 3 will present the results obtained from the tests and their discussion. Finally, a general conclusion will be shown at the end of this work.

CHAPTER 1

THEORETICAL BACKGROUND

1.1 Polymer blends

1.1.1 Introduction

Polymer blends by definition are physical mixture of structurally different homo or copolymers. Polymer blending is a useful technique for designing materials with a wide variety of properties. An important commercial advantage is that polymer blends offer a way to produce new materials by using already existing materials, which reduced development costs. However, as most polymer blends are immiscible and form heterogeneous multi-phase systems, blending often results in material properties that are strongly dependent on the processing conditions, morphology and interactions between the phases.

In recent years, research in the polymer blend domain has increased significantly (Utracki, 1989). Particularly, blends with engineering resins constitute the highest growth area in this field with annual growth rates of 17 % reported in the past (Rappaport, 1985).

Blends can result in completely new materials exhibiting high degrees of synergism compared to the original components. In other cases they serve to produce materials with an optimal cost/performance behavior. Polymer blends have allowed the gap to be filled between high cost engineering resins and low cost/low performance commodity polymers. The primary physical properties which are targeted for improvement in blending are the following in order of priority: (1) impact strength (examples: polybutadiene/polystyrene; ethylene-propylene-diene terpolymer/polyamide); (2) heat deflection (e.g. polyphenylene oxide/polyamide

blends); (3) cost/process ability (e.g. polyethylene terephthalate/polycarbonate blends). The primary uses of polymer blends are in automotive and business machine application.

Development of new multiphase polymer blend materials is related primarily to two key variables: control of the interfacial chemistry and control of the microstructure. The ultimate objective is to be able to control interfacial chemistry and microstructure at will for a wide range of systems under melt processing conditions (Favis,1991).

In the previous study, a blend of 80 volume % polystyrene (PS) and 20 % ethylene-propylene rubber (EPR) was compatibilized by using two triblock copolymers of styrene/ ethylene-butylene/styrene (SEBS) which acted as interfacial agents. They have been expected to reduce the interfacial tension, homogenize the morphology and improve adhesion between phases. The correlation between the morphology and the resulting mechanical properties of the blends was examined by combining the emulsification curve with a fracture mechanics approach. Results obtained from the emulsification curve suggested that for the lower molecular weight interfacial agent (denoted as K2), the reduction of the particle size is more effective than for the high molecular weight copolymer, K1. This resulted in an increase of four to five-fold in the Izod impact strength at interfacial agent concentrations above the critical concentration for emulsification for blends compatibilized by the low molecular weight copolymer (K2) and a transition from brittle to ductile fracture mode occurred. The Izod and Charpy impact strengths of blends compatibilized by K1, however, showed only marginal increase, and no brittle-ductile transition was observed, all samples broke in a brittle mode with the testing condition at room temperature.

In the next sections, these results will be detailed and discussed more basing on a consideration of the interrelationship between the morphology, interface and the mechanical properties of polymer blends. This work then would be a development of these results.

1.1.2 Influence of interfacial modifiers on morphology

The objective of blending is to create novel materials with homogeneous properties. In order to obtain this, good stress transfer across the interface and stabilization of the morphology to avoid Ostwald ripening and coalescence coarsening are necessary.

An efficient way of improving the performance of immiscible polymer blends is by addition of a copolymer. The copolymer must be made from polymeric segments miscible with the two homopolymers constituting the blend. It is possible for example to modify interfacial interactions by generating copolymers *in-situ* during melt processing or by addition of polymeric or low molecular weight additives as third components in the system. The copolymer migrating toward interfaces has been known to create many positive effects on the blends. It allows a reduction of the blend's interfacial tension and particle-particle coalescence rate, both accounting for the finer dispersion usually observed after copolymer addition in a blend. Presence of the copolymer at the interface also enhances chain entanglements between the two homopolymers of the blend. This later phenomenon explains the improved phase adhesion in well-compatibilized systems [21, 23, 24].

In consideration of the qualitative effect of the compatibilization of polymers, lots of attempts in various directions have been done. The emulsification curve, which has long been known in classical emulsion, is one method of quantifying the efficacy of interfacial agents in polymer blends [25-27]. This curve relates the average particle size of the minor phase to the concentration of interfacial agent added to the system. The characteristic shape of the emulsification curve shown for the various systems displays an initial rapid drop in phase size as would be expected for a system experiencing a drop in interfacial tension. A critical concentration value of interfacial modifier (C_{crit}) is subsequently observed beyond which a

quasi-equilibrium particle size is attained. The term quasi-equilibrium is used since immiscible polymer blends are never in a state of true thermodynamic equilibrium. A quasi-equilibrium morphology can be obtained as a result of the high viscosity of the individual components of the blend. In addition, this critical concentration is believed to correspond to a point of saturation of the interface. The emulsification curve has recently been used in the group of Favis and co-workers to compare the efficacy of different interfacial agents in a blend of polystyrene and ethylene-propylene rubber [34].

In the previous study of Patrick Cigana and Basil D. Favis, as noted above, two triblock copolymers of styrene/ ethylene-butylene/styrene (SEBS) which acted as interfacial agents were utilized to compatibilize a blend of 80 volume % polystyrene (PS) and 20 % ethylene-propylene rubber (EPR). The emulsifying effect of the interfacial agents used in that study was shown in Figure 1.1. It has been suggested obviously that the lower molecular weight interfacial agent, K2, is more effective at reducing the particle size than the high molecular weight copolymer, K1. In the first case, the volume average particle size is reduced from 2.72 to around 0.55 microns, a decrease of nearly 80 %, whereas the K1 triblock copolymer only decreased it to about 1.1 microns. Moreover, the greater spread observed in the K1 data was an additional indication of its poorer emulsifying ability.

The difference in effect of these two interfacial agents on reducing the particle size thus resulted in the different fracture behaviors of the blends. This will be discussed in detail in the following section.

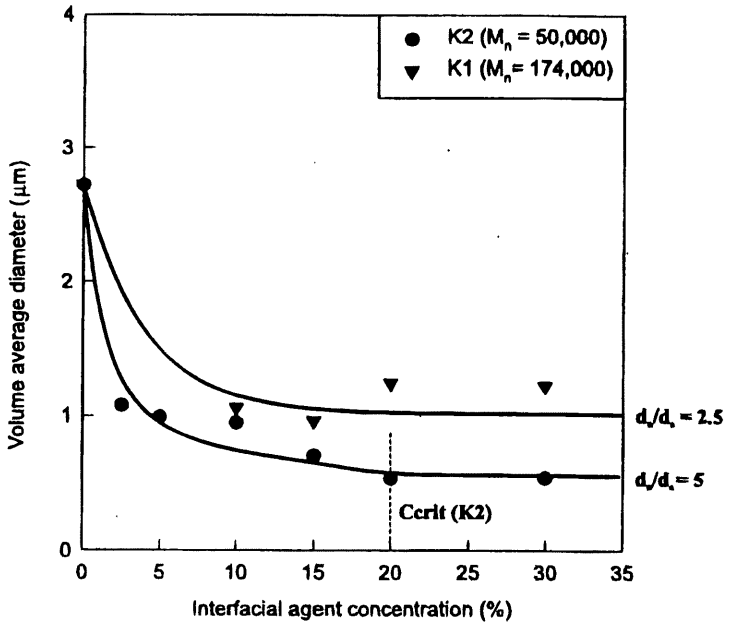

Figure 1.1: Emulsification curve for blends of 80 % polystyrene and 20 % ethylene-propylene rubber (volumetric) [1], compatibilized with Kraton 1651 (K1) and Kraton 1652 (K2). The interfacial agent concentrations are based on the volume of the minor phase.

1.1.3 Morphology- property relationship

It has been known recently that a study of the blend morphology is of central importance because it relates the properties of the blend to the manner in which it was processed. Many studies have dealt with the relationships between morphology, processing and the physical, rheological and mechanical properties of incompatible blends. Several examples of the practical application of morphological control can be found in the literature. Impact strength is one of the important mechanical properties which can be improved by blending and which is highly dependent on the size of the dispersed phase. There are several studies which discussed the impact modification of polypropylene [28, 29] and polyamide [30-33] by blending these polymers with elastomeric materials. It has been shown that the impact

strength of a blend is possibly improved by adequately controlling the size [30, 32-37] and size distribution [39-41] of the dispersed phase. This result, therefore, displays a close correlation of the C_{crit} with mechanical properties. A substantial increase in the impact strength is observed beyond the C_{crit} value. For example, in consideration of the fracture behavior of the blends compatibilized by the low weight copolymer K2 examined above, the Charpy impact strength increased significantly at interfacial agent concentrations above the critical concentration for emulsification. However, for K1, the higher molecular weight interfacial agent, the increase in impact strength was marginal and did not depend on the concentration of interfacial agent (Figure 1.2). A distinct effect was also observed, for the blends compatibilized by K2, above 15 % interfacial modifier (based on the minor phase).

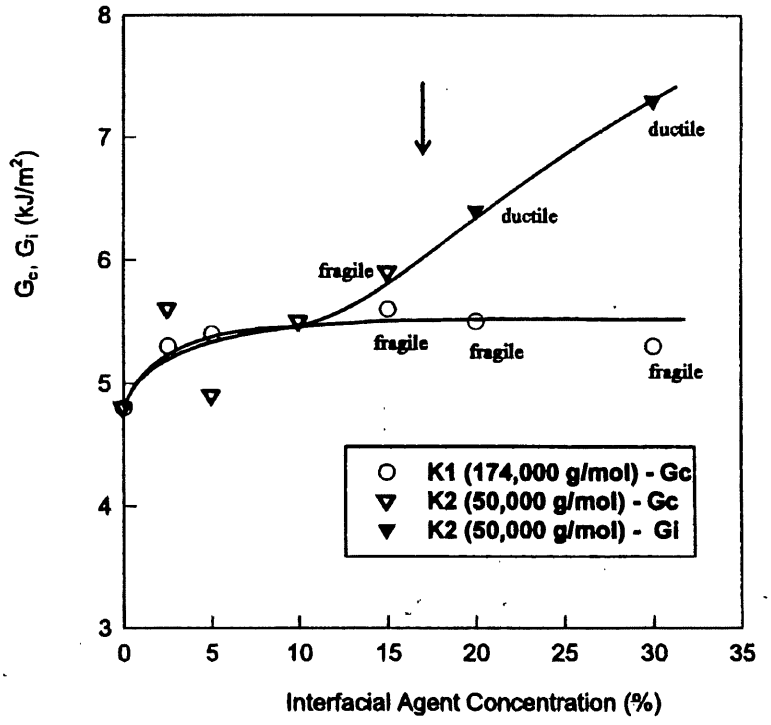

Figure 1.2: Results of the Charpy tests for blends of 80 % PS and 20 % EPR [1], compatibilized by Kraton 1651 (K1) and Kraton 1652 (K2). Values of G_c are reported for

blends with brittle fracture; values of G_i are presented for the two blends (20 % and 30 % K2) that showed stable crack propagation in ductile fracture. The arrow shows the approximate point of transition between brittle and ductile fracture mechanisms, near the critical concentration for emulsification (see Figure 1.1.)

Results suggested that a transition from brittle to ductile fracture, along with the corresponding increase in impact strength, could clearly be seen around 20 % interfacial agent. This transition seemed to occur at a concentration of interfacial modifier equal to the critical concentration for emulsification for this blend, and likely corresponded to a state of interfacial saturation. This transition, however, is not observed with the high molecular weight interfacial agent; all samples showed a brittle mode of fracture.

The different effects of K1 and K2 on the fracture performance of the blends compatibilized by these interfacial agents can be readily explained in light of the morphological analysis. The study of Favis et al. presented that since the high molecular weight interfacial agent, K1, does not effectively migrate to the interface, as shown by the emulsification curve, the interface is not saturated, adhesion is poor and the stress can not be transferred effectively from the polystyrene to the rubber phase. The interface is weak, and the samples break in a brittle way, with a low toughness. The K2, in spite of its short chains and low molecular weight (only 7,500 g/mol for each of the styrene blocks) does saturate the interface and provides an effective stress transfer across the interface, resulting in a ductile fracture mechanism once saturation has been attained (20 % interfacial agent in this case).

In the present work, with the same purpose of examining the role of the interfacial agents, K1 and K2, on the mechanical properties and fracture behavior of the blends, these two triblock copolymers (K1 and K2 with their different molecular weights: M_n (K1) = 174 000

g/mol and M_n (K2) = 50 000 g/mol) were studied again for varying the adhesion between the phases in the blend of Polystyrene/ Ethylene-Propylene Rubber (PS/EPR). In order to develop this research in a large range of different testing conditions, tensile, compression and fracture tests will be carried out over various temperatures and loading rates.

In this work, a method using the stress intensity factor was used to examine the fracture performance of the blends. This method allows us to determine the fracture resistance of the blends at crack initiation as well as during the propagation of the crack according to the $K_R(\Delta a_{eff})$ curve. The focus is put on the brittle-ductile transition in fracture and on the effects of time and temperature on the ductile fracture behavior of PS/EPR blend, modified by various concentrations of the two different interfacial agents.

Moreover, an attempt at giving a link between the yield behavior with the fracture process is done by using the Ree-Eyring's model. This model was usually used to predict the tensile and the compression yield stress of the polymer blends at various temperatures and loading rates. It has also been shown that the correlation between temperature and loading rate seems to be controlled by the molecular relaxation according to the Ree-Eyring theory. A considered relationship between the activation energy ΔH_β in the β process from the Ree-Eyring equation and the energy barrier ΔH^* of the Arrhenius form controlling the brittle-ductile transition in fracture performance of the blends, is found to give a relationship between the yield behavior with the fracture approach.

The following sections will present the major theoretical background using to resolve the issues discussed above.

1.2 Fracture characterization of polymers

1.2.1 Introduction

The materials that break in a ductile way under a simple tensile test will unfortunately be able, under certain conditions and even with weak loading, to produce a dramatic brittle fracture. The difference in these behaviors is explained by the presence of the preexistent cracks or of the defects in material and it was discovered in 1892 [44]. The basic concept is the balance between the decrease in potential energy (related to the release of stored elastic energy and work done by movement of the external loads) and the increase in surface energy resulting from the presence of the crack. This concept, developed by Griffith in 1920 [45] was thus extended to linear elastic fracture mechanics (LEFM). The main assumption of LEFM is that the material behaves like a linear elastic solid. The technique has been found to work well even for those materials where the region near the crack tip behaves inelastically but every where else shows elastic behavior. The LEFM has been applied widely to the failure of glassy polymers, e.g., [47-50] and it can clearly describe the break phenomenon properties of amorphous polymers in various cases of fracture (static, impact, cracking under a constraint of fatigue and cracks) [46].

However, LEFM is not appropriate to model the fracture behavior in viscoelastic media or where extensive plasticity is present during deformation. In practice, several polymers dissipate the absorbed energy by creating a plastic deformation at the end of the crack tip. Among these materials, one can find the ductile multiphase polymers (HIPS, ABS, the toughened nylon...) and the crystalline polymers applied in temperatures higher than their glass transition temperature like PP and PE [52]. For these cases, the LEFM has found its limitation [51] and concepts of post-yield fracture mechanics [42] and several models

proposed recently [43] can be used to characterize the crack initiation and propagation resistances of the materials.

The next sections will review some models developed recently for characterization of the fracture performance of polymers. Subsequently, the method based on the concepts of post-yield fracture mechanics using in this work will be introduced and detailed.

1.2.2 Classification of the fracture modes for polymers

The field of fracture of materials has received much attention and research effort after several catastrophic failures of major structures, usually made of high strength metallic materials. During the two decades following the second world war, a great number of investigations were carried out for catastrophic fracture, that has led to the development of fracture mechanics. Using the theories in fracture mechanics developed mainly for metals, quantitative methods have been proposed for the characterization of the fracture performance of polymers [7-9, 53, 54]. The proposed methods provide a new interpretation of the results of the common Charpy and Izod tests, but using samples containing a sharp initial crack instead in order to simulate the presence of a defect in the material. On the other hand, in the Charpy and Izod tests, only the total energy absorbed by the sample to break can be measured and it is well known that this value does not directly correspond to the fracture performance of the material [10, 13, 55]. In the recent years, characterization of the fracture resistance of the samples has been made by using the different proposed methods based on fracture mechanics, which are dependent on the type of fracture observed (brittle, semi-ductile, or ductile).

In fact, it has been pointed out that the fracture behavior of polymers is a very complex process and the fracture performance depends on both the initiation and the propagation of a defect in the material [2-6]. At various levels of loading rate and temperature, the fracture

mode and performance can be very different. Depending on the amount of plastic deformation at the crack tip and the stability of crack propagation, a given polymer can break in a brittle, semi-ductile, or ductile manner. For each type, an appropriate analysis must be used to determine the fracture resistance of the blend.

Brittle fracture usually results in the shattering phenomenon of the part. In this case, the elastic energy stored in the sample up to the point of fracture is much larger than the energy dissipated in the creation of the two fracture surfaces. The crack grows in a unstable manner. Usually, a brittle crack then jumps through the initial craze and onwards, causing rapid unloading. The excess of energy is transformed into kinetic energy and transferred to the debris so that they can fly away with a very high speed. In large structures, the kinetic energy can assist the crack to propagate rapidly without external loading and maybe leads an unexpected catastrophe. This fracture behavior is a real concern in terms of safety. A method has been proposed for this mode of fracture to determine the fracture energy at crack initiation. [7-9].

When the plastic zone at the crack tip becomes significant, the fracture has a semi-ductile character and a stable crack propagation occurs before unstable fracture. For this mode, a method using two material parameters has been proposed [10] to characterize the fracture resistance of the polymer. This method allows the determination of an average value of the fracture energy in the stable crack propagation stage and the fracture energy at instability.

The development of copolymers and polymer blends has resulted in materials exhibiting more and more ductile behavior in fracture. Ductile fracture generally occurs under a stable crack propagation, with more plastic deformation. For this mode of fracture, after initiation, the cracks can only propagate with additional supply of energy by external loads so that the character of the failure is less catastrophic. For this reason, much effort is being put on

making plastics tougher. However, toughened plastics exhibit a ductile behavior only under a certain range of temperature and loading rates. Many polymers regarded as tough under `` normal `` conditions, become brittle when the temperature is lowered or the loading rate is increased.

Three types of fracture modes in polymers can be classified according to the character of their load-extension curve, as demonstrated in Figure 1.3 below.

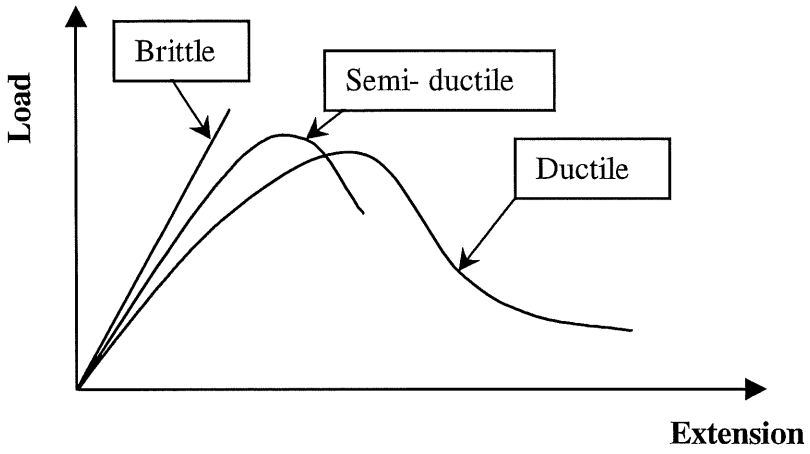

Figure 1.3: Load – Extension curves for different fracture modes of polymers

1.2.3 Brittle fracture

The characterization of brittle fracture in polymers was determined from the Turner and Williams model [9]. This method is based on the results obtained by fracture mechanics. In the energy consideration, before a crack begins to propagate, a certain amount of energy must be provided to the system. The energy balance of a cracked specimen shows that the strain energy release rate (G), which is the energy available for crack propagation, can be obtained as followed:

$$G = -\frac{1}{2} P^2 \frac{dC}{dA} \tag{1-1}$$

where P is the external force, C is the compliance of the specimen, and A is the crack surface. At the point of fracture, G reaches the critical value G_c:

$$G_c = -\frac{1}{2} P_c^2 \frac{dC}{dA} \tag{1-2}$$

P_c is the load at fracture initiation. The elastic energy stored in the sample is $U = ½ P\Delta$ where Δ is the displacement at the load application point.

In the case of brittle fracture, that is, if the fracture takes place at a constant displacement Δ, without any additional energy supplied by the external force, the energy absorbed by the specimen is equal to the strain energy U at fracture, which can be expressed by:

$$U = G_c \frac{C}{dC/dA} \tag{1-3}$$

Turner and Williams [9] expressed the term $\frac{C}{dC/dA}$ for the Charpy and Izod samples in the form:

$$U = G_c BD\Phi \tag{1-4}$$

where B is the thickness, D is the width of the sample, and Φ is a calibration factor which depends on the length of the crack and the size of the sample. The parameters Φ may be obtained numerically or determined experimentally. The values of Φ for various crack lengths and sample sizes can be obtained from tables provided in the references [8-9]. By measuring the energy absorbed after fracture in a series of samples with sharp notches of various lengths, it is possible to determine G_c from the slope of U vs. $BD\Phi$ straight line.

Brittle fracture is a completely unstable fracture phenomenon. At the point of fracture, the crack is propagated very quickly without contribution of an additional external work. The model of Turner and Williams gives satisfactory results for the measurement of the critical strain energy release rate (G_c) in brittle fracture of various materials such as PE [9,56], PMMA [8-9], PS [57] and several other materials presented in the reference [58]. Williams et al. have extended the measurement of G_c in the case of rupture where a plastic zone at the crack tip is not negligible [9,59]. By utilization of the effective crack length $a_{eff} = a_o + r_p$ the U vs. $BD\Phi$ curve shows a straight line again, except for certain conditions or for some materials, particularly for the semi-crystalline polymers [60] and the toughened polymers [61]. In these cases, the observation of the fracture surface showed that there was a mixed behavior of brittle and ductile fracture [10,60]. The method of J. G. Williams has been found to be limited to such fracture manners of these polymers and other models could be then proposed.

1.2.4 Semi-ductile fracture

Linear elastic fracture mechanics has been found not to be applicable any more to the semi - ductile materials of which the load - displacement curve is illustrated in Figure 1.3. This curve shows that after attaining the peak the load moves down a little to the break point, due to a plastic deformation. The method of correction of the plastic zone at the crack tip can not be applied correctly because its dimensions are not negligible. In this case, the U vs. $BD\Phi$ curves from the model of J. G. Williams are no longer exploitable [10,60]. The distinction between the fragile part and the ductile part in a mixed fracture, presented by the ratio of the energy of crack propagation to the total fracture energy [62], does not help to find the fracture characteristics of material.

* *Model of Vu-khanh, T. and De Charentenay, F. X. [10]*

When the polymer is more ductile, several steps of stable and unstable crack-propagation can successively occur during the fracture process of the sample. For this semi-ductile fracture mode, a method using two material parameters has been proposed to characterize the fracture resistance of polymers [10]. The method takes account of an average value of the fracture energy during the stable propagation of the crack, as well as the fracture energy at instability. In this case, the total energy absorbed by the sample to break, U, has been shown to be the sum of all the energies dissipated during the various crack propagation stages occurring in the same sample (Figure 1.4):

$$U_{total} = U_{st(1)} + U_{inst(1)} + U_{st(2)} + U_{inst(2)} + \ldots\ldots \qquad (1\text{-}5)$$

where the subscripts (1), (2) etc. refer to the first, the second step of stable or unstable crack growth etc.

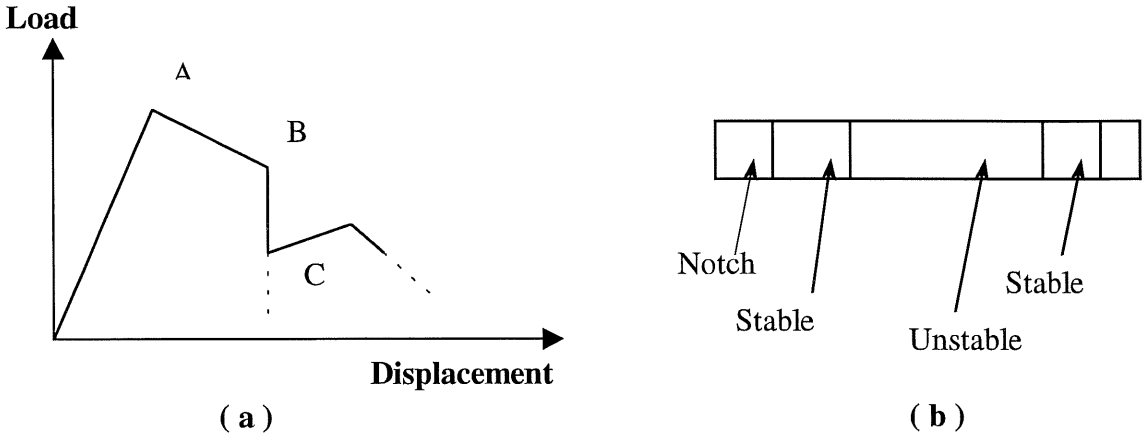

Figure 1.4: (a) theoretical load-displacement curve of a semi-ductile polymer; (b) fracture surface showing combined stable and unstable crack propagation

a/ Energy absorbed under stable propagation conditions

Assuming that the variation in G_c during stable propagation is linear, and that the mean value is G_{st}, the energy absorbed during this stage of propagation can be expressed as follows:

$$U_{st(i)} = G_{st(i)}\ A_i \tag{1-6}$$

(A_i = area of stable crack growth)

where i is the i^{th} stable propagation zone. If the G_c variation with crack growth is not linear, $G_{st(i)}$ is:

$$G_{st(i)} = \frac{1}{A_i}\int_0^{A_i} G_c(A)\,dA$$

$$= \frac{1}{a_i - a_{i-1}}\int_{a_{i-1}}^{a_i} G_c(A)\,dA \tag{1-7}$$

b/ Energy absorbed under unstable propagation conditions:

The amount of released energy produced when the crack propagates from a_1 to a_2 is given by:

$$U_{inst(1)} = BD\int_{a_1/D}^{a_2/D} G_c\ d(a/D)$$

$$= \int_{a_1/D}^{a_2/D} \frac{1}{2}\Delta^2_{(1-2)}\ \frac{1}{C^2}dC$$

$$= \frac{1}{2}\Delta^2_{(1-2)}\ \frac{1}{C(a_1/D)} - \frac{1}{2}\Delta^2_{(1-2)}\ \frac{1}{C(a_2/D)} \tag{1-8}$$

If the fracture energy at instability (G_{inst}) is assumed to be a material constant, the energy released in this stage of unstable fracture $U_{inst(1)}$ (between a_1 and a_2) can be written as a function of G_{inst}:

$$U_{inst(1)} = G_{inst}\ BD\Phi_1 - G_{inst}\ BD\Phi_1 \frac{C(a_1/D)}{C(a_2/D)} \tag{1-9}$$

where Φ_1 is the calibration factor corresponding to the crack length a_1.

c/ Proposed model for a combined mode fracture

The total energy absorbed by the sample is the sum of all the energies absorbed during the various crack propagation stages:

$$U_{tot} = G_{st(1)}\ A_1 + G_{inst}BD\Phi_1 - G_{inst}\ BD\Phi_1 \frac{C(a_1/D)}{C(a_2/D)} + G_{st(2)}\ A_2 + \ldots \tag{1-10}$$

where (1) is the first stable-unstable step.

In the impact test, if the energy lost by the hammer U is equal to the energy absorbed by the sample U_{tot} may be replaced by the measurement of U obtained on the pendulum after fracture. For a first approximation, it is possible to neglect the additional energy supplied to the sample by the hammer after the initial instability. This assumption was also verified by instrumented impact test [63] and the recorded load-displacement curve showed that the additional energy supplied by the hammer is very small in comparison with the energy stored in the sample until the first crack instability. The fracture process takes place as if there were only one stable crack propagation zone (A_1 in Figure 1.5), afterward the remaining fractures are entirely brittle. The energy balance of the combined mode fractures shown above (Equ. 1-10) can then be reduced to a simpler equation:

$$U = G_{st}\ A_1 + G_{inst}BD\Phi_1 \tag{1-11}$$

Then by plotting (U/A_1) vs. $(BD\Phi_1/A_1)$, G_{st} will be obtained by the intercept and G_{inst} will be obtained from the slope of this straight line.

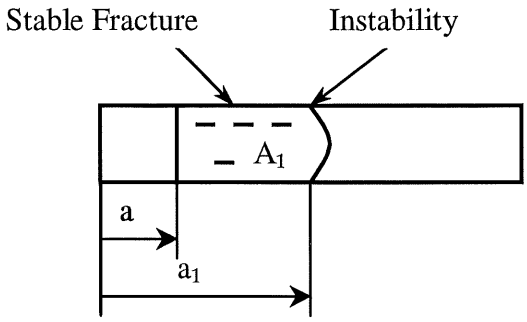

Figure 1.5: Sketch of fracture surface presenting complete brittle fracture after the stable crack propagation stage.

1.2.5 Ductile fracture

Ductile fracture is characterized by a completely stable propagation and its first quantitative approach was developed by Rice [64] using the concept of the *J*-integral with three-point bending tests at low speed. It is defined as a released energy when the crack starts to increase and is approximately equal to:

$$J_r = \frac{2U}{B(D-a)} \tag{1-12}$$

Begley and Landes suggested that its critical value (J_c) is a criterion of rupture and showed that it is a property of the material which characterizes the initiation of crack propagation in ductile materials [65]. The rate of the stability of crack propagation is expressed using the slope *dJ/da*, introduced by Paris et al. [66] with the concept of instability, which is described by a new material parameter *T*:

$$T_{mat} = \frac{E}{\sigma_{ys}^2}\frac{dJ}{da} \tag{1-13}$$

where T_{mat} is the tearing modulus of the material.

However, the criterion of the *J*-integral has limitations. For example, when it is applied in impact (very high strain rate), the practical tests are very complicated to realize. In the case

of very ductile polymers, the sample of great dimensions must be required in order to make the method practicable [65, 68]. In practice, the *J*-integral technique was used to measure the fracture toughness at crack initiation [69]. Narisawa indicated that this concept is not adapted to toughened polymers [70]. M. K. V. Chan and J. G. Williams suggested the need of another effective method for controlling the beginning of the crack propagation [67]. Y. W. Mai and Cotterell proposed a model [71] that presented the total fracture energy U_t as a sum of the energy at crack initiation U_i and the energy of crack propagation U_f in a tensile test. This method is applicable only to the polymers that break in a completely ductile manner [72, 73] and the problems may appear when there is a transition from the state of plane stress to the state of plane strain [74]. Recently, a new method for the evaluation of impact performance of ductile polymers using the common Charpy or Izod tests on sharply notched samples has been proposed by Vu-khanh.

* *Model of Vu-Khanh*

In fact, several materials which exhibit a ductile fracture behavior under impact [13, 73] showed that the curve of the absorbed energy U during the stable rupture according to the area of crack surface *A*, gives a negative intercept. This inconsistent negative intercept was also observed in the same way for those of *U* vs. $BD\Phi$ curves [13]. For this mode of fracture, it has been found that the fracture energy is not constant during the crack extension. In ductile fracture, it has been shown by J-integral measurements for many materials that the energy dissipated in the fracture process generally increases with crack propagation [75, 76]. Vu-Khanh, T. has extended the concept of the tearing modulus developed by Paris et al. [66] and has proposed a new approach taking into account the crack initiation and crack propagation

energies in the material. The approach assumes that the fracture energy of the polymer with ductile behavior varies linearly with crack extension and is given by:

$$G_r = G_i + T_a A \tag{1-14}$$

in which G_r is the actual fracture energy, G_i is the fracture energy at crack initiation, T_a represents the rate of change of G_r with crack extension and A is the fracture surface. Since the energy absorbed by the specimen is mainly dissipated in the fracture process, the energy absorbed by the specimen becomes:

$$U = \int_A G_r \, dA = G_i A + \frac{1}{2} T_a A^2 \tag{1-15}$$

From this equation one can obtain G_i by the intercept and T_a by the slope of the U/A versus A plot. Measurement performed under a low loading rate demonstrated that the fracture energy at crack initiation is in good agreement with that measured by the J-integral technique. The model also describes closely the variation of the energy absorbed by the specimen to fracture with the fracture surface. It demonstrates the cause of the abnormally high value of the fracture energy and explains the inconsistent negative intercept of the previous method.

1.3 Relation between energy rate and stress field approaches

In fact, the process of determination of each value of G_c, G_{inst} (and G_{st}) or G_i (and T_a), which correspond to the appropriate model of brittle, semi-ductile or ductile fracture behavior respectively as indicated above, requires normally a set of testing results obtained from at least 10 specimens. In the aim of reducing the number of specimens used for determining the fracture performance of the material, a method based on the tress intensity factor K is used.

Using the theories in fracture mechanics, the relation between strain energy release rate G and stress intensity factor K, has been given by [77]:

$$G = \frac{K^2}{E} \qquad \text{(plane stress)} \tag{1-16}$$

and

$$G = \frac{K^2}{E}\left(1-\upsilon^2\right) \qquad \text{(plane strain)} \tag{1-17}$$

where υ is Poisson's ratio and E is the Young modulus of the material.

The plane strain fracture toughness testing requires a small-scale yielding condition, that is, the crack length, specimen thickness and the specimen width must be much larger than the plastic zone size at the crack tip (r_p). Based on Irwin's approximation of the radius of the plane strain plastic zone size:

$$r_p = \frac{1}{6\pi}\left(K_{Ic}/\sigma_y\right)^2 \tag{1-18}$$

where K_{Ic} is the material fracture toughness and σ_y is the yield stress. The criteria of validity of K_{Ic} value recommended in the standard procedure ASTM E-399 are:

- crack length a > 2.5 $(K_{Ic}/\sigma_y)^2$ (1-19)
- specimen thickness B > > 2.5 $(K_{Ic}/\sigma_y)^2$ (1-20)

Generally, the stress intensity factor is most often found to be a practical function of stress and crack length in the form:

$$K = Y(a/D)\sigma\sqrt{a} \tag{1-21}$$

where σ is the applied stress and the function $Y(a/D)$ depends on the configuration of the cracked component and the geometric characterization of the specimen. In three-point bending test used in this work, the applied stress is determined by:

$$\sigma = \frac{3\,PS}{2\,BD^2} \tag{1-22}$$

in which P is the applied load, S is the span, B and D is respectively the thickness and the width of the sample.

Typical expressions *for Y(a/D)*, corresponding to some of the specimen configurations are given in [77]. In this work *Y(a/D)* associated with the three-point bending test can be written by :

$$Y(x) = \frac{1.99 - x(1-x)(2.15 - 3.93x + 2.7x^2)}{(1+2x)(1-x)^{3/2}} \tag{1-23}$$

in which $x = a/D$ and D is the thickness of three-point bend specimens.

From (1-21), (1-22) and (1-23) it has been fairly found that at certain stage of stress and crack length, the stress intensity factor, which represents the fracture performance of material can be completely determined. Depending on the type of fracture (brittle, semi – ductile or ductile), one can calculate the fracture resistance of the material at crack initiation as well as during the crack propagation.

1.3.1 Fracture characterization at crack initiation

In consideration of the fracture performance of the material at crack initiation, three parameters, specified by K_c , K_{inst} or K_i, which relate to three fracture modes (brittle, semi-ductile or ductile respectively) must be calculated. The fracture energy at crack initiation, G_c , G_{inst} or G_i represented for these fracture modes can be then obtained from Equ. (1-16) or Equ. (1-17).

A/ For brittle behavior:

In brittle fracture mode, the force-deflection curve shows an approximately linear increase, followed by a sharp fall in Figure 1.6. The energy absorbed by the specimen to fracture is stored elastically in the sample up to the point of fracture. In this case the crack grows in an unstable manner and a catastrophic failure can be occurred without any addition of external charge.

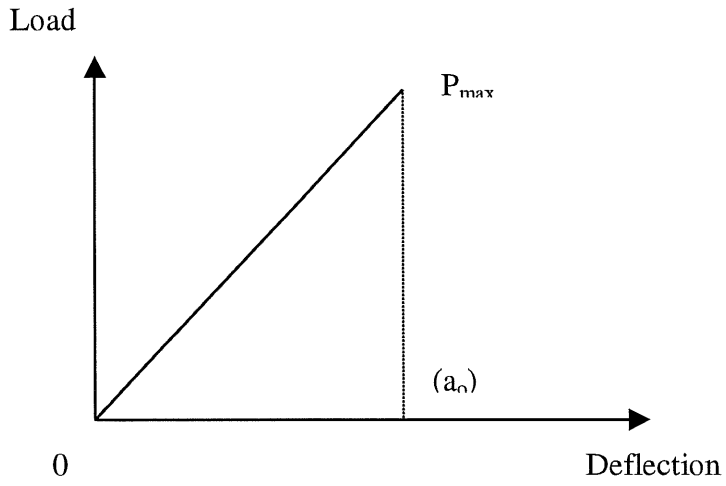

Figure 1.6: Force-Deflection curve in brittle behavior

In this case, the critical value K_c obtained at fracture can be determined from (1-21) with the form:

$$K_c = Y(a_o / D)\sigma_{\max}\sqrt{a_o} \qquad (1\text{-}24)$$

in which a_o is the initial crack length of the specimen. Therefore, it has been found that the critical value K_c of the brittle manner, with a given initial crack length a_o of the sample, depends only on the maximum force P_{max} obtained from the test.

B/ For the type of semi-ductile behavior:

In semi-ductile behavior, several steps of stable and unstable crack propagation can successively occur during the fracture process. For a first approximation, it is possible to neglect the additional energy supplied to the sample by the hammer after the first crack arrest. This assumption was also verified by instrumented impact test and the recorded load-displacement curve showed that the additional energy supplied by the hammer is indeed very small in comparison with the energy stored in the sample until the first instability of the crack. The fracture process takes place as if there were only one stable crack propagation step, afterward the remaining fracture process is entirely brittle (Figure 1.7).

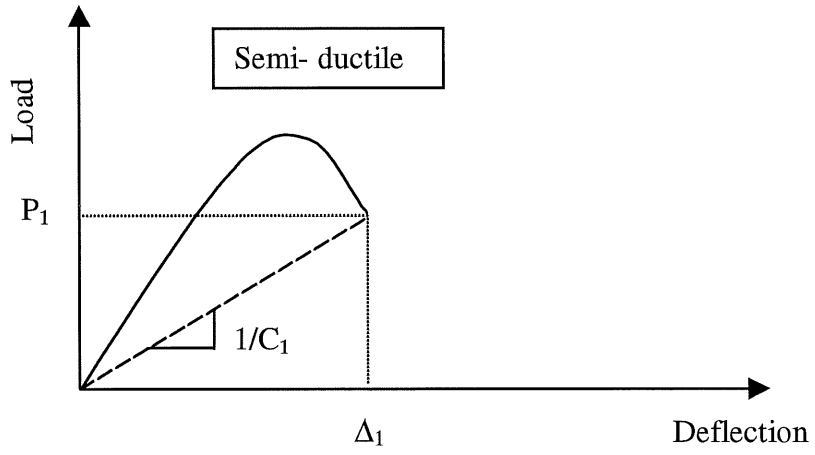

Figure 1.7: Force-Deflection curve in semi-ductile behavior

In this case, the value of K_{inst} corresponding to G_{inst}, which represents the fracture energy at instability, can be obtained by:

$$K_{inst} = Y(a_1 / D)\sigma_1\sqrt{a_1} \qquad (1\text{-}25)$$

where σ_1 and a_1 are the flexural stress and the crack length respectively at rupture. The approximation of a_1 can be obtained from calculating the compliance $C_1 = \Delta_1 / P_1$ at fracture and using afterward the *CEB (a/D)* curve, which characterized the type of three point bending test (Appendix A).

C/ For the type of ductile behavior:

In this behavior of fracture, the blend unstable fracture does not occur. The crack propagation is generally completely stable. The entire fracture surface is stress whitened, and the force-deflection curve shows a gradual decrease following the peak, indicating stable crack growth (Figure 1.8). In this case, after initiation, the cracks can only propagate with additional supply of energy by external loads so that the character of the failure is less catastrophic.

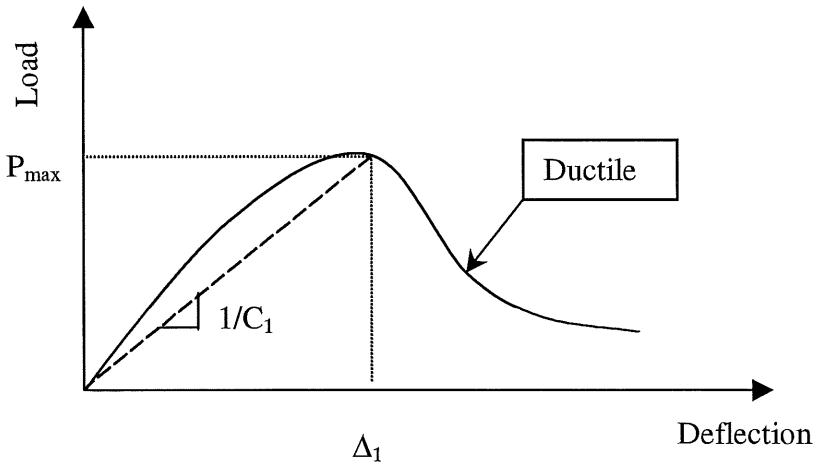

Figure 1.8: Force-Deflection curve in ductile behavior

For ductile manner, the value of K_i corresponding to G_i, which represents the fracture energy at crack initiation can be obtained with the form :

$$K_i = Y(a_1 / D)\sigma_{max}\sqrt{a_1} \qquad (1\text{-}26)$$

in which σ_{max} and a_1 in the function are the applied stress and the crack length respectively at the peak. The approximation of a_1 can be determined from calculating the compliance $C_1=\Delta_1/P_{max}$ at the peak of the force-deflection curve obtained and using afterward the *CEB(a/D)* relation which characterized the type of three point bending test (Appendix A).

1.3.2 Characterization of the material resistance during crack propagation

After the initiation, the crack growth resistance during propagation was also measured by calculating the critical stress intensity factor as a function of crack extension. This technique, called K_R-curve method [78, 79], is often used to characterize the stable crack extension resistance of thin panels when the plastic deformation ahead of the crack tip is large. It was found that the interfacial agents K1 and K2, as regarded previously, had a pronounced effect on the stable crack extension stage in PS-EPR blends considered.

The critical stress intensity factor during crack propagation is calculated using the calibration factor *f(a/D)* for three-point-bend specimens provided in [80]:

$$K_R = \frac{PS}{BD^{3/2}} f\left(\frac{a_{eff}}{D}\right) \tag{1-27}$$

where P is the load, S is the support span and a_{eff} is the effective crack length, which is the physical crack size augmented for the dimension of the plastic zone ahead of the crack tip. Considering the Equ. 1-21 and Equ. 1-22, one can note that the Equ. 1-27 above is actually a resulting formula obtained by combining these two equations. At each load level on the load-deflection diagram (Figure 1.9), the effective crack length (a_{eff}) was calculated from the instantaneous compliance, C, determined by the secant passing through the origin of the load-deflection curve as discussed previously [81] (Appendix A).

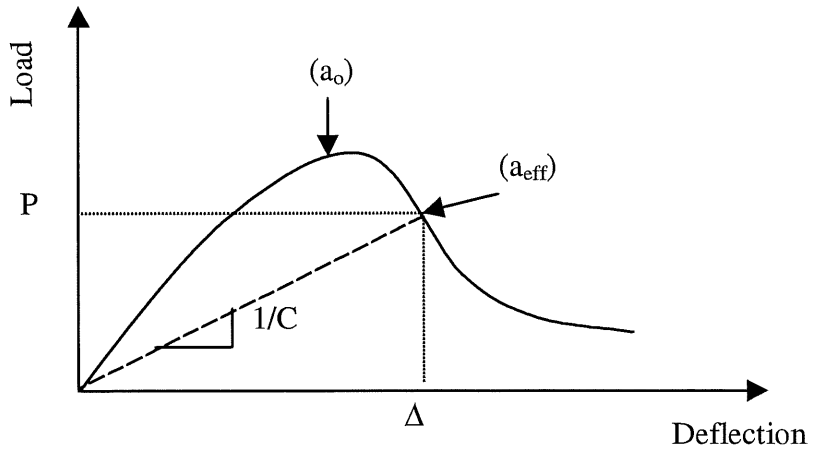

Figure 1.9: Load-Deflection diagram for obtaining a_{eff} during the crack propagation

The calculated critical stress intensity factor, which represents the crack growth resistance of the material, was then plotted as a function of effective crack growth ($a_{eff} - a_o$). It is worth noting that in order for the K analysis to be valid, the uncracked ligament of the specimen must be large to permit the plastic zone to develop. The three-point bend specimens used in this work are relatively small so that the development of the plastic zone is restricted and the measured critical stress intensity factor must be underestimated. However, even though this measurement does not represent the true crack growth resistance of the material, it can be used for the comparison purpose.

Applying the procedure discussed above for determination of fracture performance of the blend, it is well known that we can determine the appropriate fracture resistance of the material in certain test condition with only several specimens. In this work a set of 6 samples will be chosen in order to determine the mean value of stress intensity factor that can be specified by K_c , K_{inst} , K_i or K_r dependent on the type of fracture mode of each sample tested.

1.4 Brittle-ductile transition

It has been well known that the brittle-ductile transition in fracture behavior is a critical condition for the application of these materials. In almost all of polymers, like the polyamide, the polypropylene, the polystyrene... the brittle-ductile transition is observed when the experimental condition (temperature, strain rate, sample geometry, type of applied stress...) and/or the structural parameters of material (form and size of particles, glass temperature, the shear modulus...) vary. The material structure as well as the testing conditions can affect significantly the fracture mechanisms in various degrees. For a given structure, the fracture properties of a polymer (or a polymer blend) depend on the temperature and the loading speed of the test performed. Brittle fracture occurs at the high speed of deformation and/or at low temperatures. In contrast, the ductile rupture is observed in the range of high temperatures and low speeds. Between these two modes of rupture, the material exhibits a semi-ductile behavior and a stable crack propagation occurs before unstable fracture. At the low loading rates, the absorbed energy transforms into heat and can be dissipated entirely in the material. But at high speeds of deformation, transmitted heat does not have sufficient time for its total conduction. This phenomenon is called the isothermal-adiabatic transition [82]. Changes in temperature have little effect on the isothermal-adiabatic transition, but have a pronounced effect on the tough-brittle transition. Figure 1.10 shows the combined effect of the temperature and loading rate on the fracture performance. The form of each region differs from a polymer to another. The criterion of this transition from a slow and stable fracture to a high speed and unstable mode relates generally to the phenomenon of molecular relaxation [83] or to the adiabatic process at the crack tip [50, 84].

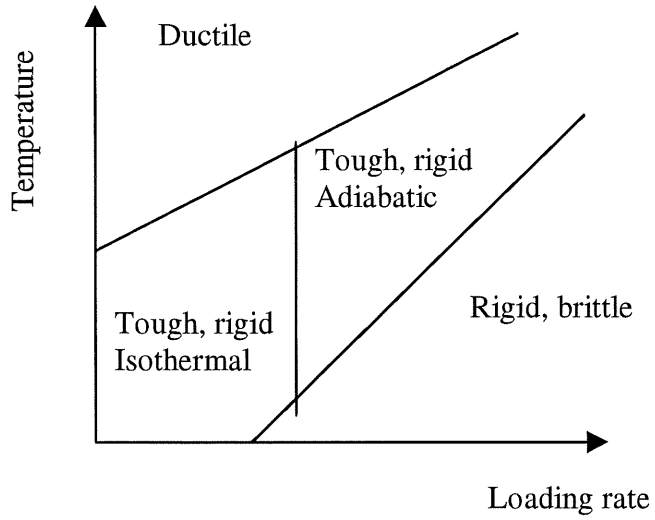

Figure 1.10: Time-temperature effect on the fracture modes.

In fact, the time-temperature dependence of fracture performance of the polymers as well as of their blends has been found to be affected by the interface and morphology. When loading rate increases, the brittle-ductile transition shifts to a higher temperature. This shift is in agreement with the superposition principle for the time-temperature dependence of the mechanical properties of polymers. The brittle behavior for temperatures below the transition implies that the molecular motions are limited. Above the transition temperature, the ductile behavior of fracture indicates that movements of certain segments or regions of macromolecules can occur, due to a thermally activated process. This suggests that the brittle-ductile transition is controlled by an energy activation process that can be expressed by the Arrhenius equation:

$$\dot{\varepsilon} = A \exp\left(\frac{-\Delta H}{RT}\right) \tag{1-28}$$

where $\dot{\varepsilon}$ is the strain rate, A is a constant, ΔH is the activation energy, R is the gas constant and T is the absolute temperature. The observed linear correlation between the brittle-ductile

temperature $T_{b\text{-}d}$ and $ln(\dot{\varepsilon})$ discussed in [14, 85] confirms that the brittle-ductile transition in fracture behavior of polymers is controlled by an energy activation process. Therefore, the Arrhenius equation can be used to predict the change in fracture behavior in order to avoid undesirable catastrophic failures in the material. From this equation, the energy barrier ΔH controlling the time-temperature dependence of fracture behavior of the material could be also deduced.

1.5 Yielding behavior

1.5.1 Introduction

The yielding behavior of polymer materials is of significant practical importance both in terms of their service performance and in manufacturing processes, such as forming, rolling and drawing. The relationship between the mechanical properties and microstructures of polymers has been studied for many years.

In tensile tests, yielding is associated with the onset of significant plastic flow and, on the molecular scale, it is associated with interchain sliding, chain separation, chain segmental motion and chain reconformation [86, 87]. Thus, the yielding process of a polymer is sensitive to changes in temperature and strain rates [88-90]. In general, such a polymer can be considered as a viscoelastic material and its yield stress increases with strain rate but decreases with temperature. Many theories and models have been proposed to describe the yielding process [91-95]. The yielding process of a polymer is usually regarded as a momentary condition of pure viscous flow because it denotes the point at which the change of stress with strain is zero for a given strain rate. It is thus considered to be a thermally activated rate process involving inter-and intramolecular motion. Eyring's viscosity theory has been used in

this case [96, 97]. Although this theory was developed for shear-induced viscous liquid flow, it has been successfully used to describe the tensile yielding process of solid polymers [98, 99]. This could be because a ductile material yields under the influence of the resolved shear stress in a tensile test. Eyring's viscosity theory has been successfully used to describe the yielding behavior of a number of polymers: for example, polymethylmethacrylate (PMMA) [100], polyethylmethacrylate (PEMA) [101], iPP [87, 102], polycarbonate [103, 104], polyvinyl chloride (PVC) [104], polyethylene (PE) [105], polyethylene terephthalate (PET) [106] and high impact polystyrene (HIPS) [107]. When this theory is used, the change in activation energy barrier height is considered to be proportional to the yield stress. Frequently, two thermally activated rate processes, named process I (α process) and process II (β process), have been required to adequately describe the yielding of a polymer over a wide range of temperatures and strain rates [100-106]. Roetling proposed that process II is associated with "main chain motion" and process I is a "side chain motion", that is, the movement of the side group relative to the main chain [100]. However, it is largely still unknown which microstructural features are associated with these two processes.

1.5.2 Ree-Eyring' s model of the flow of solids

The flow model of Eyring [96, 97] is to correlate the effects of temperature and strain rate on flow stress, and it seeks to do this from a molecular model of the flow mechanism. It has been well known that an atom or a molecule, and, for a polymer, a segment of a macromolecule, must pass over an energy barrier in moving from one position to another in the solid. In the absence of stress the segments of the polymer jump over the barrier very

infrequently and they do so in random directions. The rate of jump can be deduced from the Arrhenius equation:

$$\omega = \omega_o \exp\left(\frac{-\Delta H}{RT}\right) \tag{1-29}$$

where ω_o is the pre-exponential factor, ΔH is the activation energy, the enthalpy required to take a mole of segments from the potential well to the top of the barrier, R is the gas constant and T is the absolute temperature.

The significant point introduced by Eyring is that the application of a shear stress, σ_s, modifies the barrier height so that, in the direction of the stress, the rate of segment jumping, formerly so slow, now becomes fast enough to give rise to a measurable strain change. When a constant force is exerted on the system, the energy barrier is inclined such that the activation energy for atoms to jump over the barrier is changed. The change in the activation energy is assumed to be proportional to the load acting on the system [96, 97]. This is the basic assumption of the Eyring theory for rate processes. In the application of a shear stress, σ_s, and assuming that the strain rate, $\dot{\varepsilon}$, is proportional to the net flux rate of atoms jumping over the barrier, one can obtain the following equation:

$$\dot{\varepsilon} = \dot{\varepsilon}_o \exp\left(\frac{-\Delta H}{RT}\right)\sinh\left(\frac{\sigma_s V^*}{RT}\right) \tag{1-30}$$

where $\dot{\varepsilon}_0$ is the pre-exponential factor and V^* is known as the activation volume.

Noting that the dominant shear stress in a tensile test is the maximum shear stress, and at yield point this is $\sigma_s = \sigma_y/2$, equation (1-30) becomes

$$\dot{\varepsilon} = \dot{\varepsilon}_0 \exp\left(\frac{-\Delta H}{RT}\right)\sinh\left(\frac{\sigma_y V^*}{2RT}\right) \tag{1-31}$$

In the analysis of measurement of σ_y at varying strain rate, it is preferable to rearrange equation (1-31) by the form:

$$\frac{\sigma_y}{T} = \frac{2R}{V^*}\sinh^{-1}\left[\frac{\dot{\varepsilon}}{\dot{\varepsilon}_o}\exp\left(\frac{\Delta H}{RT}\right)\right] \tag{1-32}$$

In the range of high temperatures and low strain rates (α process), the sinh term can be simplified to an exponential by the approximation:

$$\sinh X \approx \frac{1}{2}\exp X\,. \tag{1-33}$$

therefore equation (1-32) becomes:

$$\frac{\sigma_{t_\alpha}}{T} = \frac{2R}{V^*_{t_\alpha}}\left[\frac{\Delta H_\alpha}{RT} + 2.303\log\left(\frac{2\dot{\varepsilon}}{\dot{\varepsilon}_{o_\alpha}}\right)\right] \tag{1-34}$$

in which the indices t and α refer to the tensile test and the α process, respectively.

In the same manner, we can establish the expression of the yield stress in compression related to the α process:

$$\frac{|\sigma_{c_\alpha}|}{T} = \frac{2R}{V^*_{c_\alpha}}\left[\frac{\Delta H_\alpha}{RT} + 2.303\log\left(\frac{2\dot{\varepsilon}}{\dot{\varepsilon}_{o_\alpha}}\right)\right] \tag{1-35}$$

It has been showed by Bauwens-Crowet et al. that Equ. (1-34) gave a satisfactory fit to the tensile results of polycarbonate [12]. Plots of σ_y / T against $\log \dot{\varepsilon}_y$ for polycarbonate in a large range of temperature have been showed. The experimental measurement has also confirmed the validity of the Eyring model with a set of parallel straight lines having the same

slope proportional to $1/V^*$. The activation energy ΔH of the yield process can be calculated from the horizontal distances between the straight lines. This energy has been theoretically considered to equal the activation energy related to the formation of free volume.

For various polymers, measurements of yield stress over a wide range of temperatures and strain rates by Bauwens [108-110], Roetling [100-102] and others [111] showed a nonlinear dependence on log strain rate. In order to adequately describe the yielding process over a large range of testing conditions, Equ. (1-34) was modified by Ree and Eyring [98] to allow multiple processes to be involved. The behavior could, however, be very well represented by considering that there are two Eyring processes acting in parallel so that $\sigma_y = \sigma_1 + \sigma_2$, where σ_1 and σ_2 are the stresses associated with process I and process II, respectively. Thus we obtain the expression of the resultant yield stress in tensile and in uniaxial compression tests:

$$\frac{\sigma_t}{T} = \frac{\sigma_{t_\alpha}}{T} + \frac{\sigma_{t_\beta}}{T} = \frac{2R}{V^*_{t_\alpha}}\left[\frac{\Delta H_\alpha}{RT} + 2.303\log\left(\frac{2\dot{\varepsilon}}{\dot{\varepsilon}_{o_\alpha}}\right)\right] + \frac{2R}{V^*_{t_\beta}}\sinh^{-1}\left[\frac{\dot{\varepsilon}}{\dot{\varepsilon}_{o_\beta}}\exp\left(\frac{\Delta H_\beta}{RT}\right)\right] \qquad (1\text{-}36)$$

$$\frac{|\sigma_t|}{T} = \frac{|\sigma_{c_\alpha}|}{T} + \frac{|\sigma_{c_\beta}|}{T} = \frac{2R}{V^*_{c_\alpha}}\left[\frac{\Delta H_\alpha}{RT} + 2.303\log\left(\frac{2\dot{\varepsilon}}{\dot{\varepsilon}_{o_\alpha}}\right)\right] + \frac{2R}{V^*_{c_\beta}}\sinh^{-1}\left[\frac{\dot{\varepsilon}}{\dot{\varepsilon}_{o_\beta}}\exp\left(\frac{\Delta H_\beta}{RT}\right)\right] \qquad (1\text{-}37)$$

where $V^*_{t_\beta}$, $V^*_{c_\beta}$, ΔH_β and $\dot{\varepsilon}_{o_\beta}$ have the same meaning as in (1-34) and (1-35) but are related to β process (process II). Equations (1-36) and (1-37) have been shown to agree well with experimental data for a number of polymers [108-111]. According to these two equations the diagram of σ_y/T versus logarithm strain rate can be divided into two regions: region α where process I dominated and region β where process II is activated. Between region α and region β, the curve of σ_y/T as a function of logarithm strain rate should show a noticeable change in

slope. This change can be used to find the transition boundary between these two regions by standard mathematics. When yielding in region α (i.e., when the strain rate is low and the temperature is high), the slope is approximately $\frac{4.606\,R}{V_\alpha^*}$, whereas in region β (i.e., when the strain rate is high and the temperature is low), the approximate slope is $4.606\,R\left(\frac{1}{V_\alpha^*}+\frac{1}{V_\beta^*}\right)$. For a given temperature, the transition between the two regions is defined as a critical strain rate $\dot{\varepsilon}_\beta$, at which the slope of σ_y/T equals the average of the above two approximate slopes. It can be found that the critical strain rate is:

$$\dot{\varepsilon}_\beta = \frac{\dot{\varepsilon}_{o_\beta}}{2}\exp\left(-\frac{\Delta H_\beta}{RT}\right) \tag{1-38}$$

The values of the parameters ($V_\alpha^*, \Delta H_\alpha, \dot{\varepsilon}_{0_\alpha}, V_\beta^*, \Delta H_\beta, \dot{\varepsilon}_{0_\beta}$) characterized the yielding process of a polymer (or a polymer blend) could be estimated from the diagram of σ_y/T versus logarithm strain rate due to a procedure that is presented in Appendix B.

CHAPTER 2

EXPERIMENTAL

2.1 Materials

The system investigated consists of a matrix of polystyrene (PS), supplied by Dow Chemical (Styron D685), and a minor phase of ethylene-propylene rubber (EPR), a random copolymer containing 54% ethylene, supplied by Exxon Chemical (Vistalon V-504). The interfacial agents were supplied by Shell: they consist of two styrene/ ethylene- butylene/ styrene (SEBS) triblock copolymers (Kraton 1651 and 1652, referred to as K1 and K2, respectively), containing 29% styrene. The number average molecular weights of K1 and K2 are 174,000 and 50,000 g/mol, respectively. They are essentially monodisperse. The ethylene-butylene block contains about 35 to 40% polybutylene; the high polybutylene content inhibits the crystallization of the copolymer. Some properties of these materials are listed in Table 2.1

Table 2.1: Properties of materials

Material	Commercial name	Mn (g/mol)	Mw (g/mol)	Density (g/ml)	Tg (°C)
PS	Styron D685	125,000	275,400	1.05	108
EPR	Vistalon V-504	69,000	173,000	0.85	-38
K1	Kraton 1651	174,000	-	0.91	-
K2	Kraton 1652	50,000	-	0.91	-

2.2 Sample preparation and identification

The PS matrix and EPR minor phase were blended in volumetric proportion of 80: 20. The matrix, minor phase and interfacial agent were blended using a Leistritz AG twin-screw extruder, model 30.34 (L/D = 28) operating at 100 RPM. The temperature of the screws and the die was maintained at 200°C. The extrudate was then quenched in cold water and granulated. Blends were prepared with interfacial agent concentrations of 0, 2.5, 5, 10, 15, 20 and 30% based on the minor phase. Thus, the sample denoted as K1-10 has the following composition: 80 parts PS, 20 parts EPR, and 2 parts (10% EPR content) Kraton 1651. Likewise K2-20 has a composition of 80 parts PS, 20 parts EPR, and 4 parts (20% of EPR content) Kraton 1652. About 0.1% weight of Irganox 1010 antioxidant (Ciba-Geigy) was also added to the blends.

The granules were then molded into 6mm thick plates using a Battenfeld 80-ton injection molding machine, equipped with a Unilog 8000 interface. Injection molding conditions are given in Table 2.2.

Table 2.2: Injection molding conditions

Temperature profile (°C)	240/230/210/180
Mold temperature (°C)	60
Injection pressure (bar)	145
Injection speed (mm/s)	70 (20)
Screw speed (rpm)	40 (35)
Holding time (s)	10 (20)
Holding pressure (bar)	50 (100)
Back pressure (bar)	1
Metering stroke (mm^{-1})	75 (45.5)
Cooling time (s)	20 (60)

2.3 Testing procedure

2.3.1 Tensile tests

The tensile test specimens were prepared according to ASTM - D638M, the test method for tensile properties of plastics. The sample dimensions were demonstrated in Figure 2.1. Traction tests were performed at five loading rate levels of 1 mm/min, 10 mm/min, 50 mm/min, 100 mm/min and 200 mm/min on an Instron Automatic Material Testing System, Model 4206. These tests were also carried out at a large range of temperatures from 25°C to 70°C using a temperature chamber. The temperature was measured with a thermometer placed near the specimen in the chamber; the tests were made after the specimen had remained for 1h at the required temperature.

The different test conditions presented above were applied for four various blends of K1 (K1-5, K1-15, K1-20 and K1-30) and five blends of K2 (K2-2.5, K2-5, K2-10, K2-15 and K2-30) in order to examine the effect of strain rate and temperature on mechanical properties of these materials.

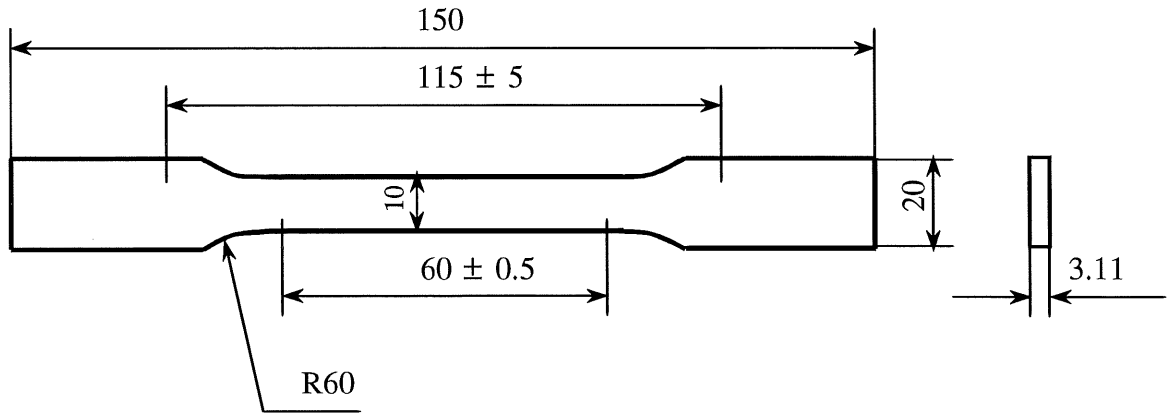

Figure 2.1: Dimensions of tensile specimens according to ASTM- D638M

The yield stress σ_t in tensile tests was calculated from the load L at the first load maximum on the load extension curve. The cross-sectional area at the yield point is calculated from the strain ε_t at the yield assuming that the specimens deformed homogeneously at constant volume up to this point. Thus:

$$\sigma_t = (L / A_o) (1 + \varepsilon_t) \qquad (2\text{-}1)$$

where A_o is the original cross-sectional area. The nominal strain rate was calculated from the initial gauge length and the crosshead speed of the Instron.

2.3.2 Compression tests

The compression yield behavior of PS/EPR/IA blends has been investigated, over a wide range of experimental condition that cannot be reached in tensile tests due to the brittle nature of the blends.

The compression test pieces were of 7 x 6 mm cross-section and they were parallel-sided with a length of 10 mm. Compression tests were performed between carefully polished and lubricated steel plates. The higher plate was connected with the tensile load cell of the Instron testing machine and the whole compression system was placed inside the temperature chamber which allowed us to regulate the temperature to – 80 °C. In consideration of the influence of temperature and loading rate, the compression tests were also performed over four decades of strain rates and at temperatures in the range of (-75 °C to 100 °C). These uniaxial compression tests have been applied for 3 blends of K1 (K1-2.5, K1-10 and K1-20).

The yield stress σ_c in compression tests was calculated also from the load *L* at the first load maximum on the load extension curve. However, with assuming that the specimens

deformed homogeneously at constant volume up to the yield point, the cross-sectional area at the yield point was calculated by:

$$A_c = A_o / (1 - \varepsilon_c) \tag{2-2}$$

where A_o is the original cross-sectional area and ε_c is the strain at the yield. Thus:

$$|\sigma_c| = (L / A_o)(1 - \varepsilon_c) \tag{2-3}$$

2.3.3 Three point bending tests on the Instron machine

Three point bending tests were performed on an Instron Automated Material Testing System, Model 4206. The samples were cut out of 6 mm thick plates to a length and width of 50 mm and 10 mm respectively using a ribbon saw (ASTM – D790M). The shape and dimensions of the specimens were demonstrated in Figure 2.2. The initial crack created in the specimen had a length varying between 10% and 80% of specimen width. A pre-notch was first made with a bend saw and the final cut was done by forcing a razor blade into the specimen with a vise. The tests were carried out at various temperatures using a temperature chamber.

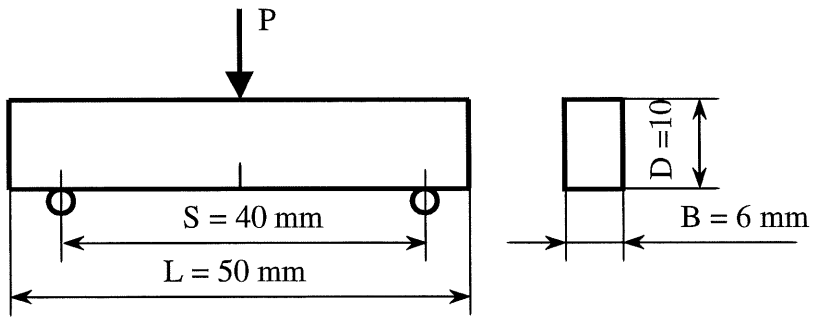

Figure 2.2: Shape and dimensions of the three point bending and Charpy specimens

In this work, the three point bending tests were carried out to examine the effect of the interfacial agents (K1 and K2) on the brittle-ductile transition in fracture behavior. For this purpose, three various blends of K1 (K1-2.5, K1-10 and K1-20) and three blends of K2 (K2-2.5, K2-15 and K2-20) were used. In consideration of the influence of loading rate, these tests were performed at four loading rate levels of 1 mm/min, 10 mm/min, 100 mm/min and 200 mm/min and over a large range of temperatures in which the blends change their fracture behavior from brittle to ductile.

Another examination, as noted previously in the introduction part, was to put the focus on the ductile fracture behavior of the blends considered. For this purpose, the three point bending tests were once again carried out for five various blends of K1 (K1-2.5, K1-5, K1-15, K1-20 and K1-30) as well as two blends of K2 (K2-20 and K2-30) at the loading speed of 100 mm/min and in a temperature range above the room temperature. By a calculating procedure, as introduced in the previous section, the fracture resistance of each blend, not only at the initiation of crack but also during the crack propagation, could be determined and analyzed. This result was also an important aspect to consider and compare the contribution of the two interfacial agents K1 and K2 on fracture performance of the PS/EPR/AI blends.

2.3.4 Impact tests (Charpy tests)

The impact test specimens of 6mm x 10mm x 50 mm (Figure 2.2) were cut out from the molded 6 mm thick plates. A sharp notch was also created in the specimens to analyze the fracture performance in terms of crack growth resistance. A pre-notch was first made by a saw cut and the final notch in the specimen was created by forcing a razor blade into the specimen in a special jig. The notch depth was varied from 10% to 80% of the specimen width.

Three point bending impact tests (Charpy tests) were done on a Monsanto Plastic Impact Machine, which was shown in Figure 2.3.

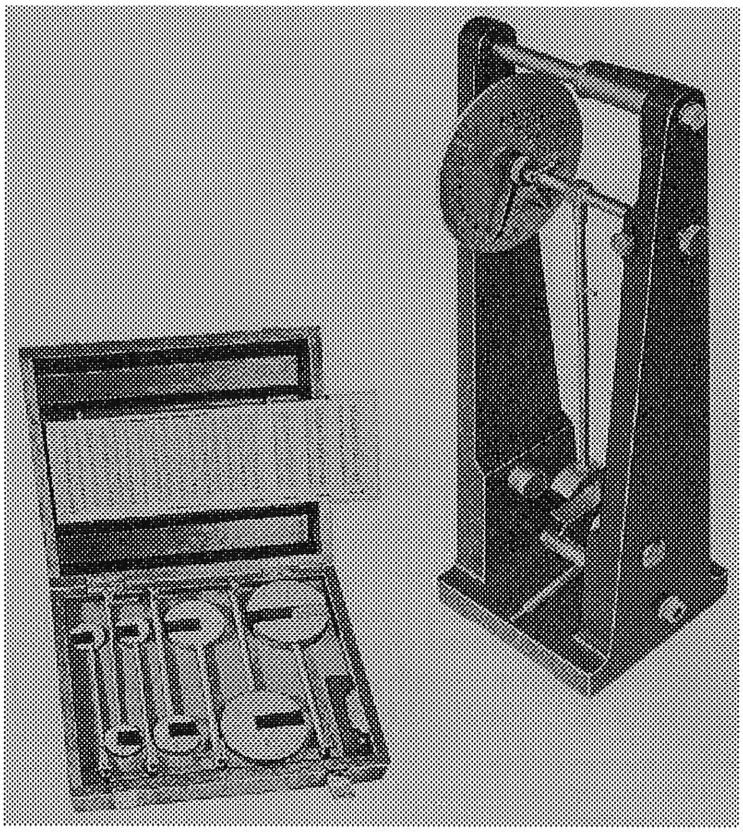

Figure 2.3: Monsanto Plastic Impact Machine

The calculated hammer speed at the beginning of the impact was 2.5 m/s. The testing temperature was varied between –10 °C and 90 °C using a temperature chamber. The striker of the impact machine was instrumented with the load captor and the load-time signal during impact was recorded by a DATA-6000 acquisition system, as shown in Figure 2.4. To reduce

the bouncing effect of the sample on the striker in impact, a small amount of plasticine was placed on the striker.

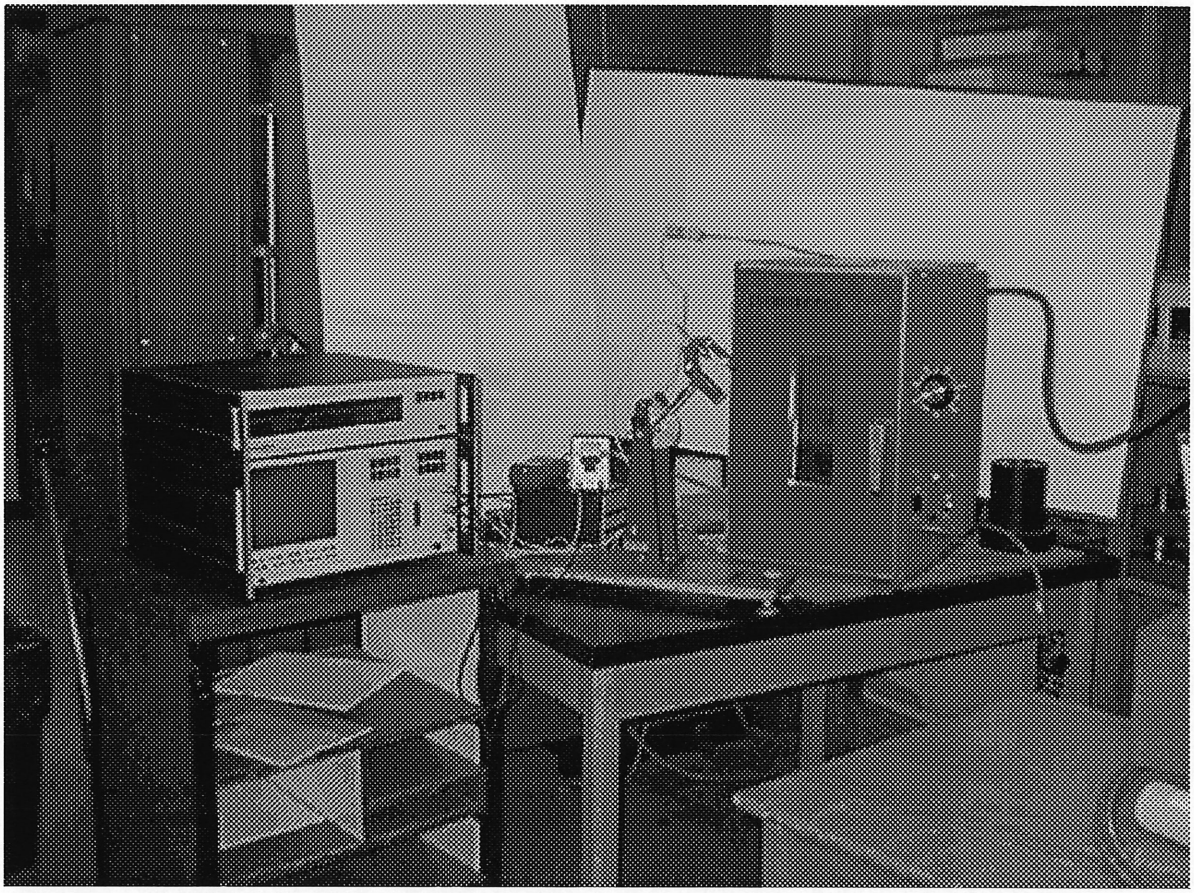

Figure 2.4: Impact machine with the DATA-6000 acquisition system

CHAPTER 3 :

RESULTS AND DISCUSSIONS

3.1 Introduction

In this chapter, the results obtained from the experimental data and their analysis based on the application of the theoretical models introduced in Chapter 1 (Theoretical background) will be presented. All experimental results, as shown by the data curves for the observed blends are demonstrated in Appendices.

The first section in this chapter shows the results obtained from the fracture tests including three-point bending tests preformed on the Instron machine and the Charpy impact tests. The focus is put on the brittle-ductile transition in fracture of the PS/EPR/SEBS blends as well as the ductile fracture resistance of these materials. The effect of two triblock copolymers K1 and K2, acting as the interfacial agents, on fracture performance of the blends will be considered and compared together.

In the second and the third sections, the results obtained from the tensile and compression tests will be shown. The Ree-Eyring model is used to study and predict the yielding behavior of the blends for both tensile and compression data. An analysis of the Ree-Eyring constants characterizing the blends in α and β yielding processes is carried out to verify the validity of the Ree-Eyring theory for tensile and compression tests. Link between the yielding behavior and fracture field will be attempted to establish.

3.2 Results obtained from fracture tests

The fracture behavior of a blend of 80 volume % polystyrene (PS) and 20% ethylene-propylene rubber (EPR), modified by two triblock copolymers of styrene/ ethylene- butylene/ styrene (SEBS), of different molecular weights has been studied recently. Favis et al. [1], by

examining the emulsification curve, suggested obviously that the lower molecular weight interfacial agent, K2, is more effective at reducing the particle size than the high molecular weight copolymer, K1. The Impact tests performed subsequently showed that for the blends modified with K2, a transition in fracture mechanisms, from brittle to ductile, occurs around 20% interfacial agent (based on the volume of the minor phase). This transition, however, is not observed with the high molecular weight interfacial agent (K1). Odje, S., in his thesis [112], presented the same significant effects of the interfacial agents, K1 and K2, on the impact fracture behavior of the PS/EPR blends. Compatibilizing the PS/EPR blends by these copolymers, acted as the coupling agents, resulted in an improvement of the impact fracture resistance of the blends. This result can be reviewed briefly in Figure 3.1 below.

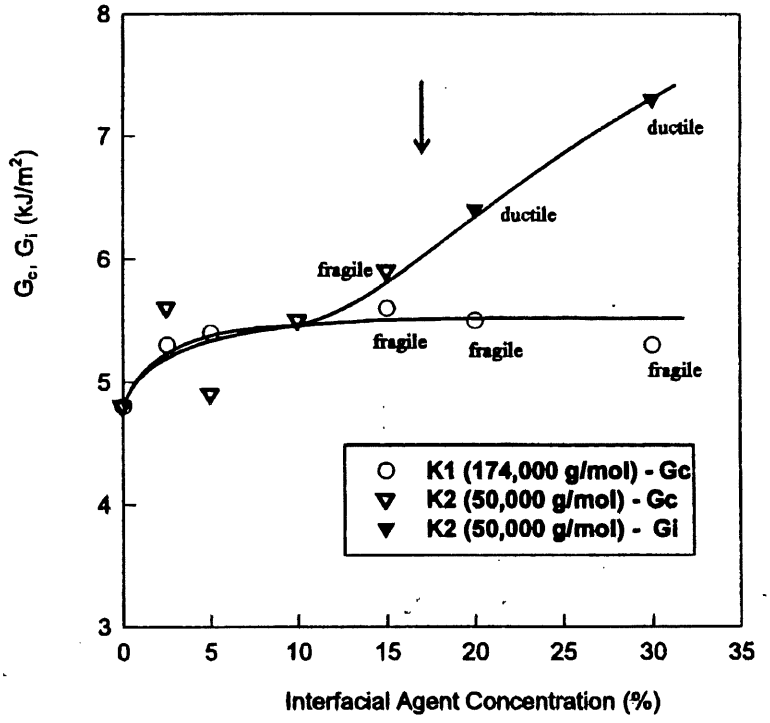

Figure 3.1: Results of the Charpy tests for blends of 80 % PS and 20 % EPR, compatibilized by K1 and K2 [1]. Values of G_c are reported for blends with brittle fracture;

values of G_i are presented for the two blends (20 % and 30 % K2) that showed stable crack propagation in ductile fracture. The arrow shows the approximate point of transition between brittle and ductile fracture mechanisms, near the critical concentration for emulsification.

In the following section, with the same purpose of examining the role of the interfacial agents, K1 and K2, on the mechanical properties and fracture behavior of the blends, a method using the stress intensity factor was used to examine the fracture performance of the blends. This method allows us to determine the fracture resistance of the blends at crack initiation as well as during the propagation of the crack according to the $K_R(\Delta a_{eff})$ curve (See section 1.3 in Chapter 1: "Theoretical background"). The focus is put on the brittle-ductile transition in fracture and on the ductile fracture characterization of PS/EPR blend, modified by various concentrations of these two different interfacial agents. The influence of time and temperature is considered by performing the tests in a different range of loading rate and temperature. The results obtained from the method using the stress intensity factor in this work will be compared later with the three fracture models, which have been proposed and used recently by Vu-Khanh, T. [43].

3.2.1 Brittle-ductile transition- Arrhenius equation

In this study, the tests were performed on six different blends: three of K1 (K1-2.5, K1-10, and K1-20) and three of K2 (K2-2.5, K2-15 and K2-20). In consideration of the influence of loading rate, these tests were performed at five loading rate levels of 1 mm/min, 10 mm/min, 100 mm/min, 200 mm/min, 2.5 m/s (Charpy impact test) and over a large range of temperatures in which the blends change their fracture behavior from brittle to ductile. Depending on the loading rate and temperature, the fracture mode and performance can be

very different. For instant, a given polymer can break in a brittle, semi-ductile or ductile manner. Figures 3.2 to 3.4 show examples of three different fracture behaviors observed in the K2-15 samples under the loading rate of 100mm/min. at various temperatures. Brittle fracture occurs at low temperature, up to about -75°C and ductile fracture takes place at higher temperature, from about -65°C. Between these temperatures, semi-ductile fracture is observed. At low temperature, below -75°C of the blend, there is little or no toughening, and fracture is quite brittle; the force-deflection curve shows an approximately linear increase, followed by a sharp fall (Figure 3.2). As the temperature is raised, a yield zone of increasing length forms near the tip of the notch, and toughness therefore increased steadily. This yield zone is usually stress whited, owing to crazing or cavitation; the remainder of the fracture surface is rough and broken. Yielding at the notch tip is reflected in non-linearity in the force-deflection curve, which is again followed by a sharp drop. This phenomenon is also known under the name `` semi-ductile `` behavior of the material (Figure 3.3). In this case the reported value corresponds to the fracture energy at instablility, K_{inst}. A further increase in test temperature causes a third transition in fracture behavior. The entire fracture surface is stress whitened, and the force-deflection curve shows a gradual decrease following the peak, indicating stable crack growth (Figure 3.4). It is clear that significant amount of energy are absorbed both before and after the initiation of a crack. Some workers regard this as true tough behavior. In the same way, all other samples can exhibit the brittle, semi-ductile or ductile behavior of fracture, depending on the temperature and loading speed of the test.

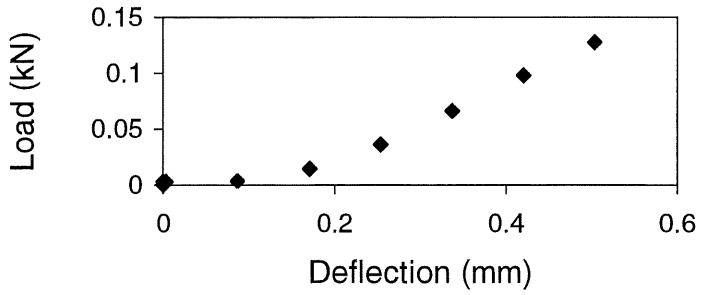

Figure 3.2 : Load-deflection curve for K2-15 blend at T= -75 °C and V = 100 mm/min.

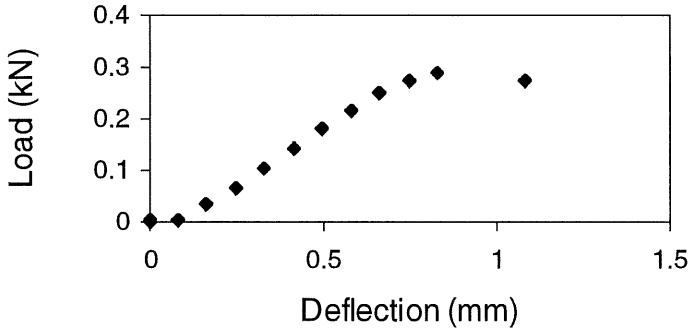

Figure 3.3 : Load-deflection curve for K2-15 blend at T= -60 °C and V = 100 mm/min.

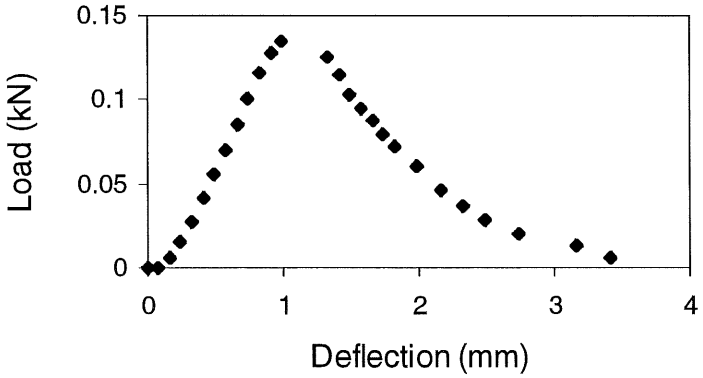

Figure 3.4 : Load-deflection curve for K2-15 blend at T= -40 °C and V = 100 mm/min.

The brittle-ductile transition for all compositions was given in Table 3.1. Adding an interfacial agent results in a lower temperature at brittle-ductile transition. In the range of interfacial agents from 2.5 % to 20 %, the more elastomer content should conduct the lower of brittle-ductile transition temperature. This effect can be observed for both two types of interfacial agent as represented also in Table 3.1.

Table 3.1: Temperatures (°C) at brittle–ductile transition for various blends :

	K1-2.5	K1-10	K1-20	K2-2.5	K2-15	K2-20
V=100 mm/min	-25 ± 5	-35 ± 5	-40 ± 5	-60 ± 10	-70 ± 5	
Impact	60 ± 10	55 ± 5	40 ± 10	30 ± 10	25 ± 10	0 ± 5

It is worth noting that one can not base only on the single values of fracture energy to determine the impact performance of the material but the type of crack propagation should also be considered. With the same value of K_c, K_{inst} or K_i, the material exhibiting a stable crack propagation performs better in terms of fracture resistance since after initiation, fracture can only continue with further supply of energy by external load. Whereas in the case of brittle fracture, the crack accelerates without any additional supply of energy from the external forces. The character of crack propagation is therefore also important in determining fracture performance.

From the relations $K= f(T)$, presented from Figure C.1 to figure C.11 in Appendix C, it can be seen that with all compositions the fracture performance of the modified blends in the temperature range studied is higher than that of the non-compatibilizied blend (NC). In these figures, the values of the strain energy release rates G_c, G_{inst}, and G_i corresponding to three fracture modes of the blend were determined from K_c, K_{inst}, and K_i according to Equa. (1-17) in Chapter 1. Over the temperature range studied and with loading rate of 100mm/min. the

fracture resistance of all compositions for both two types of K1 and K2 increases with the increase in temperature. This increase is most significant within the zone of transition temperature, that is represented by a steep slope of the curve *K(T)*. Figure 3.5, for example, shows this pronounced increase in fracture resistance as the fracture manner changes from brittle to ductile for K1-20 blends.

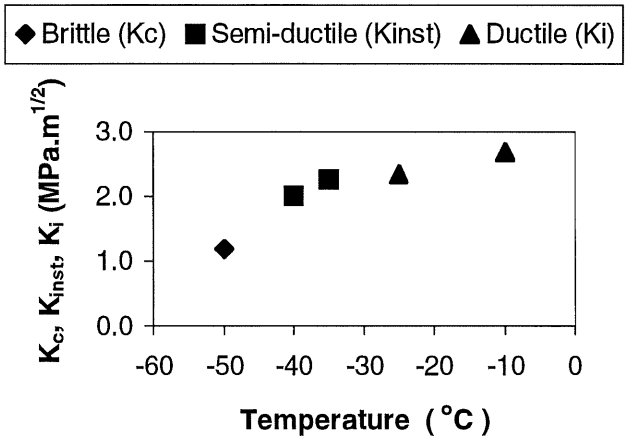

Figure 3.5: Variation of the stress intensity factor, K, as a function of temperature at V=100 mm/min for K1-20 blend.

With a blend having more content of interfacial agent, a steeper slope of the curve *K(T)* within the transition region can be found as showed from Figure C.1 to Figure C.5 (Appendix C). Moreover, for all compositions considered in the region of the transition where semi-ductile behavior must be observed, an increase in elastomer content gave an increase in K_{inst} of material for loading rate of 100mm/min., as showed in Table 3.2.

Table 3.2: Fracture resistance (K_{inst} (MPa.$\sqrt{m}$)) of blends in the region of brittle-ductile transition for tests at loading rate of 100mm/min.

Blends	K1-2.5	K1-10	K1-20	K2-2.5	K2-15
K_{inst}	1.8	1.93	2.26	2.32	3.03

However, this influence is not fairly observed under impact tests. For these samples considered under impact tests (at the loading speed of 2.5 m/s), the values of stress intensity factor did not increase gradually with the increase in temperature. As the temperature increases, a semi-ductile behavior is generally observed at the region of the peak, before the onset of ductile fracture (Figure 3.6). The same observation can be showed for all blends studied from Figure C.6 to C.11 in Appendix C. These figures also demonstrate that at the room temperature, all the samples fracture in an unstable manner except those containing 15% and 20% of the K2 interfacial agent. The result confirms again experimental data of the impact test obtained from the recent works of Favis, B. D. as well as those of Odie, S. in his thesis.

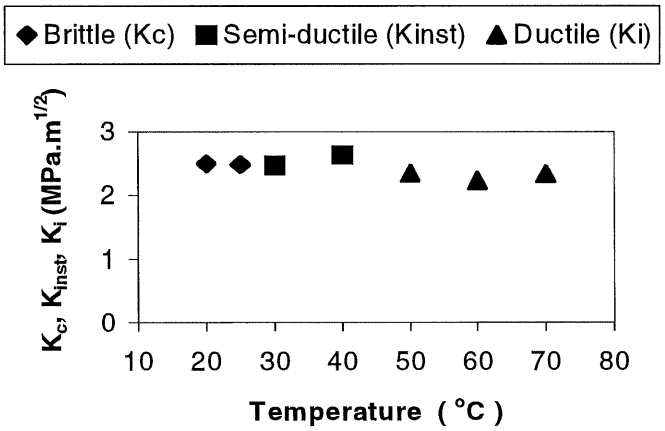

Figure 3.6: Variation of the stress intensity factor, K, as a function of temperature at V=2.5 m/s (Impact test) for K1-20 blend.

Furthermore, it can be seen that when the velocity of loading increases, the brittle-ductile transition shifts to a higher temperature. This shift is in agreement with the time-temperature superposition principle for the mechanical properties of polymers. As loading speed increases from 100mm/min to 2.5m/s, the shift in the transition temperature is significant for all compositions of both K1 and K2.

The observed peak in fracture energy has been reported in the literature and has often been related to the molecular relaxation of the polymer [113-117]. The brittle behavior for temperatures below the transition implies that the molecular motions are limited. Above the transition temperature, the ductile behavior of fracture indicates that movements of certain segments or regions of macromolecules can occur, due to a thermally activated process. The observed peak in K_i can therefore be induced by the relaxation in the irreversible deformation prior to fracture, in a similar manner to the peak of the loss factor in viscoelasticity. This confirms previous finding [14, 85] and suggests that the brittle-ductile transition is controlled by an energy activation process that can be expressed by the Arrhenius equation:

$$\dot{\varepsilon} = A \exp\left(\frac{-\Delta H}{RT}\right) \tag{3-1}$$

where $\dot{\varepsilon}$ is the strain rate, A is a constant, ΔH is the activation energy, R is the gas constant and T is the absolute temperature. For three-point-bend samples, by ignoring the effect of the crack, the nominal strain rate can be estimated by:

$$\dot{\varepsilon} = 6\frac{VD}{S^2} \tag{3-2}$$

where V is the speed of loading, D is the specimen width, and S is the span. Equation (3-1) can be rearranged as:

$$\ln \dot{\varepsilon} = A - \frac{\Delta H}{RT} \qquad (3\text{-}3)$$

In order to take into account the effect of loading rate, the temperatures at brittle-ductile transition, $T_{b\text{-}d}$, for the blends were determined at different loading rate levels of 1mm/min., 10 mm/min., 100mm/min., 200 mm/min. and 2.5 m/s (impact tests). Figure 3.7 shows the plot of $ln(\dot{\varepsilon})$ as a function of the temperature at brittle-ductile transition $T_{b\text{-}d}$ for K1-2.5. The result demonstrates a linear relationship between $1/T_{b\text{-}d}$ and $ln(\dot{\varepsilon})$ and suggests a good application of the Arrhenius equation in the fracture transition study. This observation is also be found clearly for the other blends (K1-10, K1-20, K2-2.5 and K2-15) considered in this work (Figures C.12 to C.16 in Appendix C). The observed linear correlation between the inverse brittle-ductile temperature $1/T_{b\text{-}d}$ and $ln(\dot{\varepsilon})$ confirms that the brittle-ductile transition in fracture behavior of the PS/EPR blends, modified by the interfacial agents K1 and K2, is controlled by an energy activation process. Therefore, the Arrhenius equation can be used to predict the change in fracture behavior in order to avoid undesirable catastrophic failures in the material.

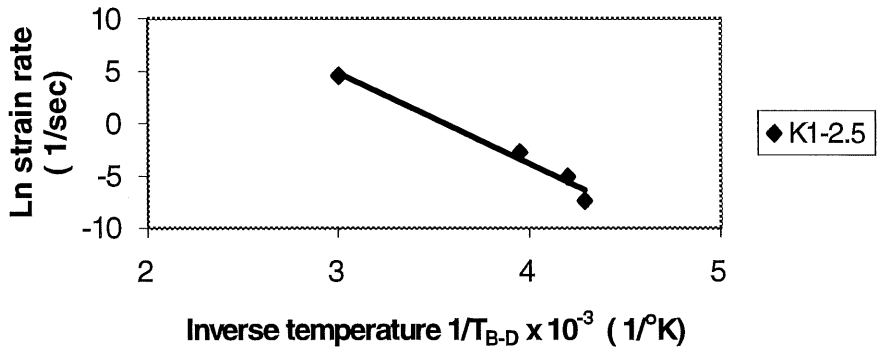

Figure 3.7: Plot of $ln(\dot{\varepsilon})$ against $1/T_{b\text{-}d}$ for K1-2.5 blend.

Furthermore, from the slope and the intercept of the plot of $ln(\dot{\varepsilon})$ against $1/T_{b\text{-}d}$, the energy barrier ΔH controlling the time-temperature dependence of fracture behavior of the material as well as the constant A could be also deduced. The values of ΔH and A obtained for various blends are shown in Table 3.3.

Table 3.3: Values of ΔH and A of Eq. (3-3) for different blends modified with the interfacial agents K1 and K2.

Blends	ΔH (kJ/mol.)	Constant A (1/s)
K1-2.5	71.87	2.18E+13
K1-10	52.08	1.84E+10
K1-20	50.56	1.77E+10
K2-2.5	45.21	5.82E+09
K2-15	38.37	5.02E+08

From the results in Table 3.3 above, it can be seen that the interfacial agent reduces the energy barrier of the blends. For the blends compatibilized by K2 interfacial agent, the decrease in the activation energy ΔH controlling the time-temperature dependence of the fracture process is more significant, resulting in a much lower in the brittle-ductile transition temperature. The difference between ΔH of K1 and K2 samples clearly shows that plasticizing effect of the SEBS triblock copolymer is more significant with a lower molecular weight. This effect is somehow similar to that of plasticizers in polymers. The plasticizing effect might be responsible for the higher impact performance observed with K2 interfacial agent as reported in [1].

3.2.2 Fracture performance of the blends in ductile behavior

While of considerable practical importance, the fracture characterization of ductile plastics is still a controversial subject. It has been known that when the material exhibits a ductile behavior in fracture, unstable fracture does not occur. The crack propagation is generally completely stable with additional supply of external energy. For this mode of fracture a method based on the assumption of constant fracture energy during the fracture process has been proposed. The energy absorbed by the sample is considered to be proportional to the fracture surface area. For many ductile plastics, this method often gives abnormally high values of fracture energy. Further more, an inconsistent negative intercept of the absorbed energy versus fracture surface plot is generally observed. Recently, a new approach taking into account the crack initiation and crack propagation energies in the material has been proposed by Vu-khanh [13]. This model, which uses two parameters G_i (the fracture energy at crack initiation) and T_a (the rate of change of actual fracture energy G_r with crack extension), was able to describe the fracture performance in ductile behavior of many polymers and blends [1, 13, 14, 55]. However, the model requires at least a series from 10 to 12 samples for the fracture characterization at each testing condition (of temperature and loading rate). This seemed to be a disadvantage because of the lack of samples provided in this work. Therefore, another method based on the correlation between the fracture energy and stress field approach (Section 1.3 in Chapter 1: "Theoretical background") is applied in the present study for examining the fracture resistance of the PS/EPR/SEBS blends over a large range of strain rate and temperature. The results are then also compared to those obtained from the recent studies [1, 112] of the same material for confirming the validity of the method using in this research. For the purpose of considering the ductile fracture behavior of the blends, the

three point bending tests were once again carried out for five various blends of K1 (K1-2.5, K1-5, K1-15, K1-20 and K1-30) as well as two blends of K2 (K2-20 and K2-30) at the loading speed of 100 mm/min and in a temperature range above the brittle-ductile transition. By a calculating procedure, as introduced in the previous section, the fracture resistance of each blend, not only at the initiation of crack but also during the crack propagation, could be determined and analyzed.

Table 3.4 shows values of the stress intensity factor at crack initiation, K_i, for the blends compatibilized by various K1 and K2 contents. From the results, it can be found that when temperatures increase from 10°C to 70°C, K_i,, presented the fracture performance at crack initiation of the material, reduce for all of the blends examined. This decrease in rupture resistance at crack initiation of the blends fractured in ductile manner is demonstrated in Figure 3.8. It is worth noting that addition of interfacial agents (K1 and K2) results in an improvement of the fracture resistance at crack initiation of PS/EPR blend and this effect has been found clearly around the room temperature. Particularly, the lower molecular weight interfacial agent, K2, is more effective at increasing the fracture resistance at crack initiation than the high molecular weight copolymer, K1 (Table 3.4). However, in the region of high temperature, adding more interfacial agents might not to lead an apparent increase in fracture performance due to a larger plastic zone developed during the thermally activated process in front of the crack tip. This is shown obviously in the case of K2-20 and K2-30 blends, which have a high fracture resistance of 2.91 and 3.63 ($mPa.m^{1/2}$) respectively at the temperature of 10°C but drop drastically to 1.54 and 1.88 ($mPa.m^{1/2}$) as the temperature goes up to 70°C. The results confirm again that adding the interfacial agents at high concentrations results in a plasticizing effect of the polystyrene matrix and a reduction in the energy barrier controlling

the fracture process. The plasticizing effect is more significant with the low molecular weight interfacial agent and would have a strong contribution to the higher impact performance observed with K2 interfacial agent as reported in [1].

Table 3.4: Values of K_i (Mpa.$\sqrt{m}$) for the blends at various temperatures with V=100 mm/min

T (°C)	K1-2.5	K1-5	K1-15	K1-20	K1-30	K2-20	K2-30
10	2.23	2.63	2.46	2.75	2.75	2.91	3.63
25	2.02	2.35	2.39	2.67	2.54	2.67	3.15
40	1.80	1.92	2.16	2.12	2.38	2.10	2.37
50	1.66	1.93	2.07	1.90	2.12	1.71	
55							2.02
60	1.61		1.86	1.71	1.99	1.58	
70	1.58	1.79	1.69	1.67	1.88	1.54	1.88

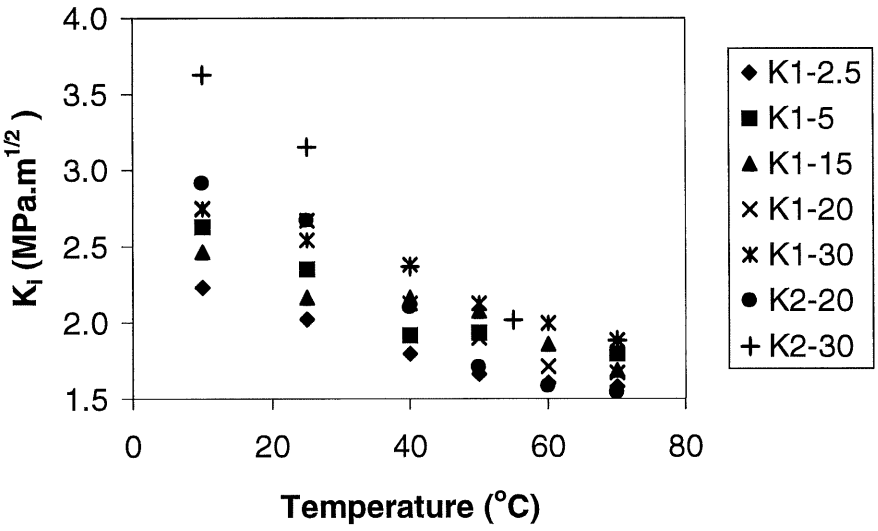

Figure 3.8: Fracture resistance at crack initiation (K_i) versus temperature for the blends modified with various interfacial agent contents of K1 and K2.

The fracture energy during the crack propagation can be characterized by calculating the variation of the critical stress intensity factor during crack extension. This variation is also called the crack growth resistance curve or *R*-curve [78]. It has been shown that there is a unique relationship between the amount of crack extension and the applied stress intensity factor for a given thickness. *R*-curve is often used to characterize the crack growth resistance of materials in which plastic deformation is large; and as the crack grows, the resistance to fracture increases due to the increased volume of plastically deformed material ahead of the crack tip. The R-curve is now an ASTM standard procedure [118] for Center-Cracked Tension panel (CCT), Compact Specimen (CS) and the Crack-Line-Wedge-Loaded specimen (CLWL). For three-point-bend specimens, the determination of the variation of the critical stress intensity factor with crack extension requires the determination of the specimen compliance versus the crack length. The compliance calculation and R-curve determination are given in Appendix A. Figure 3.9 shows R-curves for the blends modified with various interfacial agent contents at the room temperature and with the loading rate of 100 mm/min. The crack extension resistance, K_R, is plotted against the effective crack length determined by the secant method (see Appendix A); the effective crack length being the physical crack size augmented for the effects of crack tip plastic deformation. The modulus used for the calculation of the effective crack length a_{eff} is the effective modulus determined from the initial slope of the load-displacement trace as discussed in [79, 81, 119, 120].

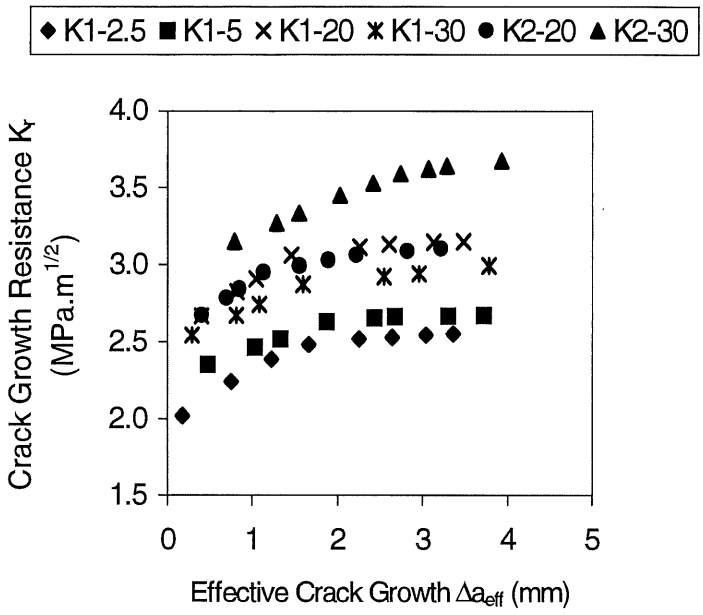

Figure 3.9: Crack growth resistance (K_R) versus effective crack extension (Δa_{eff}) for the blends modified with various interfacial agent contents of K1 and K2.

It has been shown from the results that as the crack grows, the fracture resistance of the observed blends increases and seems to approach a certain maximum value, K_{Rmax}. This increase in the fracture resistance during the crack propagation was observed previously [119, 120] and regarded as a result concerned to the increased volume of plastically deformed material ahead of the crack tip. For the blends considered, adding more interfacial agents of both K1 and K2 leads to an improvement of the fracture performance of the material during the crack propagation, represented by a shift to a higher position of the *R*-curve (Figure 3.9). . This demonstrates the considerable enhancement of fracture resistance of the PS/EPR blend when it is reinforced by up to 30 percent of triblock copolymers of K1 and K2. In the case of the blends compatibilized by the higher molecular weight interfacial agent, K1, as the content of K1 increase, the *R*-curve shifts up, attains the highest position at 20 % K1 and goes down

afterwards. This transition, however, is not observed with K2 interfacial agent; the fracture resistance of K2-30 during the crack propagation is higher than that of K2-20 and significantly higher than the fracture resistance of all K1 blends. The result also shows that the low molecular weight interfacial agent, K2, is more effective at improving the fracture performance of the PS/EPR blends than K1. This distinct effect of K2-20 and K2-30 blends on the fracture resistance during the crack propagation seems to be due to the ability of saturating the interface of the low molecular weight interfacial agent, K2, and agreed with the results obtained from the impact fracture study of these materials in [1, 112]. It can be presented obviously with the maximum values of K_R for the K1and K2 blends as shown in Table 3.5 below.

Table 3.5: Maximum values of crack growth resistance for K1 and K2 blends at 25°C (loading rate of 100 mm/min.)

Blends	K1-2.5	K1-5	K1-20	K1-30	K2-20	K2-30
K_{Rmax} (MPa.m$^{1/2}$)	2.55	2.67	3.15	2.99	3.1	3.67

3.3 Results obtained from tensile tests in α process

The yield stress was measured at different temperatures from 25° C to 70° C and at five strain rates from 3.33 x 10^{-4} to 6.67 x 10^{-2} s^{-1} (1 mm/min. to 200 mm/min.) for four various blends of K1 (K1-5, K1-15, K1-20 and K1-30) and five blends of K2 (K2-2.5, K2-5, K2-10, K2-15 and K2-30). The plots of σ_y / T as a function of $\log \dot{\varepsilon}_y$ for these blends are given from Figure D.1 to Figure D.9 in Appendix D. These figures show a good agreement between experimental data and the Eyring's theory expressed by Equa. (1-34) (in Chapter 1) for both types of interfacial agent K1 and K2. For example, Figure 3.10 gives a presentation of the linear correlation between σ_y / T and $\log \dot{\varepsilon}_y$ for K1-5 blend. With all compositions of interfacial agent for both K1 and K2, a set of parallel straight lines having almost the same slope is obtained. From these figures it can be seen that σ_y / T increases linearly with $\log \dot{\varepsilon}_y$. This result demonstrates the fact that the yield stress is fairly loading rate dependent. The linear correlation between σ_y / T and $\log \dot{\varepsilon}_y$ is found with all concentrations of the interfacial agent (for both K1 and K2) applied in the blend.

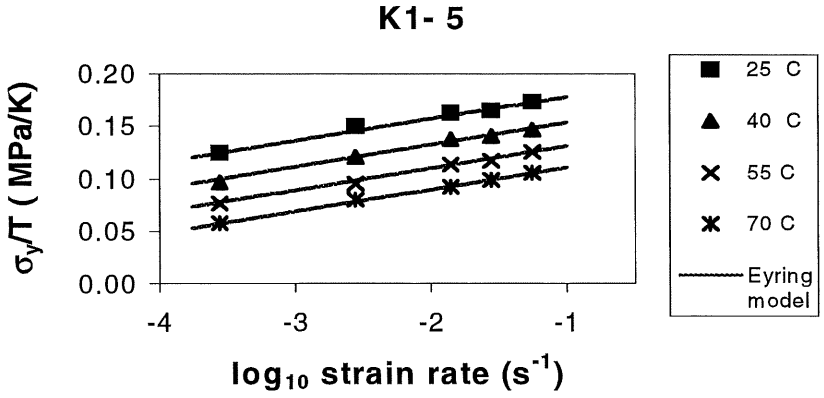

Figure 3.10: Variation of σ_y / T as a function of $\log_{10} \dot{\varepsilon}_y$ at different temperatures for K1-5 blend

However, the slope of the plots is different when the content of interfacial agents (IA) changes, as showed in Table 3.6. It is worth noting that for all concentrations of IA, the slope of the plot $\frac{\sigma_y}{T}\left(\log \dot{\varepsilon}_y\right)$ decreases gradually as the composition of IA in the blend increases. By referring to Equ. (1-34), one can note that the value of this slope is proportional to $\left(1/V^*\right)$and equal to $\left(2\times 2.303\, R/V^*\right)$. With both types of K1 and K2, an increase in copolymer additive gave a decrease in the variation of the yield stress with loading rate. The result confirms the less effect of loading rate on the yield stress for the more ductile polymers.

Table 3.6: Value of the slope d (σ_y/T) / d $(\log \dot{\varepsilon}_y)$ for various IA contents

Blends	K1				K2				
	K1-5	K1-15	K1-20	K1-30	K2-2.5	K2-5	K2-10	K2-15	K2-30
$\frac{2\times 2.303\, R}{V^*}$ (MPa.s/K)	0.0223	0.0208	0.0207	0.0199	0.0251	0.0246	0.0241	0.0234	0.0221

Furthermore, the good agreement between the Eyring's model and experimental measurement also points out that the activation volume V^* and activation enthalpy ΔH expressed in Equ. (1-34) seem to be the characters of the material and almost constant in a large range of temperatures and strain rates. From the Figures D.1 to D.9, the activation volume V^* can be easily calculated from the slope of the straight lines whereas the activation energy ΔH of the yield process can be deduced from the horizontal distances between the straight lines. In addition, the linear relationship between σ_y/T and $\log \dot{\varepsilon}_y$ for all the

observed blends at the range of tensile testing conditions considered above shows clearly that these materials exhibit a yielding behavior in only the α process (See 1.5.2 in Chapter 1). Table 3.7 demonstrates the value of $V_{t_\alpha}^*$ and ΔH_α calculated for various compositions of K1 and K2; the indices t and α refer to the tensile test and the α process, respectively. The experimental data from Table 3.7 shows that when the proportion of IA in the blend augments, the value of the activation volume $V_{t_\alpha}^*$ increases whereas to the contrary, the value of the activation enthalpy ΔH_α seems to go down lightly.

Table 3.7: Value of $V_{t_\alpha}^*$ (per jumping segment) and ΔH_α for different IA contents

	K1				K2				
	K1-5	K1-15	K1-20	K1-30	K2-2.5	K2-5	K2-10	K2-15	K2-30
$V_{t_\alpha}^*$ (nm^3)	2.85	3.05	3.07	3.20	2.54	2.59	2.64	2.72	2.87
ΔH_α (KJ/mol)	145	133.1	129	134	128	124.5	119	115.4	107.2

Indeed, as discussed previously [12], the free volume $V_{t_\alpha}^*$ is considered as a region containing n segments of macromolecules simultaneously activated and leading to yield deformation. The result obtained from the Table 3.7 could be explained by the meaning that an increase in copolymer additive would produce a larger region of more segments of macromolecules activated in the yield process, causing a relative increment in the free volume of the material. Figure 3.11 shows the linear change of $V_{t_\alpha}^*$ as a function of composition of the interfacial agents for both K1 and K2. However, this linear correlation between the activation energy ΔH_α and the IA contents is not observed clearly, as demonstrated in Figure 3.12.

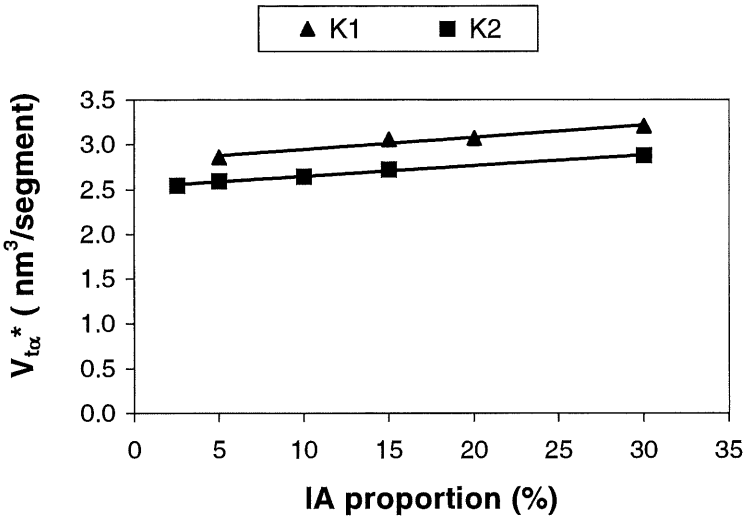

Figure 3.11: Variation of $V_{t_\alpha}^*$ as a function of interfacial agent (IA) contents (%) for various blends of K1 and K2

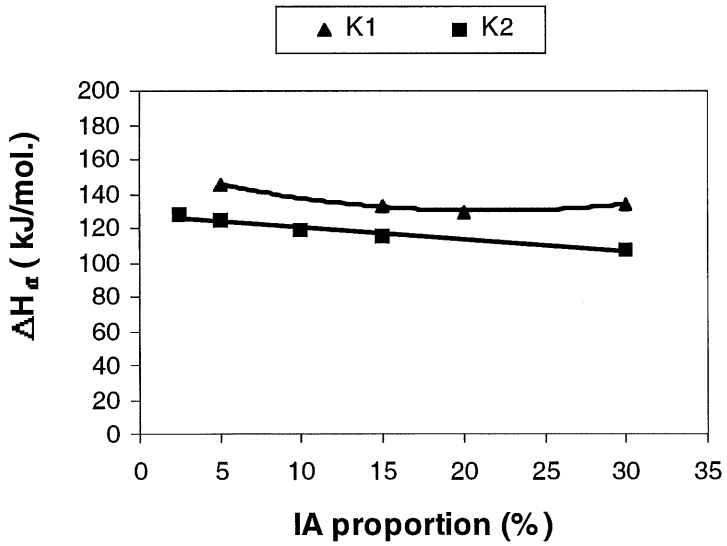

Figure 3.12: Variation of ΔH_α as a function of IA contents (%) for various blends of K1 and K2

In connecting with the energy barrier ΔH in Table 3.3, it is worth noting that the activation energy ΔH_α characterizing the yield behavior of the blend in α process as well as the energy barrier ΔH controlling the brittle-ductile transition in fracture behavior, both of

them decrease when the contents of interfacial agent (of K1 or K2) increase in the blend. This seems to display an implicit correlation between the yielding field and the fracture approaches. However, there is a considerable difference between the values of these two energies corresponding to the same blend. For each observed blend, the value of the activation energy ΔH_α in the yielding process (Table 3.7) is around two to three-fold higher than that of the energy barrier ΔH controlling the brittle-ductile fracture transition. This can be explained as one considers the different temperature range applied for determining these two parameters. ΔH_α is deduced from the yielding process in region α (at high temperatures and low loading rates) whereas ΔH is obtained in the brittle-ductile transition in fracture (at lower temperatures in the case of the same loading rate). On the other hand, it has been known that when the temperature goes down and attains the β region, the yielding behavior of the polymers could be considered as two Eyring processes acting in parallel [108-110] and two separate values of ΔH_α (in α region) and ΔH_β (in region β) can be obtained. Because the β region is near the brittle-ductile transition, it can be expected that there is a similar correlation between the activation energy ΔH_β in β yielding process and the ΔH controlling the brittle-ductile fracture transition.

3.4 Results obtained from compression tests in α and β yielding processes.

The compression yield behavior of PS/EPR/SEBS blends has been investigated, over a wide range of experimental condition that can not be reached in tensile tests due to the brittle nature of the blends. The yield stress in uniaxial compression was measured at different temperatures from -75° C to 100° C and over nearly four decades of loading rate from 0.1 to

200 mm/min. for three various blends of K1 (K1-2.5, K1-10 and K1-20). Figure 3.13 shows the plot of the compression yield stress $|\sigma_c|$ versus temperature at a constant loading rate of 100 mm/min. for K1-2.5 blend. From the figure, it has been pointed out that the yielding behavior of the observed blend can be divided into two different ranges. Over a range of temperatures, denoted as range I, from about –20 to 100 °C, the plot is a straight line and the experimental data present a good agreement with the Eyring theory, which is expressed by Equa. (1-34) (in Chapter 1: "Theoretical background"). Below –20°C, the variation of yield stress according to temperature is more significant; Equa. (1-34) is no more valid and was modified by Ree and Eyring [98] with considering that there are two Eyring processes acting in parallel so that $\sigma_y = \sigma_1 + \sigma_2$, where σ_1 and σ_2 are the stresses associated in process α and process β, respectively. Equa. (1-36) and (1-37) (applied for tensile and compression tests, respectively), which are based on the Ree-Eyring model, have been shown to agree well with experimental data for a number of polymers [108-111]. In Appendix E, figures E.2 to E.4 show the plot of the $\frac{|\sigma_c|}{T}$ as a function of logarithm of strain rate ($\dot{\varepsilon}$ in sec^{-1}) for K1-2.5, K1-10 and K1-20 blends. For instance, the time-temperature dependence of the yielding behavior of K1-2.5 blend is demonstrated in Figure 3.14. It can be found from the figure that the diagram of σ_y/T versus logarithm strain rate can be clearly separated into two regions: region α where process I dominated and region β where process II is activated. Between region α and region β, the curve of σ_y/T as a function of logarithm strain rate shows a noticeable change in slope. This change can be used to find the transition boundary between these two regions by standard mathematics. When yielding in region α (i.e., when the strain rate is low and the temperature is high), the slope is approximately $\frac{4.606\,R}{V_\alpha^*}$, whereas in region β (i.e., when the

strain rate is high and the temperature is low), the approximate slope is $4.606\,R\left(\frac{1}{V_\alpha^*}+\frac{1}{V_\beta^*}\right)$.

For a given temperature, the transition between the two regions, defined as a critical strain rate $\dot{\varepsilon}_\beta$, at which the slope of σ_y/T equals the average of the above two approximate slopes can be deduced by Equa. (1-38). A set of the points ($\dot{\varepsilon}_\beta$, T) establishes a slanting straight line d_c separating the two regions α and β (Figure 3.14). The presentation of d_c is also displayed for all observed blends in Appendix E (Figures E.2 to E.4).

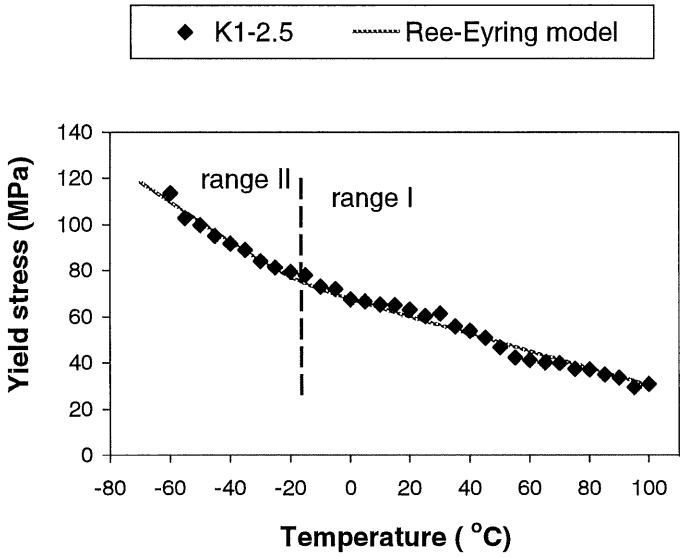

Figure 3.13: Plot of yield stress in uniaxial compression $|\sigma_c|$ versus temperature at a constant loading rate of 100 mm/min for K1-2.5 blend. The curve $|\sigma_c| = f(T)$ is calculated from Equa. (1-37) using the constants given in Table 3.8

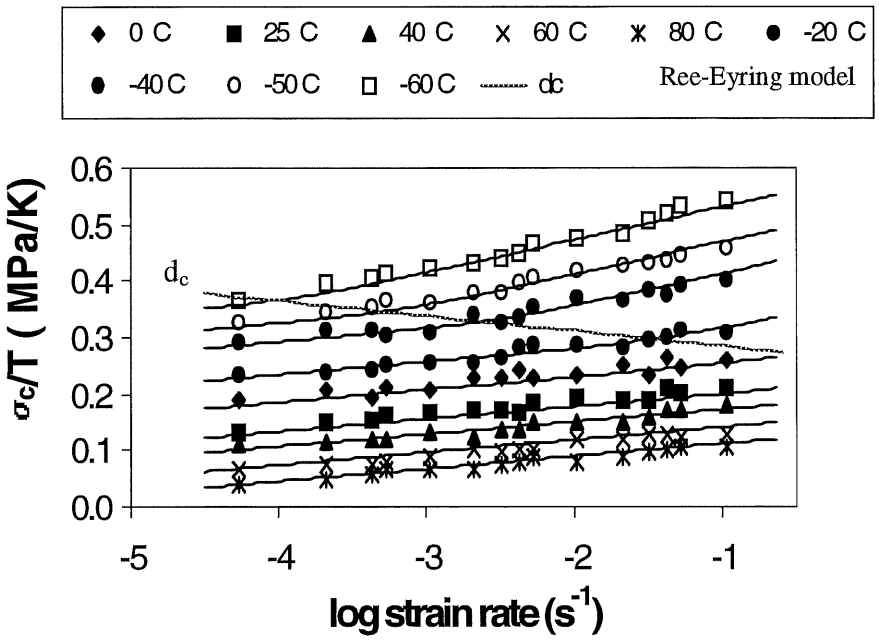

Figure 3.14: Plot of the $\frac{|\sigma_c|}{T}$ as a function of $\log_{10}\dot{\varepsilon}$ for K1-2.5 blend.

Furthermore, it is worth noting that throughout range I, the Ree-Eyring theory reduces to the Eyring theory in terms of a single simply activated flow process (denoted as the α process) and in this case, the plots of yield stresses versus log (strain-rate) or versus temperature, must give straight lines. Above d_c (range II), the existence of β yielding process is revealed in a range of temperatures and strain rates where it is necessary to assume that two activated flow processes are involved in the yield deformation of PS/EPR/SEBS blends for being allowed to apply the Eyring model. In Table 3.8, the values of the parameters ($V_\alpha^*, \Delta H_\alpha, \dot{\varepsilon}_{0_\alpha}, V_\beta^*, \Delta H_\beta, \dot{\varepsilon}_{0_\beta}$) characterized the yielding behavior for α and β processes of the blends could be estimated from the good fit of Equa. (1-37) to the data of diagrams of σ_y/T versus logarithm strain rate due to a procedure (presented in Appendix B).

Table 3.8: Constants calculated from the fit of Eq. (1-37) to the data from Figures E.2 to E.4

Blends	ΔH_α (kJ/mol)	$V^*_{c\alpha}$ (nm^3/segment)	$d\varepsilon_{0\alpha}/dt$ (s^{-1})	ΔH_β (kJ/mol)	$V^*_{c\beta}$ (nm^3/segment)	$d\varepsilon_{0\beta}/dt$ (s^{-1})
K1-2.5	145	2.85	1.59E+16	66	1.78	1.19E+13
K1-10	138.3	2.93	1.55E+15	61.1	1.83	1.50E+12
K1-20	133.5	3.16	1.78E+14	58	2.25	5.94E+09

The values of the constants given in Table 3.8 were used to generate the curve $|\sigma_c| = f(T)$ in Figure 3.13 as well as the plots of $\frac{|\sigma_c|}{T}$ as a function of logarithm of strain rate ($\dot{\varepsilon}$ in sec^{-1}) (Figures E.2 to E.4) for the observed blends. The results show a good agreement between the Ree-Eyring model and the experimental data and confirm the fact that the Ree-Eyring theory can be applied well for studying and predicting the yielding behavior of PS/EPR/SEBS blends for an arbitrary state of strain rate and temperature. From Table 3.8, moreover, it can be obviously shown that the addition of more interfacial agent results in an increase in the activation volume V^*_c and a reduction of the activation energy ΔH. This significant variation of V^*_c and ΔH can be observed for both α and β processes. In addition, the values of both of $V^*_{c\beta}$ and ΔH_β in β process are smaller than those determined from α phase. This agrees well with the results obtained in recent works [108-111] and could be explained by the reason that the β process occurs in the range of low temperature and high loading rate. The state of low temperature and high loading rate could result in reducing V^*_c, the region containing n segments of macromolecules simultaneously activated and leading to yield deformation. For each process (α or β), the increase in the activation volume obtained from the Table 3.8 shows that an increase in copolymer additive would produce a larger region of more segments of macromolecules activated in the yield process, causing a relative increment

in the activation volume of the material. Figures 3.15 and 3.16 shows the change of V_c^* and ΔH as a function of composition of the interfacial agents for K1 blends.

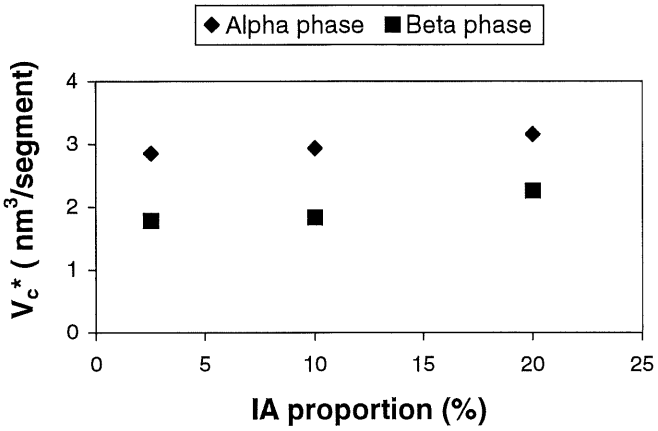

Figure 3.15: Variation of the activation volume, V_c^*, (compression) as a function of IA contents (%) for K1 blends in the α and β processes.

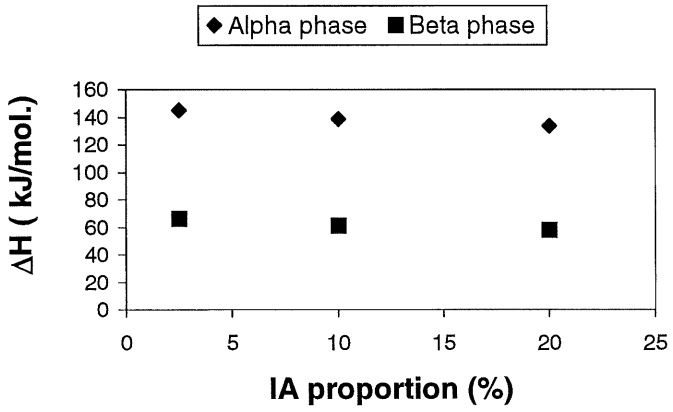

Figure 3.16: Variation of the activation energy, ΔH, as a function of IA contents (%) for K1 blends in the α and β processes.

Moreover, in considering the activation volume and activation energy characterizing the α process for tensile (Table 3.7) and compression (Table 3.8) tests, one can note that there is a similarity of these values for both two types of test. This presents the validity of the Ree-Eyring model for both two cases of tensile and compression tests, and suggests that the results determined from the compression tests in β process could be used as a consequence of the tensile tests. By comparing the activation energy ΔH_β of β process to the energy barrier ΔH controlling the brittle-ductile transition (Table 3.3), basing on the similarity of these two energies for each material, it seems to be proposed that there is an implicit correlation between the yielding behavior and the fracture approach. This result is significant and needs more considerations in the field of studying the relationship between the morphology, interface and properties of the polymer blends.

CONCLUSION

The fracture and yielding behaviors of a blend of 80 volume % polystyrene (PS) and 20 volume % ethylene- propylene rubber (EPR), compatibilized by two triblock copolymers of styrene/ ethylene- butylene/ styrene (SEBS), of different molecular weights, have been investigated over a large range of loading rates and temperatures. A study of brittle-ductile transition in fracture of the blends shows that adding an interfacial agent lowers the temperature at brittle-ductile transition. This effect, however, is much more pronounced for the lower molecular weight interfacial agent, K2. The time-temperature dependence of the brittle-ductile transition in fracture performance of the blends is controlled by an energy activation process and can be predicted by the Arrhenius equation. Adding the interfacial agents at high concentrations results in a plasticizing effect of the polystyrene matrix and a reduction in the energy barrier ΔH controlling the fracture process. The fracture resistance at crack initiation as well as during the crack propagation of the blends, which is determined by using the R-curve method, shows that the low molecular weight interfacial agent, K2, is more effective at improving the fracture performance of the PS/EPR blends than K1. Particularly, the distinct contribution of K2-20 and K2-30 blends to the higher fracture resistance seems to be due to the ability of saturating the interface of the low molecular weight interfacial agent, K2, and agreed with the results obtained from the impact fracture study of these materials in [1, 112].

The yield stress measured in tensile and uniaxial compression tests over a large range of temperatures and loading rates reveals that the yielding behavior of the blends is controlled by two Eyring processes (α and β processes) acting in parallel. A good agreement between experimental data and the Ree-Eyring model confirms the fact that the Ree-Eyring theory can

be applied well for studying and predicting the yielding behavior of PS/EPR/SEBS blends for an arbitrary state of strain rate and temperature. Furthermore, the similar values of activation energy and activation volume in α process for both two types of test show the validity of the Ree-Eyring model for two cases of tensile and compression tests. The addition of K1 and K2 interfacial agents results in a reduction of the activation energy ΔH and an increase in the activation volume V^* for both α and β processes. Besides, it has been found that for each observed blend, the value of ΔH_β in β yielding process is nearly the same of the energy barrier ΔH controlling the brittle-ductile transition in fracture. This result seems to be significant in terms of studying the correlation between the yielding behavior and fracture approach and requires more considerations in the future.

APPENDIX A:

CEB CURVE FOR FRACTURE TESTS

The stress intensity factor for a three-point-bend specimen is given [67] by:

$$K = \frac{PS}{BD^{3/2}} f(a/D) \tag{A-1}$$

where:

P : the external force

S : the span of bending test

B : the thickness of the sample

D : the width of the sample

$f(a/D)$: a calibration factor provided in Ref. 80. In this work, $f(a/D)$ associated with the three-point bending test can be written by:

$$f(x) = \frac{3x^{1/2}\left[1.99 - x(1-x)\left(2.15 - 3.93x + 2.7x^2\right)\right]}{2\,(1+2x)(1-x)^{\frac{3}{2}}} \tag{A-2}$$

(with x = a/D)

The strain energy release rate is expressed as [121]:

$$G = \frac{1}{2} P^2 \frac{dC}{dA} = \frac{K^2}{E} \tag{A-3}$$

in which:

C : the compliance of the specimen

A : the crack surface

E : Young modulus of the material

Then, combining Equa. (A-1) and Equa. (A-3), dC/dA and C can be written as a function of a/D as follows:

$$\frac{dC}{dA} = \frac{dC}{d(a/D)BD} = \frac{2S^2 f^2(a/D)}{EB^2D^3} \tag{A-4}$$

$$C = C_0 + \frac{2S^2}{EBD^2} \int_0^{a/D} f^2(a/D)\, d(a/D) \tag{A-5}$$

where :

C_0 is the specimen compliance for $a/D = 0$, and expressed by:

$$C_0 = \frac{\Delta_0}{P_0} = \frac{S^3}{4BD^3E} \tag{A-6}$$

With $\frac{S}{D} = 4$ using for this work, Equa. (A-5) becomes:

$$CEB = 16 + 32 \int_0^{a/D} f^2(a/D)\, d(a/D) \tag{A-7}$$

By connecting Equa. (A-2) to Equa. (A-7) and numerically calculating *CEB*, one can obtain the values of *CEB* as a function of *a/D* as shown in Figure A.1.

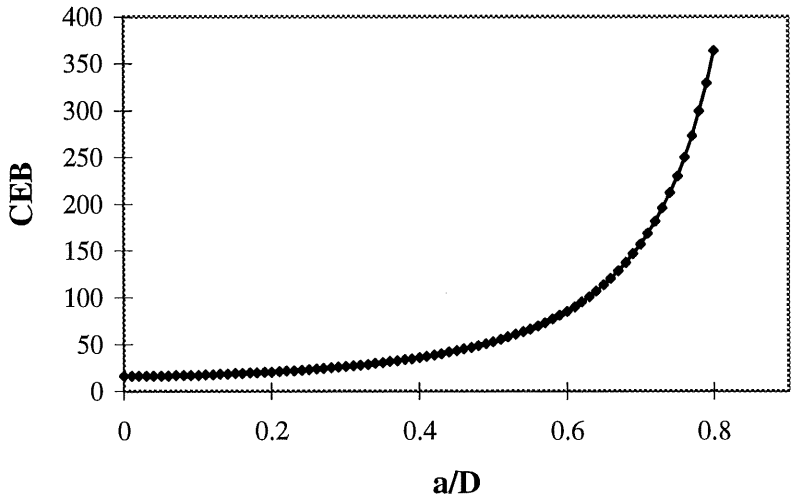

Figure A.1: *CEB* values as a function of *a/D* in three-point bending tests (*S/D* = 4)

From the numerical values of *CEB*, the stress intensity factor during crack propagation can be obtained from Equa. (A-1) as a function of crack length *a/D* at different values of deformation Δ. Knowing the relationship between the specimen compliance and the crack length, the effective crack length at any load level *P* can be determined as illustrated in Figure A-2.

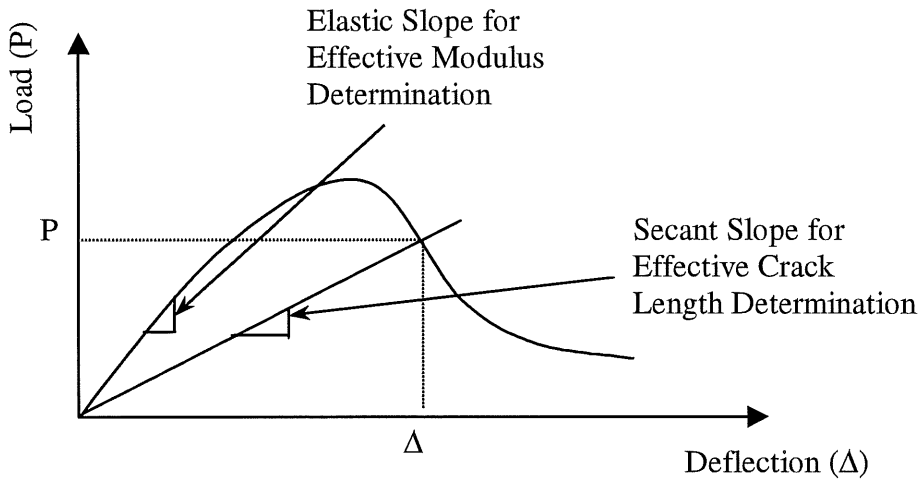

Figure A.2: Schematic drawing of effective crack length determination from the load-deflection curve.

APPENDIX B:

Evaluation of the constants: $V_\alpha^*, \Delta H_\alpha, \dot{\varepsilon}_{0_\alpha}$ and $V_\beta^*, \Delta H_\beta, \dot{\varepsilon}_{0_\beta}$ in Ree-Eyring model for tensile and compression tests

The Ree-Eyring equation using in tensile and compression tests may be written as follows:

$$\frac{\sigma_t}{T} = \frac{\sigma_{t_\alpha}}{T} + \frac{\sigma_{t_\beta}}{T} = \frac{2R}{V_{t_\alpha}^*}\left[\frac{\Delta H_\alpha}{RT} + 2.303\log\left(\frac{2\dot{\varepsilon}}{\dot{\varepsilon}_{o_\alpha}}\right)\right] + \frac{2R}{V_{t_\beta}^*}\sinh^{-1}\left[\frac{\dot{\varepsilon}}{\dot{\varepsilon}_{o_\beta}}\exp\left(\frac{\Delta H_\beta}{RT}\right)\right] \qquad \text{(B-1)}$$

$$\frac{|\sigma_t|}{T} = \frac{|\sigma_{c_\alpha}|}{T} + \frac{|\sigma_{c_\beta}|}{T} = \frac{2R}{V_{c_\alpha}^*}\left[\frac{\Delta H_\alpha}{RT} + 2.303\log\left(\frac{2\dot{\varepsilon}}{\dot{\varepsilon}_{o_\alpha}}\right)\right] + \frac{2R}{V_{c_\beta}^*}\sinh^{-1}\left[\frac{\dot{\varepsilon}}{\dot{\varepsilon}_{o_\beta}}\exp\left(\frac{\Delta H_\beta}{RT}\right)\right] \qquad \text{(B-2)}$$

(Equation (1-36) and (1-37) in Chapter 1: Theoretical background)

Because the parameters $V_\alpha^*, \Delta H_\alpha, \dot{\varepsilon}_{0_\alpha}$ and $V_\beta^*, \Delta H_\beta, \dot{\varepsilon}_{0_\beta}$ (characterized for α and β process respectively) have the same meanings in both tensile and compression tests, the procedure of evaluating these constants, as described below, will be presented in the case of the tensile test. The same procedure can be also applied for analysis of uniaxial compression results.

If one assumes that two rate processes, α and β, are involved in the deformation at yield, the Ree-Eyring theory as well as Bauwen's treatment [110] predict that the asymptotes of a given curve are expressed by:

$$\frac{\sigma_t}{T} = \frac{2R}{V_{t_\alpha}^*}\left[\frac{\Delta H_\alpha}{RT} + 2.303\log\left(\frac{2\dot{\varepsilon}}{\dot{\varepsilon}_{o_\alpha}}\right)\right] \qquad \text{for} \qquad \dot{\varepsilon}_\alpha \le \dot{\varepsilon} \le \dot{\varepsilon}_\beta \qquad \text{(B-3)}$$

and

$$\frac{\sigma_t}{T} = \frac{2R}{V_{t_\alpha}^*}\left[\frac{\Delta H_\alpha}{RT} + 2.303\log\left(\frac{2\dot{\varepsilon}}{\dot{\varepsilon}_{o_\alpha}}\right)\right] + \frac{2R}{V_{t_\beta}^*}\left[\frac{\Delta H_\beta}{RT} + 2.303\log\left(\frac{2\dot{\varepsilon}}{\dot{\varepsilon}_{o_\beta}}\right)\right] \quad \text{for } \dot{\varepsilon} > \dot{\varepsilon}_\beta \qquad \text{(B-4)}$$

where ΔH_α, ΔH_β are the activation energies; $V_{t_\alpha}^*$, $V_{t_\beta}^*$ are the activation volumes; $\dot{\varepsilon}_{o_\alpha}$, $\dot{\varepsilon}_{o_\beta}$ are constants containing a frequency factor related to the α and β processes respectively. $\dot{\varepsilon}_\beta$ is the value of the strain rate corresponding to the intersection of the two asymptotes and $\dot{\varepsilon}_\alpha$ denotes the value of the strain rate obtained by extrapolating the curve to zero stress. For a given temperature, it follows that:

$$\dot{\varepsilon}_\beta = \frac{\dot{\varepsilon}_{o_\beta}}{2}\exp\left(-\frac{\Delta H_\beta}{RT}\right) \qquad \text{(B-5)}$$

and

$$\dot{\varepsilon}_\alpha = \frac{\dot{\varepsilon}_{o_\alpha}}{2}\exp\left(-\frac{\Delta H_\alpha}{RT}\right) \qquad \text{(B-6)}$$

Let us consider two curves (shown in Figure B.1) respectively related to temperatures T_1 and T_2 in the β region and let s_x (T_1, T_2) denote the horizontal component of the shift factor between these two curves; it therefore follows from both treatments that:

$$s_x(T_1, T_2) = \frac{\Delta H_\beta}{2.303\,R}\left(\frac{1}{T_2} - \frac{1}{T_1}\right) \qquad (T_1 > T_2) \qquad \text{(B-7)}$$

The values of the parameters, denoted above, are estimated, as follows from the data of Figure B.1.

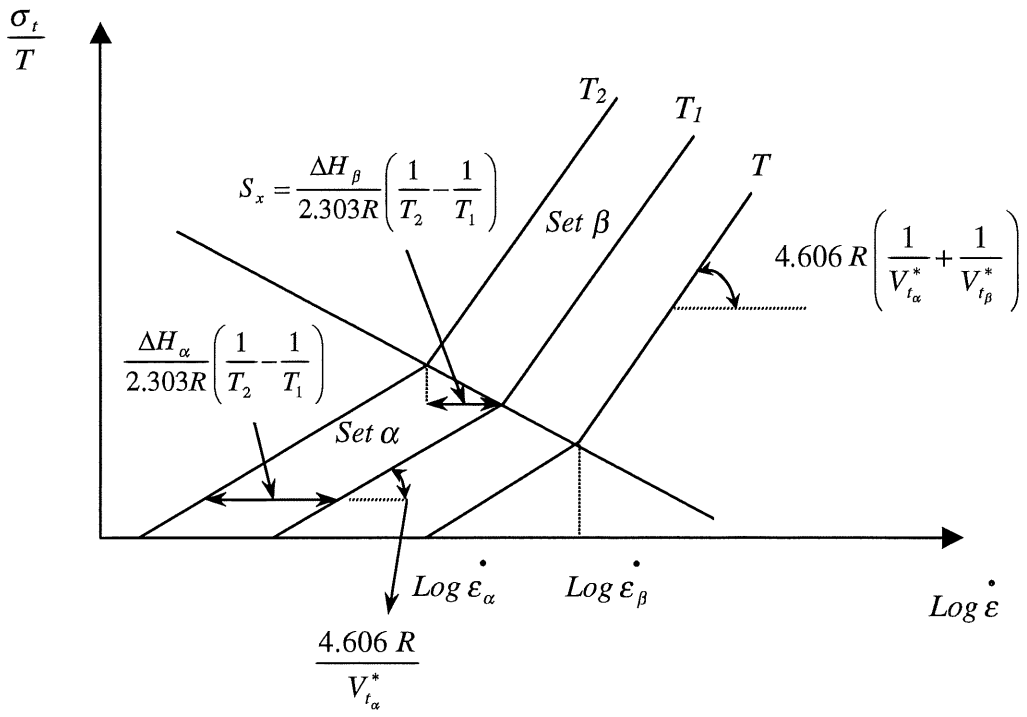

Figure B.1: Graphical method of evaluating the constants of Equations (B-3) and (B-4)

It is first assumed that the curves related to the highest and the lowest temperature regions reach the asymptote expressed by Equ. (B-3) or (B-4) respectively, within the explored range of experimental conditions. A set of straight lines is then drawn throughout the data associated with the highest temperatures and the lowest strain rate. The mean slope is taken as $\frac{4.606\,R}{V^*_{t_\alpha}}$ and the value of the activation volume $V^*_{t_\alpha}$ can be then obtained.

A set of parallel straight lines having a slope equal to $\frac{4.606\,R}{V^*_{t_\alpha}}$ is tried; from the horizontal shift of these lines and from the extrapolated value of the abscissas for $\frac{\sigma_t}{T} = 0$, mean values of ΔH_α and $\dot{\varepsilon}_{o_\alpha}$ are calculated respectively. After that, a set of parallel straight lines (called set α) is recalculated from Equ. (B-3) using the mean values of $V^*_{t_\alpha}$, ΔH_α, $\dot{\varepsilon}_{o_\alpha}$ for the all temperatures in α region at which the tests have been performed.

Another set of straight lines is then tried throughout the data, in the region of Figure B.1 related to the highest strain rates and the lowest temperatures. From the mean slope, $V_{t_\beta}^*$ is evaluated. A set of parallel straight lines (called set β) is drawn which meets set α in such a way that the locus of the intersections of straight lines, related, in both sets, to the same temperature, is a straight line called d_c (see Figure B.1). This procedure allows one to consider that the asymptotes, so obtained at each temperature, can be superimposed by a slanting translation along d_c. From measurements of s_x (expressed by Equ. (B-7)), the horizontal component of the shift factor, ΔH_β will be evaluated; and from the abscissa of the intersection of two asymptotes at a given temperature, $\dot{\varepsilon}_{o_\beta}$ can be determined using Equa. (B-5).

C.1 BRITTLE-DUCTILE TRANSITION OF THE BLENDS

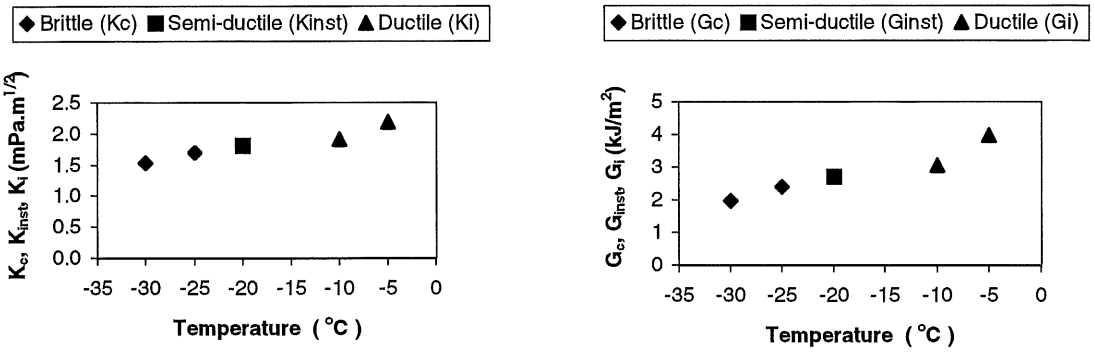

(a) (b)

Figure C.1: Variation of K (Figure a) and G (Figure b) as a function of temperature at V = 100 mm/min for K1-2.5 blend

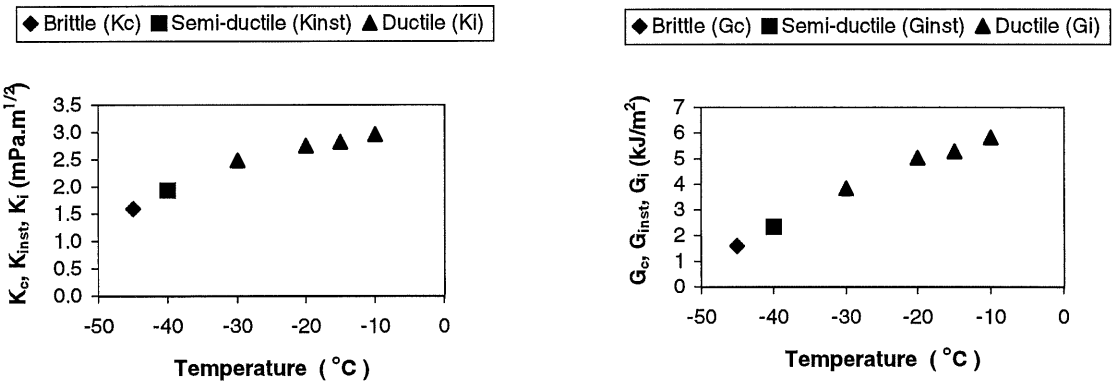

(a) (b)

Figure C.2: Variation of K (Figure a) and G (Figure b) as a function of temperature at V = 100 mm/min for K1-10 blend

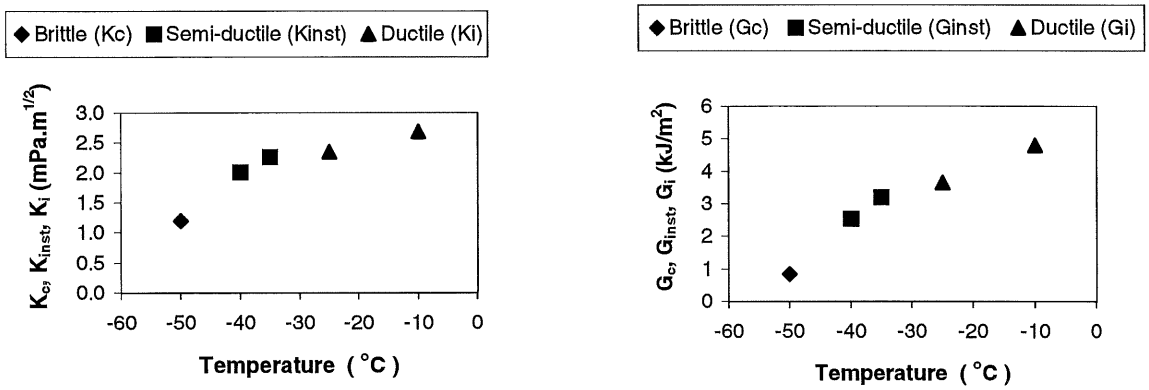

(a) (b)

Figure C.3: Variation of K (Figure a) and G (Figure b) as a function of temperature at V = 100 mm/min for K1-20 blend

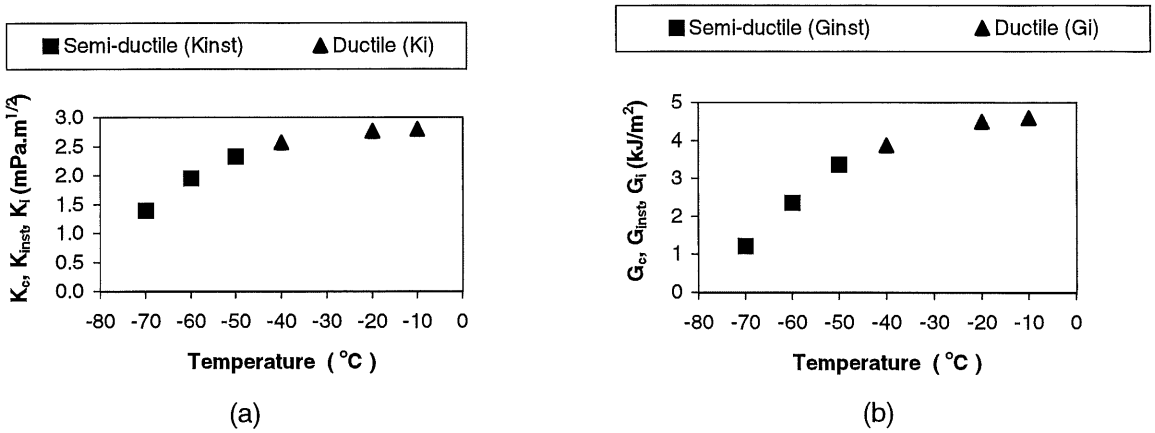

Figure C.4: Variation of K (Figure a) and G (Figure b) as a function of temperature at V = 100 mm/min for K2-2.5 blend

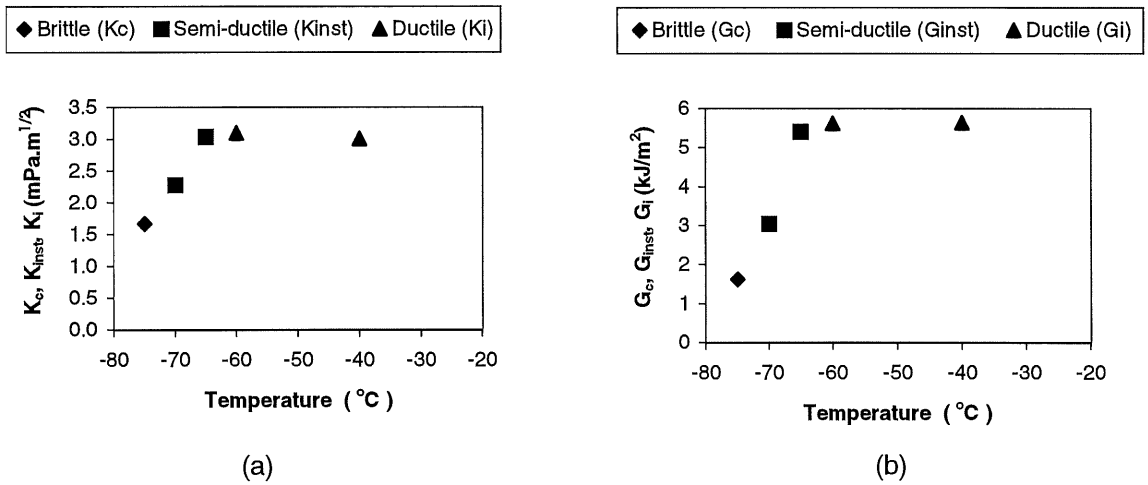

Figure C.5: Variation of K (Figure a) and G (Figure b) as a function of temperature at V = 100 mm/min for K2-15 blend

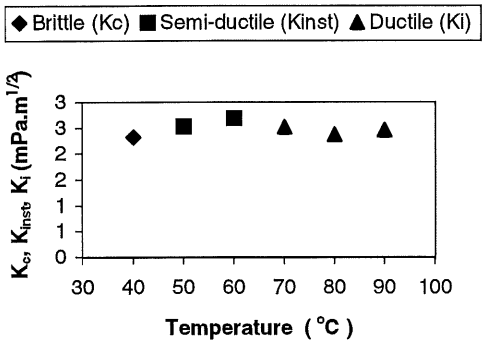

(a)

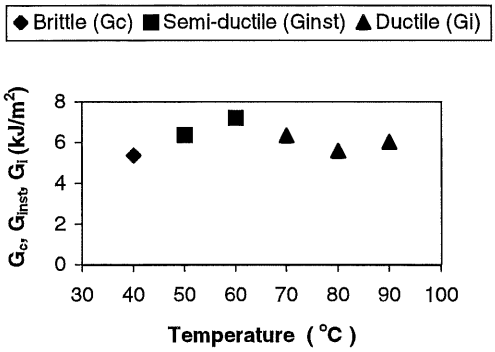

(b)

Figure C.6: Variation of K (Figure a) and G (Figure b) as a function of temperature at V = 2.5 m/s (Impact test) for K1-2.5 blend

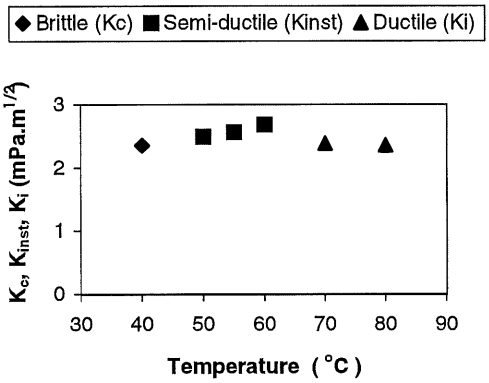

(a)

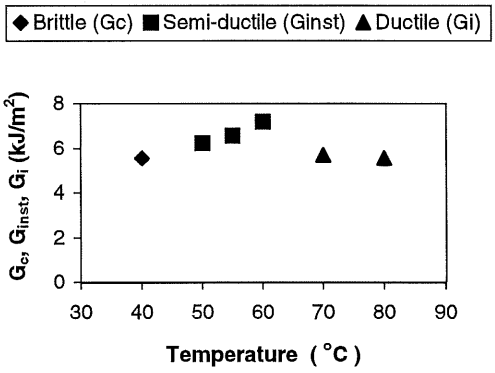

(b)

Figure C.7: Variation of K (Figure a) and G (Figure b) as a function of temperature at V = 2.5 m/s (Impact test) for K1-10 blend

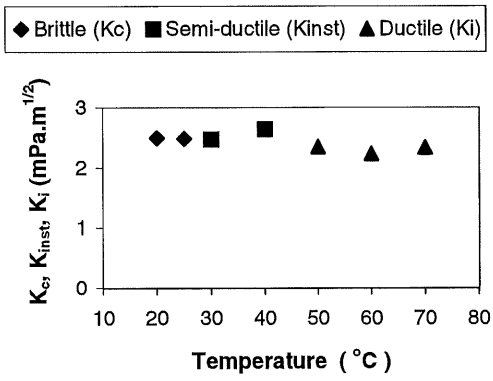

(a)

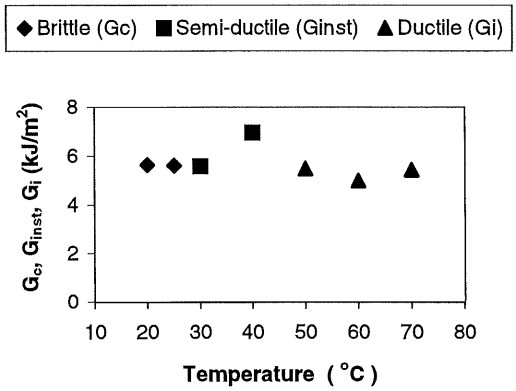

(b)

Figure C.8: Variation of K (Figure a) and G (Figure b) as a function of temperature at V = 2.5 m/s (Impact test) for K1-20 blend

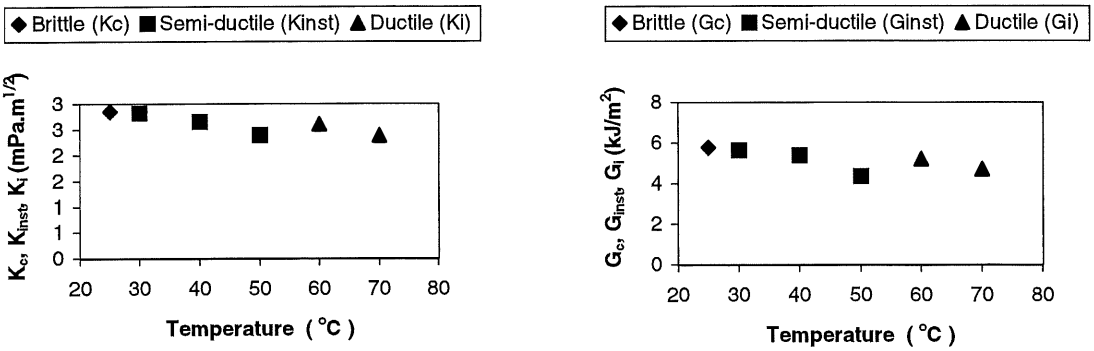

(a) (b)

Figure C.9: Variation of K (Figure a) and G (Figure b) as a function of temperature at V = 2.5 m/s (Impact test) for K2-2.5 blend

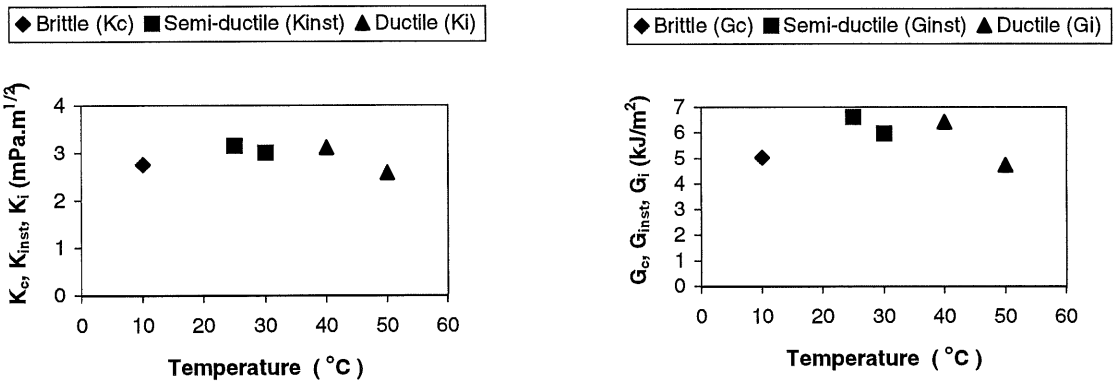

(a) (b)

Figure C.10: Variation of K (Figure a) and G (Figure b) as a function of temperature at V = 2.5 m/s (Impact test) for K2-15 blend

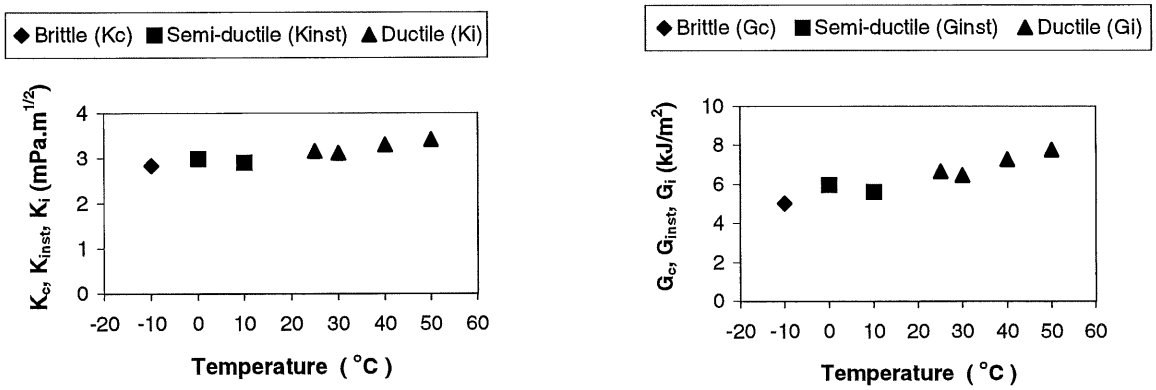

(a) (b)

Figure C.11: Variation of K (Figure a) and G (Figure b) as a function of temperature at V = 2.5 m/s (Impact test) for K2-20 blend

C.2 APPLICATION OF THE ARRHENIUS EQUATION IN THE BRITTLE-DUCTILE TRANSITION PREDICTION

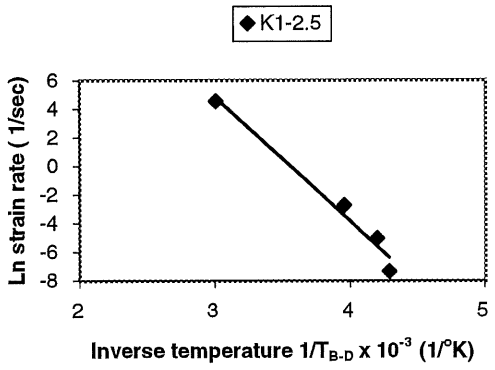

Figure C.12 : Plot of $\ln \dot{\varepsilon}$ against $1/T_{b-d}$ for K1-2.5 blend

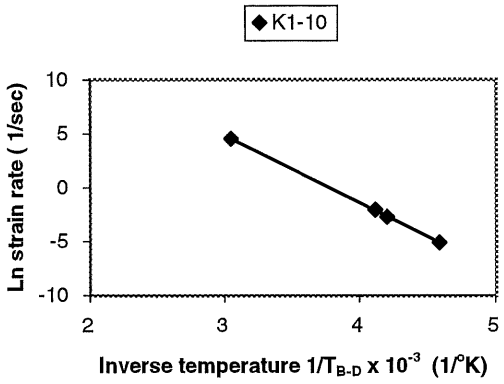

Figure C.13 : Plot of $\ln \dot{\varepsilon}$ against $1/T_{b-d}$ for K1-10 blend

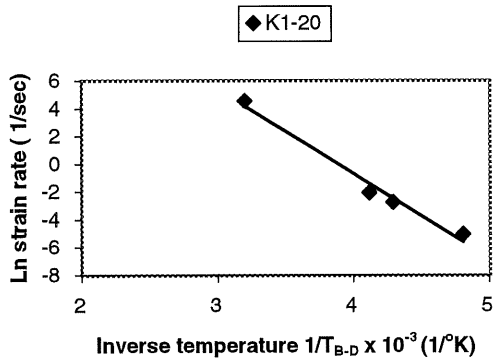

Figure C.14 : Plot of $\ln \dot{\varepsilon}$ against $1/T_{b-d}$ for K1-20 blend

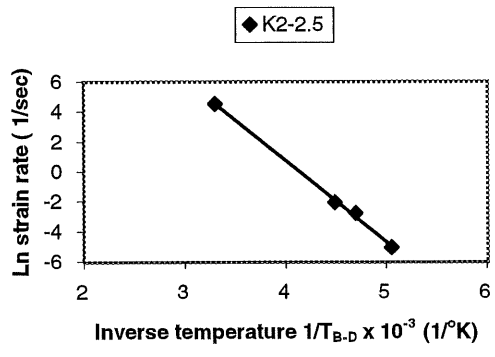

Figure C.15 : Plot of $\ln \dot{\varepsilon}$ against $1/T_{b-d}$ for K2-2.5 blend

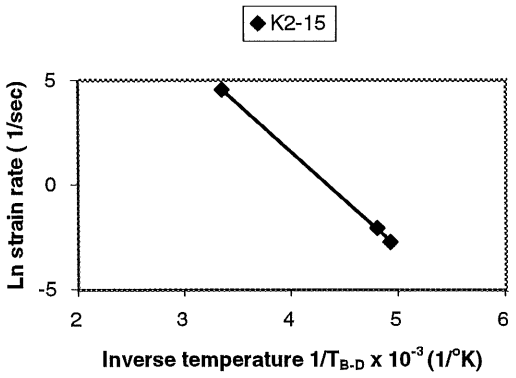

Figure C.16 : Plot of $\ln \dot{\varepsilon}$ against $1/T_{b-d}$ for K2-15 blend

APPENDIX D: CURVES OF THE TENSILE TESTS

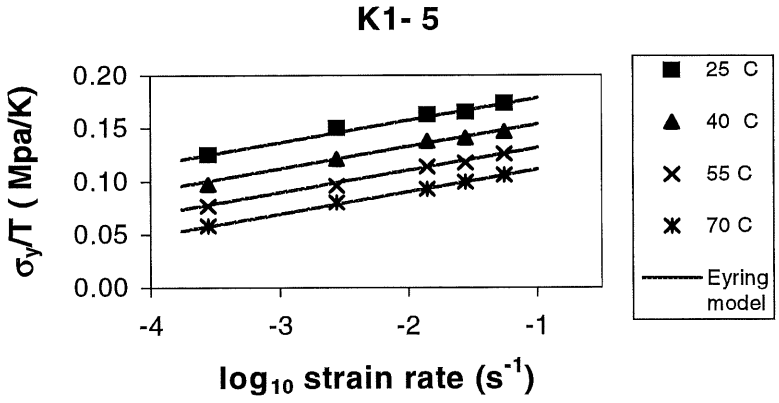

Figure D.1: Variation of σ_y / T as a function of $\log_{10} \dot{\varepsilon}_y$ at different temperatures for K1-5 blend

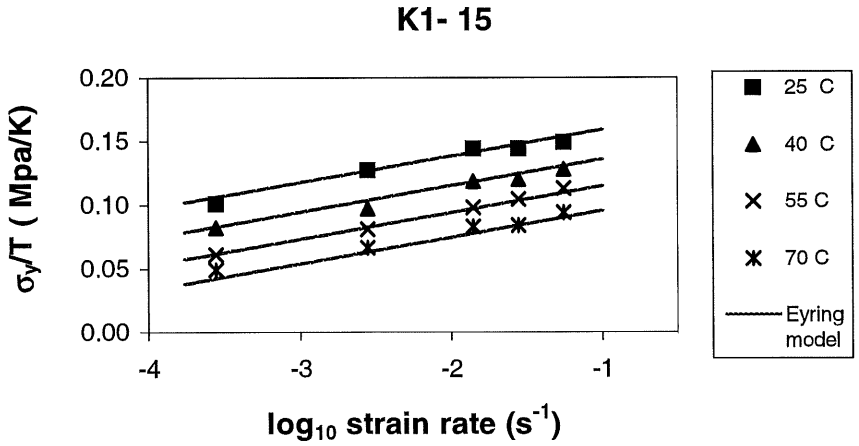

Figure D.2: Variation of σ_y / T as a function of $\log_{10} \dot{\varepsilon}_y$ at different temperatures for K1-15 blend

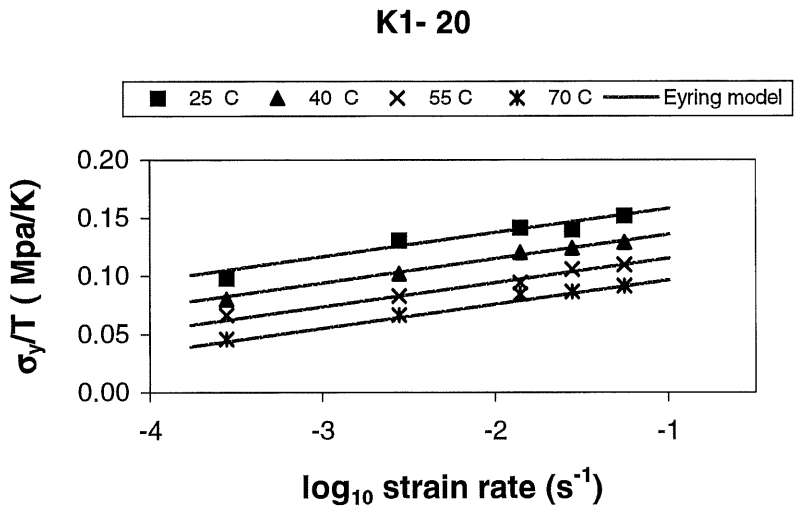

Figure D.3: Variation of σ_y / T as a function of $\log_{10} \dot{\varepsilon}_y$ at different temperatures for K1-20 blend

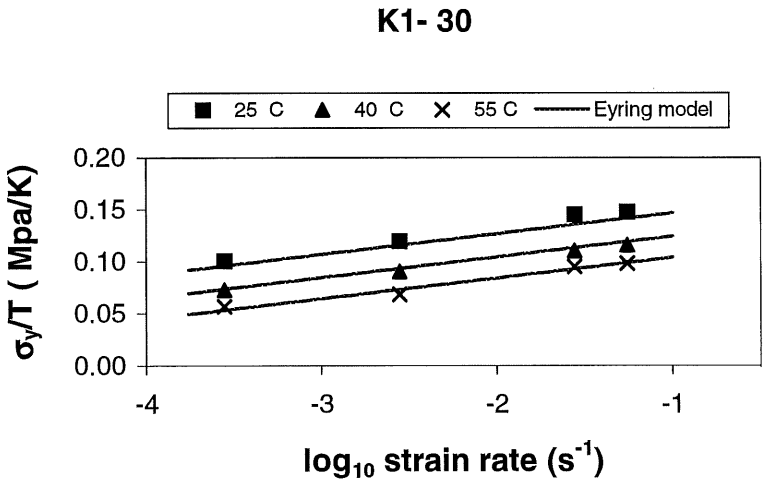

Figure D.4: Variation of σ_y / T as a function of $\log_{10} \dot{\varepsilon}_y$ at different temperatures for K1-30 blend

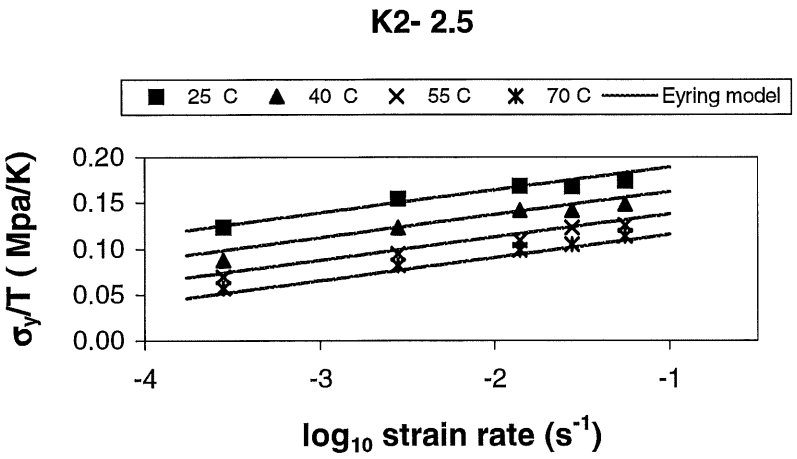

Figure D.5: Variation of σ_y / T as a function of $\log_{10} \dot{\varepsilon}_y$ at different temperatures for K2-2.5 blend

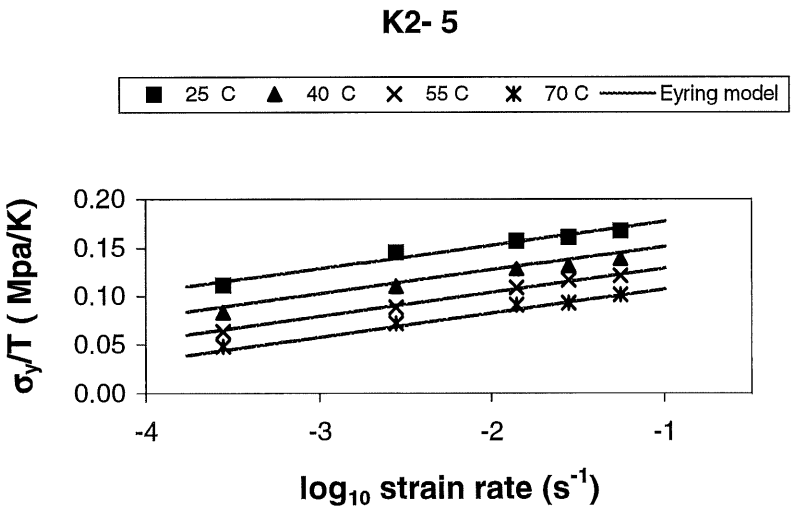

Figure D.6: Variation of σ_y / T as a function of $\log_{10} \dot{\varepsilon}_y$ at different temperatures for K2-5 blend

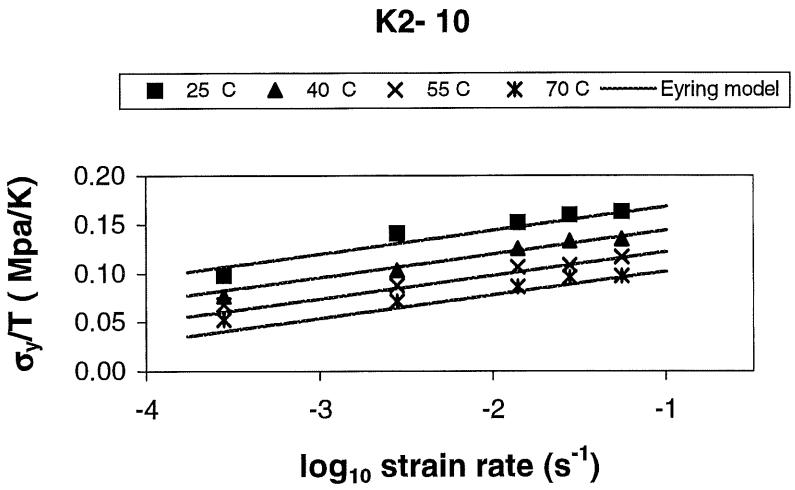

Figure D.7: Variation of σ_y / T as a function of $\log_{10} \dot{\varepsilon}_y$ at different temperatures for K2-10 blend

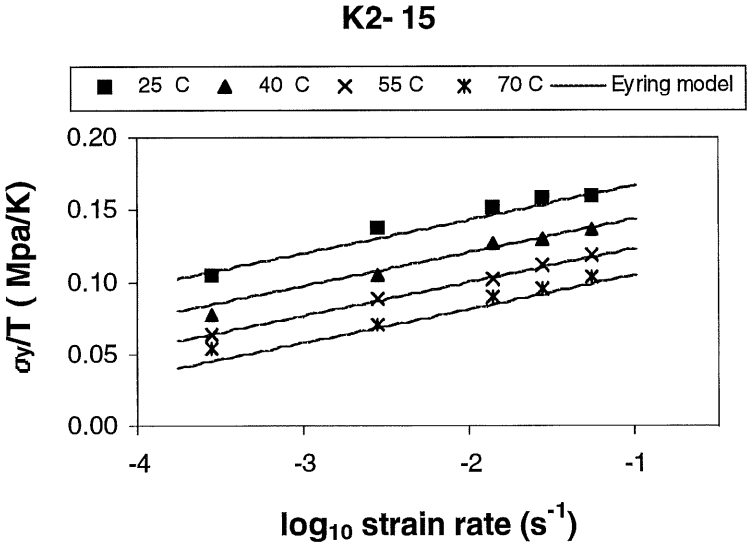

Figure D.8: Variation of σ_y / T as a function of $\log_{10} \dot{\varepsilon}_y$ at different temperatures for K2-15 blend

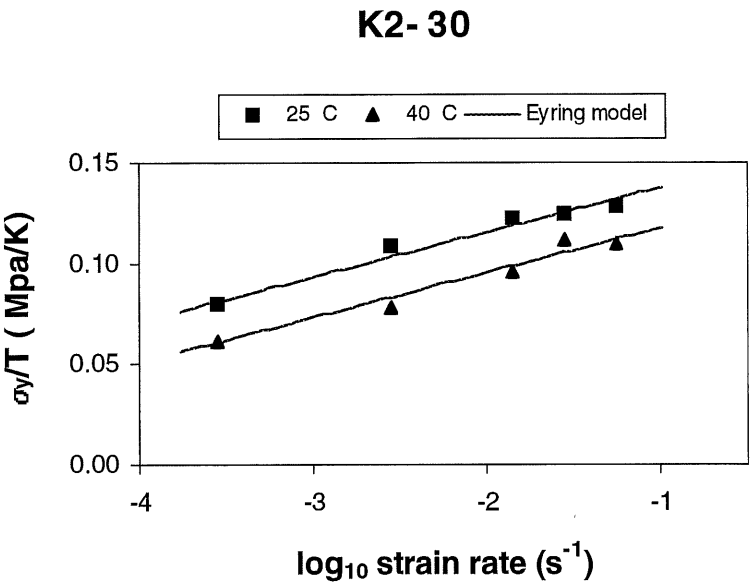

Figure D.9: Variation of σ_y / T as a function of $\log_{10} \dot{\varepsilon}_y$ at different temperatures for K2-30 blend

APPENDIX E : CURVES OF THE COMPRESSION TESTS

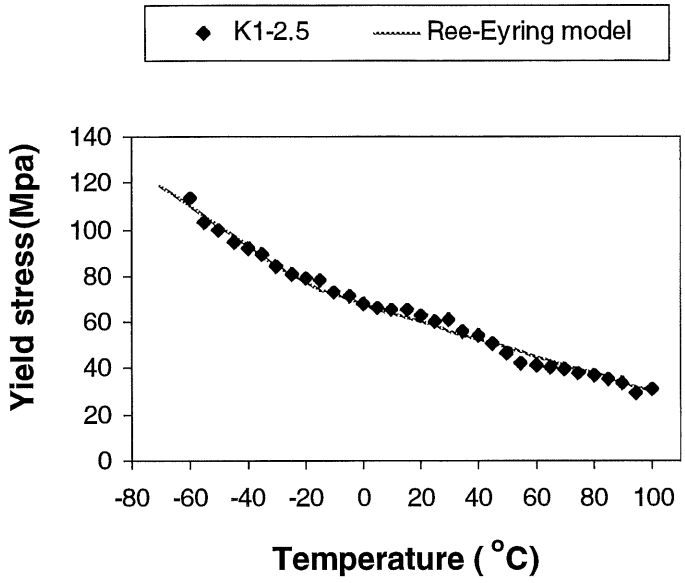

Figure E.1: Plot of yield stress in uniaxial compression $|\sigma_c|$ versus temperature at a constant rate $\dot{\varepsilon} = 100\,\text{mm/min}$ for K1-2.5 blend

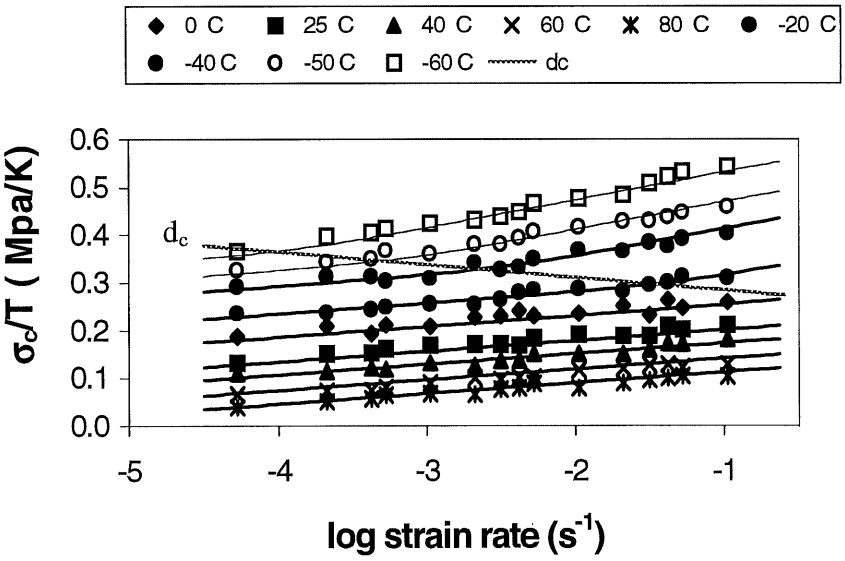

Figure E.2: Plot of the $\frac{|\sigma_c|}{T}$ as a function of $\log_{10} \dot{\varepsilon}$ for K1-2.5 blend.

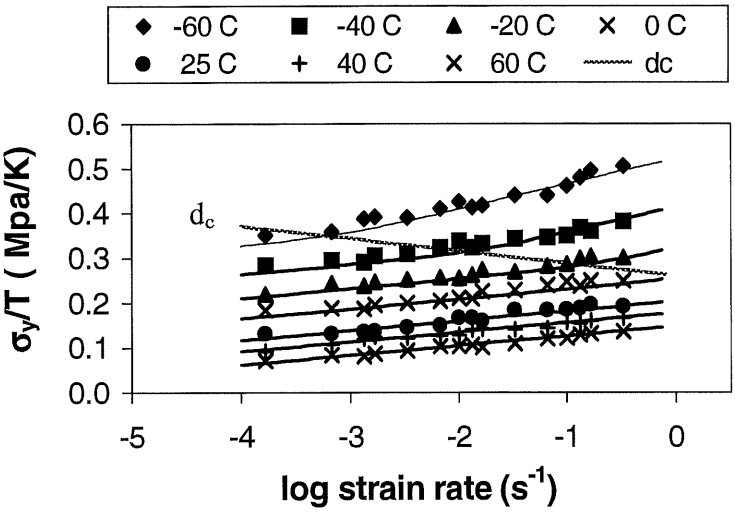

Figure E.3: Plot of the $\frac{|\sigma_c|}{T}$ as a function of $\log_{10} \dot{\varepsilon}$ for K1-10 blend.

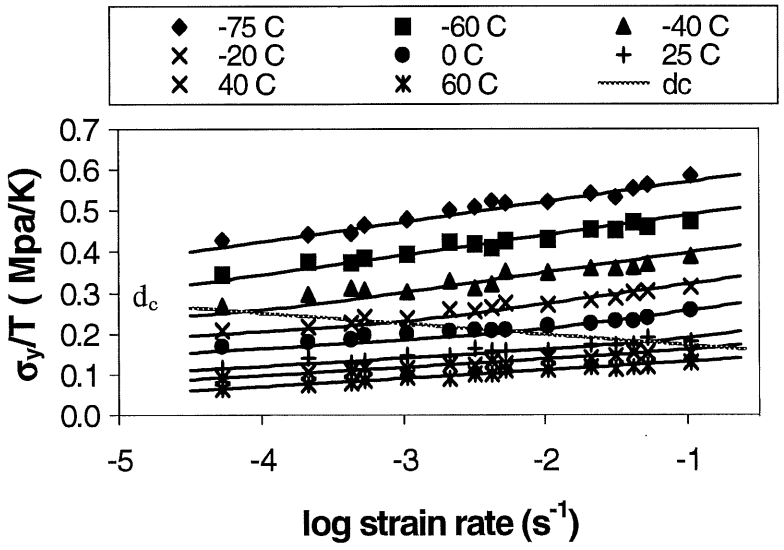

Figure E.4: Plot of the $\frac{|\sigma_c|}{T}$ as a function of $\log_{10} \dot{\varepsilon}$ for K1-20 blend.

References

1. Cigana, P., Favis, B. D., Albert, C., Vu-Khanh, T., *Macromolecules,* vol. 30, n° 14 (1997), pp. 4163-4169
2. Sih, G. C., and MacDonald, B., "Fracture mechanics applied to engineering problems: strain energy density criterion", *Engineering Fracture Mechanics,* vol. 6, n° 2 (1974), pp.361-386
3. Kipp and Sih, G. C, "The strain energy density failure criterion applied to notched elastic solids", *International Journal of Solids and Structures,* vol. 11, n° 2 (1975), pp. 153-173
4. Sih, G. C., "Some basic problems in fracture mechanics and new concept", *Engineering Fracture Mechanics,* vol. *5* (1983), p. 365
5. Sih, G. C. and Madenci E., "Crack growth resistance characterized by the strain energy density function", *Engineering Fracture Mechanics,* vol. 18, n° 6 (1983), pp. 1159-1171
6. Vu-Khanh, T. and Fisa, B., "Effects of Fillers on Fracture Performance of Thermoplastics: Strain Energy Density Criterion", *Theoretical and Applied Fracture Mechanics,* vol. 13, n°1 (1990), pp. 11-19
7. Turner, C. E., " Fracture Toughness and Specific Fracture Energy: A Re-analysis of Results", *Materials Science Engineering,* vol. 11, n° 5 (1973), pp. 275-282
8. Marshall, G. P., Williams, J. G. and Turner, C. E., " Fracture Toughness and Absorbed Energy Measurement in Impact Tests on Brittle Materials", *Journal of Materials Science,* vol. 9, n° 7, (1973), p. 949-956
9. Plati. E. and Williams, J. G., "The Determination of the Fracture Parameters for Polymers in Impact", *Polymer Engineering and Science,* vol. 15, n° 6, (1975), pp. 470-477

10. Vu-Khanh, T. and de Charentenay, F. X., "Mechanics and mechanisms of impact fracture in semi-ductile polymers", *Polymer Engineering and Science,* vol. 25, n° 13 (1985), pp. 841-850

11. McCrum, N. G., Buckley, C. P. and Bucknall, C. B., Principles of Polymer Engineering, 1988, Oxford University Press, Newyork, p.172

12. Bauwens-Crowet, C. and Bauwens, J. C., " Annealing of Polycarbonate below the Glass Transition: Quantitative Interpretation of the Effect on Yield Stress and Differential Scanning Calorimetry Measurements", *Polymer,* vol. 23, n° 11 (1982), pp. 1599-1604

13. Vu-Khanh, T., "Determination of the impact fracture parameters in ductile polymers", *Polymer,* vol. 29 (1988), pp. 1979-1984

14. Vu-Khanh, T., "Time-temperature dependence in fracture behavior of high impact polystyrene", *Theoretical and Applied Fracture Mechanics (Netherlands)*, vol. 29, n° 2, June (1998), pp.75-83

15. Favis, B. D., "Polymers alloys and blends: recent advances", *The Canadian Journal of Chemical Engineering*, vol. 69, June (1991) , pp. 619-625

16. Bucknall, C. B., Clayton, D. and Keast, W. E., " Rubber-toughening of Plastics. Part 2: Creep mechanisms in HIPS/PPO blends", *Journal of Materials Science* vol. 7 (1972), pp. 1443-1453

17. Bucknall, C. B., Clayton, D. and Keast, W. E., " Rubber-toughening of Plastics. Part 3: Strain damage in HIPS and HIPS/PPO blends", *Journal of Materials Science* vol. 8 (1973), pp. 514-524

18. Bucknall, C. B. and Drinkwater, I. C., " Rubber-toughening of Plastics. Part 4: Creep mechanisms in ABS emulsion polymer", *Journal of Materials Science* vol. 8 (1973), pp. 1800-1808

19. Bucknall, C. B. and Page, C. J., "Rubber-toughening of Plastics. Part 6: Effects of rubber particles on the kinetics of creep in polypropylene", *Journal of Materials Science* vol. 17 (1982), pp. 808-816

20. Bucknall, C. B., Heather, P. S. and Lazzeri, A., " Rubber Toughening of Plastics. XII. Deformation Mechanisms in Toughened Nylon 6,6", *Journal of Materials Science,* vol. 16 (1989), pp. 2255-2261

21. Creton, C., Kramer, E. J., Hui, C. and Brown, H. R., " Failure Mechanisms of Polymer Interfaces Reinforced With Block Copolymers", *Macromolecules* vol. 25 (1992), pp.3075-3088

22. Washiyama, J., Kramer, E. J., Creton, C. and Hui, C., " Chain Pullout Fracture of Polymer Interfaces", *Macromolecules* vol. 27 (1994), pp. 2019-2024

23. Brown, H. R., " Effect of a diblock copolymer on the adhesion between incompatible polymers", *Macromolecules*, vol. 22 (1989), pp. 2859-2860

24. Creton, C., Kramer, E. J and Hadziioannou, *Macromolecules*, vol. 24 (1991), p. 1846

25. Willis, J. M. and Favis, B. D., "Processing-morphology relationships of compatibilized polyolefin/polyamide blends. Part 1: The effect of an ionomer compatibilizer on blend morphology ", *Polymer Engineering and Science*, vol. 28 (1988), pp.1416-1426

26. Willis, J. M., Favis. B. D. and Lunt, J., " Reactive Processing of Polystyrene-Co-Maleic Anhydride/Elastomer Blends: Processing--Morphology—Property Relationships", *Polymer Engineering and Science*, vol. 30 (1990), p. 1073

27. Favis, B. D., " Phase size/interface relationships in polymer blends: The emulsification curve " *Polymer*, vol. 35 (1994), pp. 1552-1555

28. Galli, P., Danesi, S. and Simonazzi, T., *Polymer Engineering and Science*, vol. 24 (1984), p. 544

29. Karger-Kocsis, J., Kallo, A. and Kuleznev, V. N., " Phase structure of impact-modified polypropylene blends", *Polymer*, vol. 25 (1984), pp. 279-286

30. Cimmino, S., Coppola, F., Orazio, L. D., Greco, R., Maglio, G., Malinconico, M., Mancarella, C., Martuscelli, E. and Ragosta, G., " Ternary nylon-6/rubber/modified rubber blends: effect of the mixing procedure on morphology, mechanical and impact properties", *Polymer*, vol. 27 (1986), pp. 1874-1884

31. Greco, R., Malinconico, M., Martuscelli, E., Ragosta, G. and Scarinzi, G., *Polymer*, vol.28 (1987), p. 1185

32. Hobbs, S. Y., Bopp, R. C. and Watkins, V. H., " Toughened nylon resins", *Polymer Engineering and Science*, vol. 23 (1983), pp. 380-389

33. Borggreve, R. J. M., Gaymans, R. J., Schuijer, J. and Ingen Housz, J. F., " Brittle-tough transition in nylon-rubber blends: effect of rubber concentration and particle size ", *Polymer*, vol. 28 (1987) pp. 1489-1496

34. Matos, M., Favis, B. D. and Lomellini, P., " Interfacial modification of polymer blends - the emulsification curve: 1. Influence of molecular weight and chemical composition of the interfacial modifier ", *Polymer*, vol. 36 (1995), p. 3899

35. Zang, B. Z., Uhlmann, D. R. and Vandersande, J. B., " Rubber-roughening in polypropylene", *Journal of Applied Polymer Science,* vol. 30 (1985), pp. 2485-2504

36. Wu, S., *Polymer*, vol. 26 (1985), p. 1855

37. Silberberg, J. and Han, C. D., " Effect of rubber particle size on the mechanical properties of high-impact polystyrene", *Journal of Applied Polymer Science,* vol. 22 (1978), pp. 599-609

38. Donald, A. M. and Kramer, E. J., *Journal of Materials Science,* vol. 17 (1982), p.1765

39. Hobbs, S. Y., " Effect of rubber particle size on the impact properties of high impact polystyrene (HIPS) blends", *Polymer Engineering and Science*, vol. 26 , n° 1 (1986), pp. 74-81

40. Zang, B. Z., Uhlmann, D. R. and Vandersande, J. B., " Rubber particle size dependence of crazing in polypropylene", *Polymer Engineering and Science*, vol.5, n° 10 (1985), pp. 643-651

41. Bucknall, C. B., Cote, F. F. P. and Partridge, I. K., *Journal of Materials Science*, vol. 21 (1986), p. 301

42. Vu-khanh, T. and Fisa, B., " Fracture behavior of mica-reinforced polypropylene: effects of coupling agent, flake orientation, and degradation ", *Polymer composites*, vol. 7 (1986), pp. 219-226

43. Vu-khanh, T., *Trends in Polymer Science (UK)*, vol. 5, n° 11 (1997), pp. 356-360

44. Sih, G.C., "*Handbook of stress Intensity Factors for Researchers and Engineers*", Institute of Fracture and Solids Mechanics, Lehigh University, Bethelehem, PA (1973)

45. Griffith, A.A., Phil., *Trans. Royal Soc.*, (London) A221 (1921), p.163

46. Williams, J.G., " Failure in Polymers", *Advanced in Polymer Science 27*, Springer-Verlag New-York (1978)

47. Berry, J. P., *Journal of Polymer Science*, vol. 50 (1961), p. 107

48. Broutman, L. J. and McGarry, F. J., *Journal of Applied Polymer Science*, vol. 9 (1965), p. 589

49. Kambour, R. P., *Journal of Applied Polymer Science (Symposia)*, vol. 7 (1968), p. 215

50. Marshall, G. P., Coutts, L. H. and Williams, J. G., " Temperature effects in the fracture of PMMA", *Journal of Materials Science*, vol. 9 (1974), pp. 1409-1419

51. Casiraghi, T., Castiglioni, G. and Ronchetti, T., "Fracture Mechanics of Polymers: Critical Evaluation for Linear Elastic Behavior at High Speed Testing", *Journal of Materials Science*, vol. 23 (1988), pp. 459-466

52. Narisawa, I., "Fracture and Toughness of Crystalline Polymer Solids", *Polymer Engineering and Science*, vol. 27, n° 1 (1987) , pp. 41-45

53. Newmann, L. V. and Williams, " Impact behavior of ABS over a range of temperatures", J. G., *Polymer Engineering and Science*, vol. 18 (1978), pp.893-899

54. Turner, C. E. in *Fracture Mechanics: Twelfth Conference (ASTM STP 700)*, American Society for Testing and Materials (1980), pp. 314-337

55. Vu-khanh, T., "Impact fracture characterization of polymer with ductile behavior", *Theoretical and Applied Fracture Mechanics*, vol. 21 (1994), pp. 83-90

56. Birch, M.W. and Williams, J. G., " The effect of Rate on the Impact Fracture toughness of Polymers", *International Journal of Fracture*, vol. 14, n° 1 (1978), pp. 69-84

57. Nikpur, K. and Williams, J. G., " An impact strength Analysis of some Rubber-modified Polystyrenes", *Plastics and Rubbers: Materials and Applications* , vol. 3 (1978), pp. 163-166

58. Williams, J. G., "Fracture Mechanics of Polymers", Ellis Horwwood, Chichester (1984)

59. Williams, J. G. and Birch, M. W., "Fracture", International Fracture Conference part 4, vol. 1, University of Waterloo, Canada (1977), p. 501

60. De Charentenay, F. X., Robin, J. J., Francois Xavier and Vu-khanh, T., " Impact fracture mechanics of semi-ductile polymers", Fifth International Conference on Deformation, Yield and Fracture of Polymers, Cambridge, England, March 29-April 1 (1982), pp. 33.1-33.6

61. Bucknall, C. B., "Toughened Plastics", Applied Science Publishers l. t. d. (1977)

62. Beaumont, P. W. R., Riewald, R. G. and Zweben, C., *ASTM STP 568* (1974), p. 134

63. Vu-khanh, T., Docteur-ingénieur Thesis, University of Compiègne, France (1982)

64. Rice, J. R., *Journal of Applied Mechanics*, vol. 35 (1968), p. 379

65. Landes, J. D. and Begley, J. A., *ASTM STP 560* (1974)

66. Paris, P. C., Tada, H., Zahoor, A. and Ernst, H., ''Elastic-Plastic Fracture: First Symposium'', *ASTM STP 668*, 5 (1979)

67. Chan, M. K. V. and Williams, J. G., " J-integral studies of crack initiation of a tough high density polyethylene", *International Journal of Fracture*, vol. 23 (1983), pp.145-159

68. Hashemi, S. and Williams, J. G., ''Single and Multiple-specimen R-Curve Method for J1c Determination of Toughened Nylons'', *Journal of Materials Science*, vol. 26 (1991), pp. 621-630

69. "E-813 Standard Test Method for J_{IC}, a Measure of Fracture Toughness", *Annual Book of ASTM Standards*, American Society for Testing and Materials, Philadelphia (1983)

70. Narisawa, I. and Takemori, M. T., "Fracture Toughness of Impact Modified Polymers based on J-Integral", *Polymer Engineering and Science*, vol. 29, n° 10 (1989), pp. 671-678

71. Mai, Y. W. and Cotterell, B., "On the Essential Work of Ductile Fracture in Polymers", *International Journal of Fracture*, vol. 32 (1986), pp. 105-125

72. Mai, Y. W. and Cotterell, B., Horlyck, R. and Vigna, F., "The Essential Work of Plane Stress Ductile Fracture of Linear Polyethylenes", *Polymer Engineering and Science*, vol.27, n° 11 (1987), pp. 804-809

73. Vu-khanh, T., Communication privée

74. Saleemi, A. S. and Nairn, J. A., "The Plane-Strain Essential Work of Fracture as a Measure of the Fracture Toughness of Ductile Polymers", *Polymer Engineering and Science*, vol. 30, n° 4 (1990), pp. 211-218

75. Logsdon, W. A., *ASTM STP 590*, 43 (1976)

76. Ernst, H. A., *ASTM STP 803*, I-19L (1983)

77. Hertzberg, R. W., "Deformation and fracture mechanics of engineering materials", John Wiley & Sons (1989)

78. Heyer, R. H., *ASTM STP 527*, 3 (1973)

79. McCabe, D. E. and Landes, J. D., *ASTM STP 668*, 288 (1979)

80. E 399 Standard Test Method for Plane Strain Fracture Toughness of Metallic Materials, Annual Book of ASTM Standards (1983)

81. Vu-khanh, T., Sanschagrin, B. and Fisa, B., Composites 85 Symposium, NRCC/IMRI, Boucherville, Quebec, Canada, Nov. 20 (1984), pp. 9.1-9.47

82. Vincent, P. I., "The Tough-Brittle Transition in Thermoplastics", *Polymer*, vol. 1 (1960), p.425

83. Johnson, F. A. and Randon, J. C., *National Physics Science*, 239, Oct. (1978)

84. Williams, J. G. and Crouch, B. A., "Thermal Crack Tip Blunting in High Speed Fracture of Polymers", Sixth International Conference: Deformation, Yield and Fracture of Polymers, 1-4 April, (1985), pp. 30. 1-30. 4

85. Vu-khanh, T. and Yu, Z., "Mechanism of Brittle-Ductile Transition in Toughened Thermoplastics", *Theoretical and Applied Fracture Mechanics*, vol. 26 (1997), pp. 177-183

86. Marshall, I. and Thompson, A. B., *Proceedings of the Royal Society (London) A*, 221 (1954), p. 541

87. Liu, Y. and Truss, R. W., " Tensile yielding and microstructures of blends of isotactic polypropylene and linear low-density polyethylene ", *Journal of Polymer Science*: Part B: Polymer Physics, vol. 33 (1995), pp. 813-822

88. Argon, A. S., Andrews, R. D., Godrick, J. A. and Whitney, W., *Journal of Applied Physics*, vol. 39 (1968), p. 1899

89. Brown, N., *Materials Science Engineering*, vol. 8 (1971), p. 69

90. Bochum, A. S., *Kunststoffe*, vol. 72 (1982), p. 791

91. Tobolsky, A. V. and Andrews, R. D., *J. Chem. Phys.*, vol. 13 (1945), p. 3

92. Robertson, R. E., *J. Chem. Phys*, vol. 44 (1966), p. 3950

93. Argon, A. S., *Philosophical Magazine*, vol. 28 (1973), p. 839

94. Bowden, P. B. and Raha, S., " Molecular model for yield and flow in amorphous glassy polymers making use of a dislocation analogue", *Philosophical Magazine*, vol. 29 (1974), pp. 149-166

95. Tate, K. R., Perrin, A. R. and Woodhams, R. T., " Tensile flow stress model for oriented polypropylene", *Polymer Engineering and Science,* vol. 28 (1988), pp. 740-742

96. Eyring, H., *J. Chem. Phys.*, vol. 4 (1936), p. 283

97. Glasstone, S., Laidler, K. J. and Eyring, H., "The theory of Rate Processes", McGraw-Hill, New York (1941), pp. 480-483

98. Ree, T. and Eyring, H., *Journal of Applied Physics*, vol. 26 (1955), p. 793

99. Robertson, R. E., *Journal of Applied Polymer Science,* vol. 7 (1963), p. 443

100. Roetling, J. A., *Polymer*, vol. 6 (1965), p. 311

101. Roetling, J. A., *Polymer*, vol. 6 (1965), p. 615

102. Roetling, J. A., *Polymer*, vol. 7 (1966), p. 303

103. Duckett, R. A., Goswami, B. C., Smith, L. S. A., Ward, I. M. and Zihlif, A. M., " Yielding and crazing behaviour of polycarbonate in torsion under superposed hydrostatic pressure " *British Polymer Journal*, vol. 10 (1978), pp. 11-16

104. Bauwens-Crowet, C., Bauwens, J. C and Hommes, G., *Journal of Polymer Science*, A-2, vol. 7 (1969), p. 735

105. Truss, R. W., Clarke, P. L., Duckett, R. A. and Ward, I. M., " Dependence of yield behavior on temperature, pressure, and strain rate for linear polyethylenes of different molecular weight and morphology", *Journal of Polymer Science*: Part B: Polymer Physics, vol. 22 (1984), pp. 191-209

106. Foot, J. S., Truss, R. W., Ward, I. M. and Duckett, R. A., " Yield behaviour of amorphous polyethylene terephthalate: an activated rate theory approach ", *Journal of Materials Science,* vol. 22, (1987), pp. 1437-1442

107. Bucknall, C. B., Davies, P. and Partridge, I. K., *Journal of Materials Science*, vol. 21 (1986), pp. 307-313

108. Bauwens-Crowet, C., Bauwens, J. C. and Homes, G., *Journal of Materials Science*, vol.7 (1972), p. 176

109. Bauwens, J. C., " Vinyl chloride yield condition and propagation of lueders' lines in tension- torsion experiments on poly", *Journal of Polymer Science*, A-2, vol. 8 (1970), pp. 893-901

110. Bauwens-Crowet, C., " Compression yield behaviour of polymethyl methacrylate over a wide range of temperatures and strain-rates ", *Journal of Materials Science*, vol. 8 (1973), pp. 968-979

111. Yoon, H. N., Pae, K. D. and Sauer, J. A., " Effects of combined pressure-temperature on mechanical behavior of polypropylene", *Journal of Polymer Science,* Part B: Polymer Physics, vol. 14 (1976), pp. 1611-1627

112. Odje, S., "Rupture du mélange de polymères polystyrène/caoutchouc ethylène propylène: mécanismes de rupture, interfaces et morphologie", Thesis for the Degree of Master of Science, Mechanical engineering, Université de Sherbrooke (1997)

113. Heifboer, J., "Dynamic mechanical properties and impact strength", *Journal of Polymer Science, Part C*, vol. 16 (1968), pp. 3755-3763

114. Boyer, R. F., "Dependence of mechanical properties on molecular motion in polymers", *Polymer Engineering and Science*, vol. 8 (1968), pp. 161-185

115. Vincent, P. I., "Impact strength and mechanical losses in thermoplastics", *Polymer*, vol.15 (1974), pp. 3639-3650

116. Hartmann, B. and Lee, G. F., "Impact resistance and secondary transitions", *Journal of Applied Polymer Science*, vol. 23 (1979), pp. 3639-3650

117. Woo, L., Westphal, S. and Ling, M. T. K., "Dynamic mechanical analysis and its relationship to impact transitions, *Polymer Engineering and Science*, vol. 34 (1994), pp.420-427

118. E 561 Standard Practice for R-Curve Determination, Annual Book of ASTM Standards.

119. Vu-Khanh, T. Sanschagrin, B. and Fisa, B., "Fracture of Mica-Reinforced Polypropylene: Mica Concentration Effect", *Polymer Composites*, vol. 6, No. 4, October (1985), pp. 249-260

120. Vu-Khanh, T. and Fisa, B., "Fracture Behavior of Mica-Reinforced Polypropylene: Effects of Coupling Agent, Flake, Orientation, and Degradation", *Polymer Composites*, vol. 7, No. 4, August (1986), pp. 219-226

121. Knott, J. F., "Fundamentals of Fracture Mechanics", Butter-worth, London (1973)